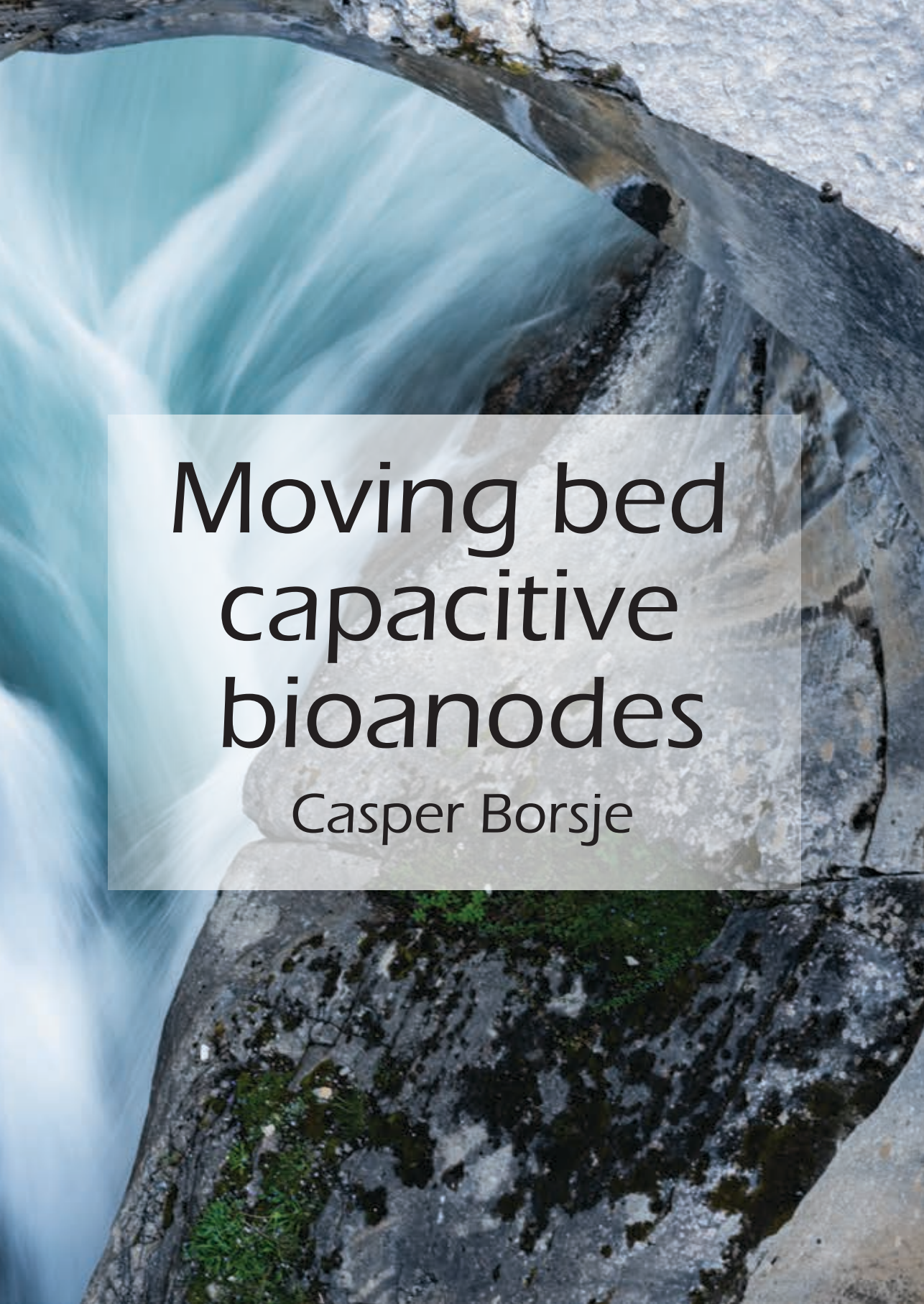

Moving bed capacitive bioanodes

Casper Borsje

Propositions

1. Decoupling redox processes from the electrochemical cell using capacitive electrodes opens perspectives for scaling up bioelectrochemical systems. (This thesis)

2. Moving bed capacitive bioanodes are limited by electrical resistance. (This thesis)

3. Profit from publicly funded research should be used for funding new research.

4. Resources for scientific research are wasted by lack of resources for publication of negative findings and experimental failures.

5. Translation of scientific insight, to manage the public's understanding and expectations, is required to maintain public trust in science.

6. Creative hobbies are essential for academic researchers.

Propositions belonging to the thesis, entitled:

"Moving bed capacitive bioanodes"

Casper Borsje

28 May 2021

Moving bed capacitive bioanodes

Casper Borsje

Thesis committee

Promotor

Prof. Dr C.J.N. Buisman

Professor Biological Recovery and Reuse Technology

Wageningen University & Research

Co-promotors

Dr A. ter Heijne

Associate professor, Environmental Technology

Wageningen University & Research

Dr T. Sleutels

Scientific program manager

Wetsus, European Centre of Excellence for Sustainable Watertechnology, Leeuwarden

Other members

Prof. Dr K.J. Keesman, Wageningen University & Research

Prof. Dr I.A. Ieropoulos, University of the West of England, Bristol, UK

Dr L. Jourdin, Delft University of Technology

Dr P.F.H. van den Brink, Evides Waterbedrijf N.V., Rotterdam

This research was conducted under the auspices of the Graduate School for Socio-Economic and Natural Sciences of the Environment (SENSE)

Moving bed capacitive bioanodes

Casper Borsje

Thesis

submitted in fulfilment of the requirements for the degree of doctor
at Wageningen University
by the authority of the Rector Magnificus,
Prof. Dr A.P.J. Mol,
in the presence of the
Thesis Committee appointed by the Academic Board
to be defended in public
on Friday 28 May 2021
at 1:30 p.m. in the Aula

Casper Borsje
Moving bed capacitive bioanodes, page 155 pages.

PhD thesis, Wageningen University, Wageningen, the Netherlands (2021)
With references, with summary in English

ISBN 978-94-6395-732-8
DOI https://doi.org/10.18174/542629

Be kind to yourself

Table of contents

Eldhraun lava field, Iceland

Chapter 1

General introduction

1.1. Wastewater treatment technology for removal of organic material

Environmental challenge

In modern society, municipalities and industry produce significant volumes of wastewater. Globally, on average 95 m^3 wastewater is produced per capita per year, with in Europe 124 m^3/capita/year and North America at 231 m^3/capita/year: a global total of 380×10^9 m^3 per year (2015 data) [1]. Wastewater contains a mixture of several pollutants, such as dissolved organics, and nitrogen and phosphorus compounds, with differing effects on the environment and ecosystems. In nature, the dissolved organics are degraded by aerobic bacteria, resulting in the deoxygenation of the water. This is especially problematic for wastewater discharged into surface waters, which host important ecosystems that rely on oxygen in the water. Nitrogen and phosphorus discharge can result in eutrophication, which in turn leads to reduced biodiversity and possible toxicity due to proliferation of certain algae species [2,3]. At the end of the 19th century, wastewater treatment – rather than disposal – became more important as these consequences became clear [4]. Wastewater treatment plants (WWTPs) were constructed, connecting in 78% of the population in the EU to primary and secondary treatment (EU-28, status in 2017) [5]. The wastewater treatment process consists of several steps, including but not limited to: primary treatment for the removal of (suspended) solids, secondary for removal of organics, and tertiary for removal of nutrients, minerals, metals, inorganics, taste, color, odor and pathogens [6]. Traditionally, aerobic treatment has been used to remove these organics, but the recovery of energy contained in the organics, has become a goal in itself: firstly, to make the WWTPs less energy intensive and more self-sustainable and secondly to export the energy for use in society. Aerobic treatment and recovery of the energy from organics in wastewater using anaerobic digestion processes and bioelectrochemical systems will be discussed in the following paragraphs [7,8].

Aerobic treatment

Aerobic treatment utilizes oxygen for the oxidation of dissolved organics by aerobic bacteria in the controlled environment of WWTPs. Traditional treatment uses large ponds to flow the wastewater through. Oxygen is forced into the water stream at various points in the pools, and the required oxygen is consumed by the growing bacteria while degrading the organic material. The aerobic biomass is collectively called activated sludge. The aeration requires significant amounts of energy. In the last decade, the aeration step consumed between 0.1 and 0.6 kWh/m^3wastewater in various WWTPs around the world, depending, among others, on climate, size, technology, and chemical oxygen demand (COD) and total nitrogen requirements of influent and effluent [7]. For typical wastewater, 0.5 kgCOD/m^3 [9], the aerobic energy costs are 0.2 to 1.2 kWh/kg COD. The growth of aerobic microorganisms results in a large volume of sludge in suspension in the wastewater stream: the sludge volume is proportional to the organic loading rate [10] (commonly expressed as kg COD per m^3 per day). Waste aerobic sludge can then be used in various ways: production of biogas (via anaerobic digestion, see section 1.1.) [7,11], VFAs [12], PHA (bioplastic precursor) [13], biochar [14], hydrogen [15]. The sludge can also be applied as fertilizer, directly or after treatment [10] for pollutants such as heavy metals [16], antibiotics [17] and nanoplastics [18]. The incineration [10] of the dewatered sludge or of the produced biogas can be directly used to increase the energy balance of WWTPs by recovery of the electrical power and heat [7]. An alternative use of aerobic treatment is the production of bioflocculants using MBRs [19].

Technological developments into the activated granular sludge (AGS) process, have improved the energy efficiency of aerobic treatment process. The NEREDA® AGS process was shown to reduce the energy requirements of aerobic treatment by 40%. The AGS processes utilize anaerobic treatment in combination with aerobic treatment [8]. For instance, the granular nature of the AGS process combines the anaerobic environment inside the granules with the aerobic environment of the outer layers of the granules. The NEREDA® granules also contains nitrifying and denitrifying bacteria which remove N and P from the wastewater. A full scale AGS study, in the Netherlands (2014), reported 6.9 mgN/L and 0.4 mgP/L effluent, while the same wastewater was treated in the WWTP, with aerobic treatment and chemical P removal, to 9.9 mgN/L and 0.9 mgP/L [12]. The AGS process reduced the energy costs for the treatment by about 1/3rd, reaching lower effluent concentrations that the traditional aerobic treatment combined with chemical P removal [12].

Thus, though aerobic treatment allows for the protection of surface waters, there are major downsides in the costs of energy and surface area for wastewater treatment facilities. Technological developments have diminished these concerns, but the energy contained in the organic content of wastewater is only partially recovered through secondary processes such as anaerobic digestion of the activated sludge.

Anaerobic digestion

An alternative to aerobic treatment is the anaerobic digestion (AD) process, which produces biogas directly from the wastewater. Anaerobic digestion occurs via several steps: from hydrolysis to acidogenesis and methanogenesis [20]. High-rate digestion was first developed with up flow anaerobic sludge bed (UASB) reactors [21], which were further developed in the last decades [22]. The technology uses anaerobic granular sludge with a high activity per volume of reactor: less sludge is produced by the same organic loading rate compared to aerobic treatment [23]. The produced biogas is a mixture of CH_4 and CO_2 (~80% methane) [24]. For efficient combustion, upgrading the biogas by removal of CO_2 is preferred [25]: on average, about 30% of the energy in biogas can be recovered as electrical power and the remaining energy is converted to heat. The recovered electrical power is about 1 kWh/kg COD, or 26% of the theoretical energy from COD (3.86 kWh/kgCOD [9]), and 400 $W/m^3_{reactor}$ [26]. The heat and electrical power can be used to improve the energy balance of WWTPs [26], where the heat has to be used to heat the digestion process, which increases the anaerobic activity [24], and electrical power for pumping and other appliances [26]. The combustion of biogas is also used in greenhouses, as an alternative to natural gas, to produce CO_2 to enhance plant growth [27].

The production of biogas thus allows for the recovery of energy from wastewater, while reducing the energy costs, sludge production and footprint. To fully recover the energy as electrical power however, the biogas requires several post-treatment steps: upgrading the biogas to methane requires removal of CO_2 [25] and H_2S [28]. Removal of H_2S is essential as it is a toxic gas, but also would result in the formation of SO_2 during combustion of the biogas. SO_2 leads to the formation of sulfuric acid, which causes corrosion in combustion engines [28], and acid rain. Acid rain globally destroyed forests and ecosystems, leading to extensive legislation for pollution control [2].

Nutrient removal, N and P, in anaerobic digesters is insufficient for effluent requirements to prevent eutrophication [24], though recent developments have shown biogas production, and thus treatment of organics, with simultaneous precipitation of CaP granules for P removal was possible using calcium dosing [29].

Bioelectrochemical systems

Bioelectrochemical systems (BESs) have been proposed as an alternative for anaerobic digestion. The technology, called Microbial Electrochemical Technology (MET), makes use of microorganisms that interact with electrodes. The biological electroactivity, where bacteria created an electrical current, was first discovered in 1911 by Potter [30], and further developed as a Microbial Fuel Cell (MFC) in 1931 [31] and the 1960s [32,33]. Since the 1990s, BESs have gained scientific and industrial interest for energy recovery, wastewater treatment and MFC powered sensor platforms [34].

In electrochemical systems, an anode and a cathode are connected in an electrical circuit. The anode and cathode electrolyte compartments are often separated by an ion exchange membrane. The use of electron donating microorganisms, combined with the anode, result in a bioanode, where the electrons freed in the oxidation of organics are accepted by the anode. Electron accepting microorganisms, in combination with a cathode, is called a biocathode, where the electrons are transferred from the cathode to the microorganisms [35].

The electrical current produced by bioanodes can be used to produce electrical power or drive production or separation processes. The cathodic reaction determines if power is produced or consumed (see section 1.2.). For instance, if oxygen is reduced to water at the cathode, the cell voltage becomes positive and electrical power is produced: this is called a Microbial Fuel Cell (MFC) (**Figure 1.1A**) [36]. Oxygen reduction at the cathode can also be used to produce H_2O_2 [37] alongside electrical power. Alternatively, the bioanode current can be used to produce products, for which an applied voltage is required: such a system is called a Microbial Electrolysis Cell (MEC) (**Figure 1.1B**) [38].

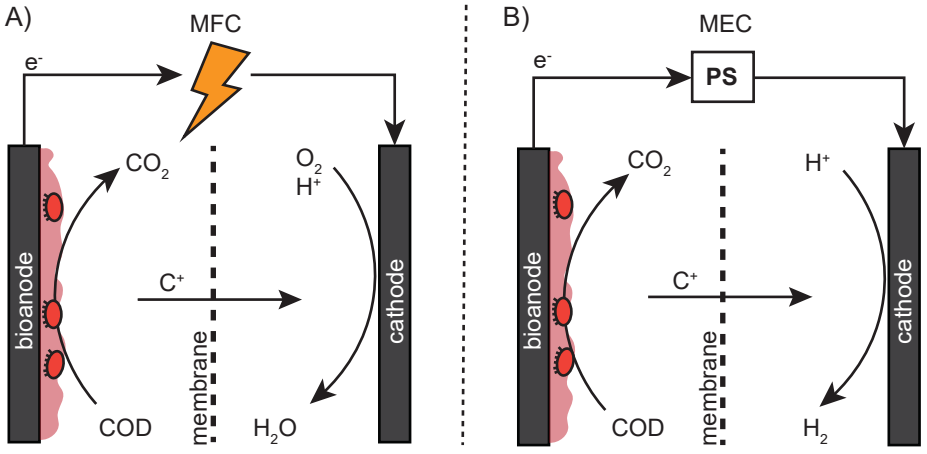

Figure 1.1. Bioanodes applied in a Microbial Fuel Cell (MFC) and a Microbial Electrolysis Cell (MEC). The MFC produces electrical power, while the MEC requires a power supply (PS). The anode and cathode compartment are separated by an ion exchange membrane (here for cations), over which ions travel to balance the charge of the electron transfer via the electrical circuit.

The hydrogen evolution reaction (HER) allows for the production of H_2 gas [38–42] and NaOH [35]. The increase in pH as a result of the HER can be used to separate NH_3 due to the shift in equilibrium with NH_4^+ [43], as well as provide a locally favorable pH for the precipitation of calcium hydroxyapatite, resulting in the recovery of phosphorous [44]. In addition, the current can be used for desalination in MFCs with multiple membrane separated electrolyte compartments [45]. A biocathode can be used to reduce CO_2 to organics, a process called bioelectrosynthesis in Microbial Electrosynthesis Systems (MESs), where microorganisms perform reduction reactions to produce various products such as methane [46–49], formate [50], acetate [51,52], butyrate [53,54] and longer chain fatty acids [53,55].

In this thesis, I focus on bioanodes, and further description of electroactive bacteria will only refer to those which oxidize dissolved organic material. The following paragraphs describe both the microbial electroactive processes and the electrochemical processes in the application of bioanodes in more detail.

1.2. Electrical current from bioanodes

Electroactive bacteria for oxidation of organics

Electroactive bacteria (EAB), also called electrogens, gain energy from the oxidation of organics [56,57]. The charge that is freed in the oxidation reaction requires a reduction reaction as the terminal electron acceptor (see next section for examples of oxidation and reduction reactions in MFCs and MECs). In bioelectrochemical systems, the interaction of EAB with the electrodes is studied. EAB can affect extracellular electron transfer (EET), which is what makes them electro-active. ***Geobacter*** and ***Shewanella*** are common species found in bioanodes, when grown in open and mixed microbial communities of real wastewater treatment. However many more species have been found to be electroactive [58,59]. EET mechanisms are categorized in A) direct contact with the anode, B) electron shuttling between EAB and the anode, and C) EAB in a conductive solid matrix [60]. **Figure 1.2** shows illustrative examples of EET.

Direct contact allows EAB to directly interact with the anode: charge is transferred via cytochrome-c proteins [56,61,62] or nanowires [63]. However, only a thin layer of EAB can have direct contact with the anode: this results in a low current density [60].

Electron shuttling involves the use redox mediators in thicker layers of EAB biofilms [60] and by planktonic EAB. The redox mediators can be secreted organic compounds, such as flavins, metal ions or metal oxides, such as MnO_2/Mn^{2+}, or other compounds, such as $2H^+/H_2$, NO_3^-/NO_2^- [35]. The mediators are reduced by the EAB and then oxidized again at the anode. If the mediator is mobile, and can store and transfer charge bidirectionally, it can be used by planktonic EAB to transfer electrons to the anode. This includes solid charge carriers, such as activated carbon which can store charge in electrical double layers (see section 1.3.) [64]. The current density is limited by diffusion of the mediators to the anode [60], or in the case of solid charge carriers limited by contact incidence with the anode. EAB themselves can also store charge [65]. The likely mechanism is the use of the cytochromes and other redox-active proteins [66]. The charge storage is essential for the planktonic EAB to function when no electron acceptor is readily available, but also useful for biofilms which can remain active even if the electrical circuit is not accepting electrons (open circuit) [67].

The highest current densities are produced using the solid conductive matrix, the final of the three EET mechanisms, which allows thicker biofilm layers to grow while maintaining electrical contact with the anode, if the biofilm conductivity is high [60]. Eventually, the current density will be limited by proton diffusion out of the biofilm [68,69]. Thus, electron transfer in a conductive matrix, as an EAB biofilm, results in higher current densities. Flat plate electrodes have reached about 10 A/m^2, but in combination with large electrode surface area per volume, biofilms of EAB produced high current densities in small lab scale reactors: up to 390 $A/m^2_{projected}$ or 22×10^3 $A/m^3_{reactor}$ [70].

Application of bioanodes in MFCs and MECs

Bioanodes produce an electrical current that can be used in MFCs and MECs to produce electric power or products like hydrogen or peroxide [71]. **Table 1.1** shows common oxidation and reduction reactions in bioanode systems. The oxidation of organics at the anode is often studied in synthetic wastewater by using volatile fatty acids as model substrates, mostly acetate [35]. The oxidation of acetate (Reaction 1) releases bicarbonate, protons, and electrons. In MFCs, the electrons are transported via the electrical circuit and used in the oxygen reduction reaction (ORR) to reduce oxygen to water or hydroxide (depending on the local pH) (Reactions 2 and 3). In MECs, the hydrogen evolution reaction (HER) takes place at the cathode (reaction 4). The reaction potential, which depends on the local concentrations of products and reactants, is expressed as a voltage compared to a reference electrode. In this thesis, the Ag/AgCl/3M KCl reference is used, which equates to +205 mV versus the standard hydrogen electrode (SHE).

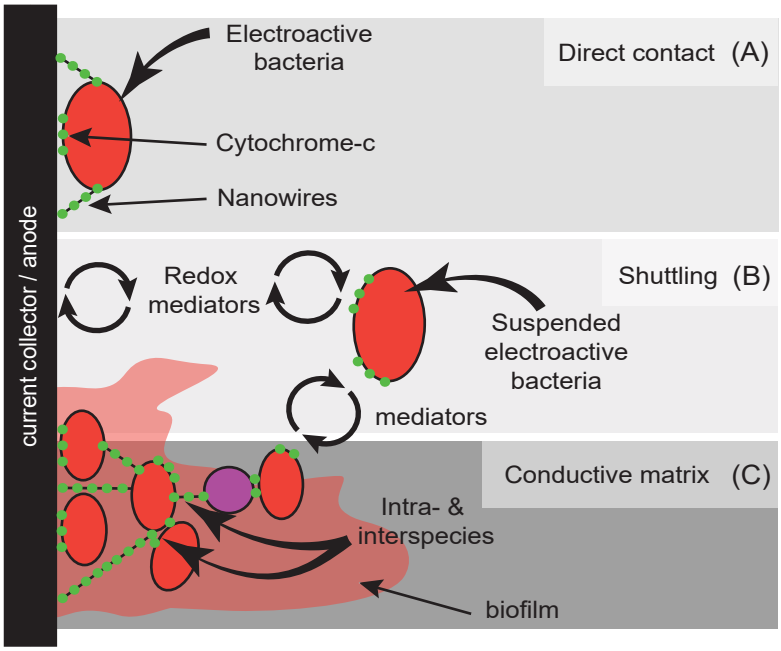

Figure 1.2. Extracellular electron transfer of mechanisms used by electroactive bacteria in bioanodes.

Table 1.1. Common electrochemical reactions in bioanode systems.

Half-cell reactions		Thermodynamic equilibrium potential (V vs Ag/AgCl)
Reaction 1	$CH_3COO^- + 4H_2O \rightarrow 2HCO_3^- + 9H^+ + 8e^-$	-0.49 [a]
Reaction 2	$O_2 + 4H^+ + 4e^- \rightarrow 2H_2O$	+0.59 [b]
Reaction 3	$O_2 + 2H_2O + 4e^- \rightarrow 4OH^-$	+0.31 [c]
Reaction 4	$2H_2O + 2e^- \rightarrow H_2 + 2OH^-$	-0.91 [d]

a) 28° C, pH 7, 20 mM acetate, 80 mM HCO_3^-
b) 28° C, pH 7, pO_2 0.21 atm (saturated)
c) 28° C, pH 12, pO_2 0.21 atm (saturated)
d) 28° C, pH 12, pH_2 1 atm

Electrons are used at the cathode in a reduction reaction, after travelling through the electrical circuit. Charge neutrality is maintained by ion transport through the electrolyte between the two electrodes. An ion exchange membrane, between the anode and cathode compartments, allows for product purity and reduced cross-over of oxygen, which reduces the efficiency of the oxidation, or hydrogen, which can be consumed by the bacteria, to the anode, as well as reduced transport of organics to the cathode [72,73].

The resulting cell voltage is positive for MFCs, producing electrical power: for instance, reactions 1 and 3 result in a theoretical cell voltage of +0.8 V. A MEC requires an applied voltage: reactions 1 and 4 result in a theoretical voltage requirement of -0.42 V.

A major benefit of MFCs is the type of energy recovered. MFCs can produce electrical power directly, and with a theoretical conversion of organics to electrical current of almost 100% (minus biological yield), resulting in 50% total conversion efficiency at maximum power, due to resistance losses [74]. Using the theoretical energy from oxidation of COD [9], the 50% conversion efficiency of MFCs leads to 1.9 kWh/kgCOD. In comparison, for AD on average 26% of energy is recovered as electrical power [25,28]. Laboratory MECs consumed 0.6 kWh/kgCOD, though the energy requirements should be compared to water electrolysis cells. MECs require on average 3 times less theoretical energy input than conventional water electrolysis: reactions 1 and 4 result in -0.42 V, and reactions 3 and 4 in -1.22 V.

This cell voltage is reduced (MFCs), or increased (MECs), due to voltage losses resulting from: A) a pH gradient, B) membrane transport resistance, C) ionic resistance, and D) potential losses at the anode and cathode resulting from for instance electrode material resistance, biofilm conductivity, and diffusion gradients into and out of the biofilm [69].

The pH gradient builds up when an ion exchange membrane is used. In the anode compartment, the oxidation reaction produces protons, decreasing the pH. Because this acidifies the bioanode, the bioanode activity is reduced [68,69]. In the cathode compartment, the ORR and HER result in an increased pH, due to the consumption of protons (reactions 2 and 4) or the production of hydroxide (reaction 3). As a result, a pH difference is created between the anode and cathode compartments, which results in a voltage loss. For instance, a difference between pH 7 and pH 12 results in 0.3 V loss: 59 mV per pH unit [41,75]. Aside from a pH gradient, the ion exchange membrane is a barrier in the current-driven migration and the diffusion of ions. The resulting membrane potential is a loss for the voltage produced or applied [75].

The ionic resistance is an effect of the concentration of ions in the electrolyte. Municipal wastewater streams have conductivities in the order of 1 mS/cm [76]. Over a cell width of 1 cm, and an exposed membrane area of 100 cm^2, the resistance of the solution is 10 Ohm. With a current density of 10 A/m^2, the ionic voltage loss is 1 V.

If we include the losses due to the pH gradient and ionic conductivity, as described above, the losses combine to 1.3 V. For a MEC, this results in about 1.7 V applied, while water electrolysis in the same setup would require 2.5 V. For an optimized electrolysis cell, the cell voltage would be about 1.8 V, though at higher hydrogen production rates [7,77]. However, a MFC cannot produce power due to these losses, as the net voltage would be negative. In stacked MFCs, where multiple cells are electrically connected in series, this causes voltage reversal due to overdrawing the electrical current [78]. At maximum power density, the resistance limits the current density [74]: if the maximum power is at 50%, then the voltage losses can be (reactions 1 and 3) at most 0.4 V. If the pH gradient is the same as in the example above, as well as the wastewater conductivity, the ionic voltage loss is limited to 0.1 V, which means the current density is limited to 1 A/m^2, and the volumetric power density is 40 $W/m^3_{reactor}$.

Challenges for BESs in wastewater treatment

Wastewater contains both solid and dissolved organics, and conditions such as the pH and concentrations of organics and nutrients, can vary widely [2]. Wastewater can thus pose challenges for the application of BESs in the treatment facilities. In this thesis, I focus on bioavailable wastewater conditions in which bioanodes operated, using synthetic wastewater, which reduces limitations for the current generated by bioanodes.

The low concentration of ions in wastewater, especially in municipal wastewater, results in low ionic conductivity. This results in increased resistance in MFCs, which increases the voltage loss over the cell and limits the current density. As the ionic resistance is directly proportional to the width of the cell, a thin electrochemical cell is desired [79,80], since increasing the conductivity of the wastewater is not a practical option.

As described in the previous paragraph, a thin electrochemical cell is desired to reduce voltage losses. Suspended solids in wastewater streams form a challenge with thin spaces [79]. The anode and cathode compartments are often filled with porous structures, such as carbon felt [73,81–83] or granules [84–88], to enhance the available surface area per volume, for biofilm attachment and reaction surface for hydrogen evolution, resulting in high current densities [80,89]. The filled compartments provide challenges for wastewater with suspended solids [90,91]. To reduce the chance of clogging, the compartments of bioanodes are often wider, resulting in increased ohmic losses from ionic resistance losses. This results in higher operational costs of MECs due to the increased voltage requirements and decreases the electrical power produced by MFCs, thereby reducing the feasibility of bioanodes for wastewater treatment [71]. In addition to clogging by suspended solids, the growth and ageing of the biofilm lead to accumulation of biomass, which in turn leads to increased diffusion losses over the thickness of the membrane and to passivation of the electrode, as the thicker biofilm is not necessarily as conductive as a new biofilm. Though the accumulated biofilm can be washed out using periodically higher pumping rates, increasing the energy costs of the system, biofilms are known to adapt to the created shear stress, increasing the pumping requirements for washout even more [92].

Methanogenic archaea, or methanogens, which are the main driving force behind AD, prosper in similar conditions as those optimal for electrogens, for instance: temperature, pH, substrate concentrations. The methanogens thus compete with electrogens for substrate and space. The electrogens are at a disadvantage in MFCs due to their dependency on an electrical conductive surface, whereas methanogens can grow in suspension, on any type of surface, as well as form granular sludge, which is retained well in reactors (depending on the conditions) [74]. Due to this competition, larger scale bioanodes often produce biogas as well, thereby reducing the coulombic efficiency (charge recovered as electrical current/charge in consumed substrate) [93].

Recent studies have determined the competitive advantage of electrogens can be shifted in their favor by using substrate concentration or loading rates, together with control over the thermodynamic conditions by use of the anode potential [74,94]. By designing the reactor so that the available anode area per volume (m^2/m^3) matches to the activity and substrate loading rate, the electrogens can win the competition over methanogens if the anode potential is higher than -0.4 V vs Ag/AgCl. Increasing the anode potential, however, decreases the cell voltage for MFCs, thereby reducing the voltage efficiency and total efficiency of the MFC [74]. For substrate loading rates in the order of 1 $kgCOD/m^3.d$, electrogens outcompete methanogens in MFCs [74], which would mean 35 W/m^3 in the example system (1.2.). This is lower than AD, which can treat loading rates of 5 – 25 $kgCOD/m^3.d$ to produce 400 W/m^3 of power [26], at a voltage efficiency of 40% [22]. Increasing the area to volume ratio in MFC, accomplished by three-dimensional electrodes such as granular bed electrodes [95], would increase the activity and potentially allow for higher organic loading rates than 1 $kgCOD/m^3.d$.

The challenges mentioned here all contribute to decreasing the current density of bioanodes. Deeke and colleagues analyzed the power densities of MFCs between 2002 and 2012. The improvements of recent developments have too small increments [96] to reach the desired 400 W/m^3 with which MFCs can compete with AD [26]. Though the benefits of bioanodes can be found in a wider range than AD processes, where the current can be used to drive the formation of valuable products and separation processes, the low current densities associated with low power densities remain a challenge for application of bioanodes. To compete with high performance AD reactors, the goal is treating 5 – 25 $kgCOD/m^3_{reactor}.d$ [26]. This translates to 700 – 3500 $A/m^3_{reactor}$ in terms of volumetric current density [34], however the 1 $kgCOD/m^3.d$ for outcompeting methanogens [74] would imply 140 $A/m^3_{reactor}$. Higher OLR can be treated if the surface area per volume (m^2/m^3) is higher, resulting in high removal rates for the low substrate concentration in the reactor.

Though mL-scale setups have shown current densities surpassing to the highest target (391 $A/m^2_{projected}$ or 22×10^3 $A/m^3_{reactor}$ with a high surface area anode of 56 $m^2_{geometric}/m^3$) [70], larger scale studies have yet to reach such current densities (0.14 $A/m^3_{reactor}$ for a 10 L setup [97] to 30 $A/m^3_{reactor}$ in a 20 L setup [98] and 1.7 $A/m^3_{reactor}$ in a 250 L MFC [99]). Improving the current density is thus important for the application of bioanodes in the consideration for replacing aerobic sludge and anaerobic digestion processes. High current densities are reached at high anode potentials [70]. Thus, unless the resistance is very low, the anode control requires an applied voltage and a MEC system is required.

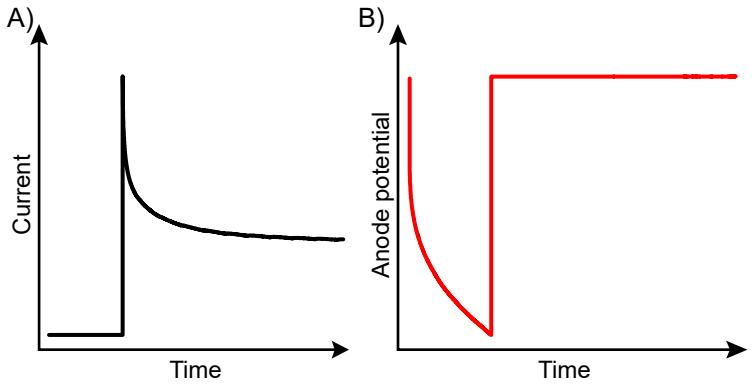

Figure 1.3. A single charging and discharging cycle of a fixed capacitive bioanode. Adapted from [87].

Table 1.2. Activated carbon electrode materials for supercapacitive charge storage, with capacitance (C).

Material	Density (g/cm^3)	Pore area (m^2/g)	Predicted C [83] F/cm^3)	Electrolyte	Measured C (F/cm^3)	References
Felt	0.1	1150[a]	16	High	23	Super-capacitor [83]
Cloth	0.2	1300 [109][a]	31	High	30	Super-capacitor [103]
GAC granules	0.5	885[b]	44	Low	22	Capacitive bioanode [87,88]
PK granules	0.3	764[b]	23	Low	13	Capacitive bioanode [87,88]
HR granules	0.5	1100[b]	54	Low	36	Capacitive anode [107], Chapter 5
				High	50	

a) BET analysis of N_2 adsorption spectrometry.
b) NLDFT analysis of N_2 adsorption spectrometry

1.3. Capacitive bioanodes for intermittent charge storage

In this thesis, I have studied capacitive bioanodes with the aim to increase the current density by using charge storage of capacitive electrodes. A capacitive discharge current is released from the stored charge. The capacitive current is released on top of the current produced directly by the bioanode [100], thus increasing the current density. The best performing non-capacitive granular bed bioanode produced 1063 $A/m^3_{reactor}$ [95]. The first capacitive bioanode used an external capacitor [101], and Deeke and colleagues developed an integrated capacitive bioanode using a graphite plate coated with activated carbon. The capacitive bioanode produced 1.2 A/m^2 or 81 $A/m^3_{reactor}$ [67,85]. Though the experiments comparing non-capacitive and capacitive bioanodes show the benefits of intermittent use of charge storage, application of capacitive bioanodes has not resulted in high current densities.

In the following paragraphs, I explain the process of intermittent charge storage and which challenges we envision capacitive bioanodes to solve.

Capacitive bioanodes

Capacitive electrodes allow for charge storage by electro-sorption of ions from the solution. In combination with a bioanode, the capacitive bioanode can be charged by the EAB via oxidation of organics. In BESs, the capacitance is charged in open circuit (the circuit is not accepting electrons), if other electron acceptors, such as dissolved oxygen, are absent: the capacitance functions as the electron acceptor (until the charge storage is full). During discharging the capacitive bioanode, the capacitive current is added to the faradaic current from the oxidation by the EAB. When fully discharged, only the faradaic current is produced. Though capacitive bioanodes are best constructed using capacitive electrode materials (see next section), the charge storage mechanism of EAB adds to the capacitance [65,66].

Figure 1.3 shows the current (A) and potential (B) profiles of intermittent charging and discharging. The charge is stored during charging, in open circuit (a current of 0 mA), which decreases potential of the granule towards the thermodynamic equilibrium potential: -0.49 V for acetate oxidation by a bioanode (**Table 1.1**). The stored charge is harvested during discharging, by applying a higher potential than the potential of the charged capacitance (**Figure 1.3**). During discharging, the current of capacitive bioanodes consists of two components: the faradaic current produced by the bioanode, which is dependent on the poised potential of the current collector, and the capacitive current which is dependent on the potential difference between the poised potential and the charged potential (see also **Figure 1.4B**). The capacitive current results in a peak current which decreases towards the level of the faradaic current. As the charge is discharged, the potential of the capacitance increases and thereby decreases the potential difference and thus the capacitive current [85].

Fixed capacitive bioanodes, as opposed to fluidized (see next section), require intermittency of the current in cycles of charging and discharging. They employ similar cell designs as conventional, non-capacitive, bioanode systems [85]. They are therefore prone to the same clogging challenges. Though the current density can be increased significantly, it is still limited by the periods of open circuit changing.

When using intermittent charging and discharging, capacitive bioanodes were shown to produce more charge over the total time, than a non-capacitive bioanode produced in continuous operation [85].

The intermittent operation was also found to affect the structure of the biofilm when studied on a non-capacitive flat electrode: a more open structure was formed with "mushroom-like" extrusions. The authors hypothesized that the extrusions allow for the higher charge recovery due to increased surface area per volume of biofilm [102], as diffusion, of substrate and reaction products (bicarbonate, protons), over the thickness of the biofilm limited the activity of the EAB less [69]. Thus, the use of charge storage was shown to be beneficial for the activity of the EAB, as well as produce a high current during discharging.

Capacitive electrodes can be made from porous activated carbon. Various activated carbon structures have been studied for use in supercapacitive electrochemical systems, among which felt [83], cloth [103], and particles. The particles can be used as powder, for a coating on a solid electrode (with a binder) [85,86] or as granules [87,88], in a granular bed. In general, a distinction can be made between fixed and fluidized capacitive bioanodes. For the fixed capacitive bioanodes, activated carbon felt, cloth, veil, and a packed bed of granules have been used. Fluidized capacitive bioanodes (see next section) have thus far only used activated carbon granules [87,88,96,104–108]. **Table 1.2** shows material properties of some activated carbon materials commonly used in BESs.

This thesis concerns the use of activated carbon granules. A granular bed results in a high-density electrode structure compared to other activated carbon materials (see the bulk density in **Table 1.2**), while maintaining an open interparticle structure, also called void space (1 – bulk density), for electrolyte access. The EAB can grow on the external surface of the granules: if assumed the granules are spherical, the surface area to volume ratio is

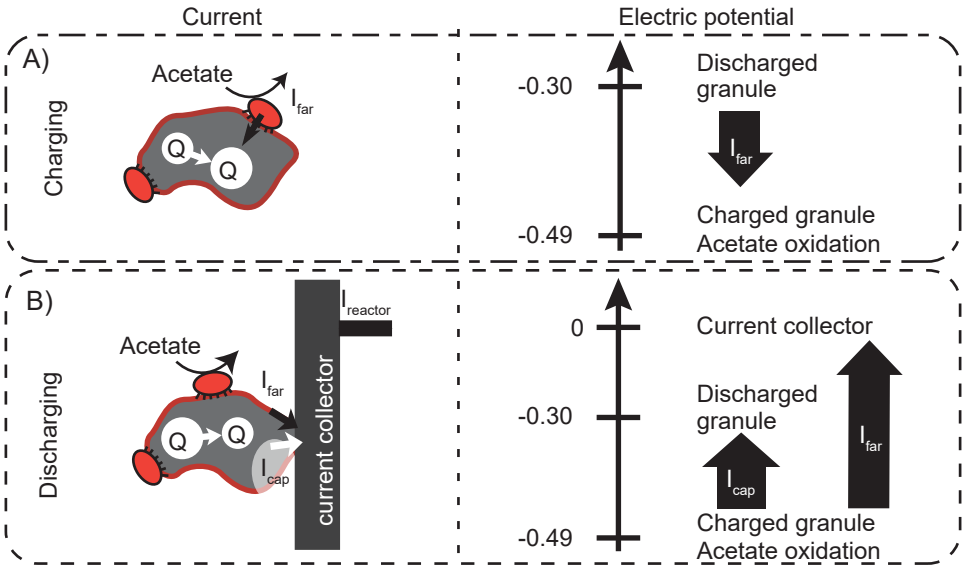

Figure 1.4. Charging and discharging of capacitive bioanode granules. Electric potentials are shown versus Ag/AgCl/3M KCl reference. Reproduced from [116], published by Elsevier Ltd., CC BY 4.0 (http://creativecommons.org/licenses/by/4.0/).

Table 1.3. Challenges for bioanodes and the effect of implementation fluidized bed reactors.

	Bioanode challenges	Effect of fluidized bed reactors
A	Low conductivity wastewater	Local higher conductivity due to discharging
B	High clogging risk due to narrow openings and accumulation of biomass	Low clogging risk due to fluidization and removal of biomass through shear stress and washout
C	Low loading rate required for selective pressure for electrogens	High surface area per reactor volume for selective pressure for electrogens
D	Low current densities	Combined faradaic and capacitive discharge

6/diameter and thus smaller granules have a higher area for growth [88]. The downside of smaller granules is a reduced interparticle space in the granular bed which can limit access of substrate to the biofilm (activity of the EAB) and of ions to the membrane (voltage losses). For structures like felt and cloth, the void space is much greater, but surface area per volume may be lower (depending on the diameter of the granules in comparison).

The amount of charge stored in the porosity of activated carbon is proportional to the surface area: the electrical double layer (EDL) capacitance can be estimated as 10% of the BET area [83]. Activated carbon has an internal surface area in the order of 1000 m^2/g, which would result in a capacitance of 100 F/g.

Intermittent charging and discharging in fluidized bed bioanodes

Fluidized bed electrodes use fluidization of particles to create a three-dimensional electrode. The fluidization results in a convective contact between particles and current collector. The fluidized nature allows for improved diffusion of substrate and reaction products [96,106,110]. Fluidized bed reactors were originally studied for copper plating on non-capacitive spheres, but the voltage losses were too great for the improved diffusion rates [111] to be beneficial for the electroplating process [112,113]. Bioanodes have been developed using activated carbon granules as charge carriers, which were fluidized via mechanical stirring [104], or liquid [105,114,115] or gas flow [96]. Intermittent contact with the anode discharges the stored charge, which was stored via oxidation of organics by EAB on the surface of the granules. **Figure 1.4** shows the faradaic current (I_{far}) and capacitive current (I_{cap}), as well as the electrical potential, during charging and discharging of granules. Though the granules are in intermittent contact, and thus charged when not in contact, a continuous current ($I_{reactor}$) is produced by the granules discharging to the current collector.

Fluidized bioanodes to resolve challenges for implementation of bioanodes

The main challenges for bioanodes (section 1.2.) are A) low conductivity, B) clogging, C) methanogen competition, and D) low current densities. Fluidized bioanodes could potentially resolve these challenges and have the potential to reduce material costs per volume of reactor. **Table 1.3** gives an overview of the challenges bioanode reactors face when traditional cell designs are used (section 1.2.) and the effect of implementing capacitive bioanodes in fluidized bed reactors are envisioned to have.

When discharging the stored charge in the discharge cell, cations – originally adsorbed during charging – are released during discharging, which is expected to increase the local ionic conductivity [96]. Additionally, the released cations are likely to be mainly Na^+ and K^+, as they make up the majority of cations in wastewater [75]: the pH is unlikely to vary greatly as a result of the anodic current, unlike the acidification as a result of high current density in fixed bioanode systems [69]. Discharge of high volumetric capacitance would result in large amounts of cations released, thus increasing the local conductivity significantly [97].

A fluidized bed is constantly moving. As a result, suspended solids, in real wastewater, can flow with the electrolyte through the reactor without causing clogging. Undigested suspended solids can be washed out due to differences in specific density, as well as size differences with the granules. Preferably, the fluidization of the granular bed will induce some shear stress in order to control the biofilm on the surface of the granules, and thus prevent diffusion limitations observed in thicker biofilms [69]. The detached biomass will be washed out with the other suspended solids.

As for the competition between electrogens and methanogens, sufficient discharging would result in a gradient of electric potential: the capacitive bioanode granules would have a high potential after discharging, which becomes lower during charging [85]. The large surface area per reactor volume, due to the large granular bed volume, would translate the potential gradient into an electroactive activity gradient. The result would be low substrate concentrations when the potential gradient is matched to a substrate gradient via the local organic loading rate. The substrate consumption can also be spread over a larger volume, thereby reducing the pH stress on the biofilm, and ensuring low substrate concentrations, even at high organic loading rates.

With thin biofilms (shear stress), high $m^2_{bioanode}/m^3_{reactor}$, low substrate concentrations, and washout of slow growing microorganisms (due to low substrate concentrations, see section 1.2.), the electrogens are envisioned to win the competition from methanogens [74].

Capacitive bioanodes produce a discharge current, which is a combination of the faradaic current and capacitive current. In a fluidized bed, the charge is stored during charging, by oxidation of organics, and continuously harvested in the electrochemical discharge cell, producing a continuous discharge current. By using the charge storage capacity to separate the charging from the electrical current production in the discharge cell, the membrane and current collectors can be smaller than the total volume of the reactor [96], making scaling up more feasible. A high discharge current would allow for a small electrochemical cell, compared to the total reactor volume.

Reactors using fluidized granules, before 2015, produced between 0.4 $A/m^3_{reactor}$ (1L reactor) [115] and 260 $A/m^3_{reactor}$ (7 mL reactor) [104] in large and small scale setups [104,105,114,115]. These current densities are insufficient for competition with large scale AD (section 1.2.). As such, the promise of high current densities by using capacitive bioanode granules has not yet been realized.

The benefits of applying capacitive bioanodes in fluidized bed reactors require a high discharge current, before any optimization steps for the charging can be made. This thesis therefore focusses on investigating granular capacitive bioanodes to produce an electrical current.

1.4. Thesis aims and outline

In this thesis, the main goal was the development of a fluidized bed reactor which produces a high current density from the conversion of organic substrate by electroactive bacteria, by using intermittent contact of capacitive bioanode granules with the discharge anode. After identifying the possible current density from discharging capacitive granules, a concept reactor was developed. The reactor design was further studied to understand the discharge processes to identify future improvement strategies.

In **Chapter 2**, bioanode granules were studied to determine the performance of different types of single carbon granules in terms of current density during intermittent charging and discharging as well as continuous operation. This understanding was used to compare to granular bed bioanodes in both capacitive and non-capacitive reactors. With this comparison, the potential for improvement was identified.

In **Chapter 3**, the moving granular bed reactor is presented. The aim was to build a reactor in which the contact time for discharging was improved. The reactor performance was studied in terms of reactor current density, activity of the granules outside of the reactor and SEM imaging to understand the development of the biofilm on the granules. The results were compared to previous bioanodes.

In **Chapter 4**, the goal was to determine how to best use capacitive current: to see whether a moving granular capacitive bioanode improved the current density as compared to a fixed bed of capacitive bioanode granules, in a similar discharge cell setup. The discharge cell configuration was further studied as well.

In **Chapter 5**, the discharge characteristics of the moving granular bed were studied in abiotic conditions. The aim was to determine the effect of process parameters on the discharging of the charged granules: the potential difference with the current collector, the effect of electrical and ionic resistance, and the effect of the flowrate of the moving bed through the discharge cell, were studied.

In the **Chapter 6**, I discuss the results of the experiments and identify various topics for further study and improvement, to increase the current density from the moving bed reactor. Then I discuss the future for capacitive bioanodes and the moving granular bed electrode.

Criel-sur-Mer, France

Chapter 2

Performance of single carbon granules as perspective for larger scale capacitive bioanodes

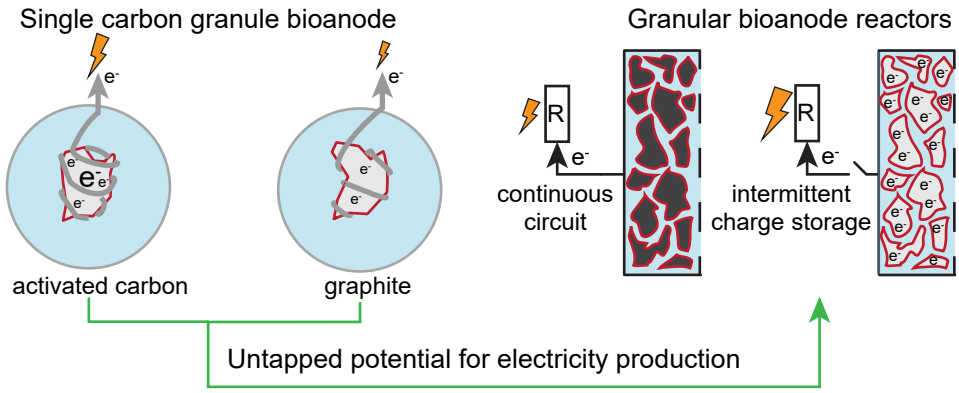

This chapter has been published as:

C. Borsje, D. Liu, T.H.J.A. Sleutels, C.J.N. Buisman, A. ter Heijne, Performance of single carbon granules as perspective for larger scale capacitive bioanodes, J. Power Sources. 325 (2016) 690–696. doi:10.1016/j.jpowsour.2016.06.092.

Abstract

The use of high surface area electrodes, like carbon-based felt or granules, in Bioelectrochemical Systems is crucial for high volumetric current production. In case activated carbon granules are used, charge can also be stored in the form of an electric double layer in the pores, which has been shown to improve bioanode performance. So far, it is not known how much current can be generated by a single granule. In this study, we investigate the current production and charge storage behavior of a single carbon granule. Two types of activated carbon granules and one graphite granule are tested to find the untapped potential of granular bioanodes. A single activated carbon granule produces up to 0.6 mA, corresponding to 60 mA/cm^3 granule volume at -300 mV vs. Ag/AgCl anode potential. Charge – discharge experiments show that capacitive granules produced 1.3-2.0 times more charge compared to a graphite granule with low surface area. When extrapolated to other granular systems, our study indicates that the current generated by granular bioanodes can be improved with several orders of magnitude, which could form the basis of an economically feasible Microbial Fuel Cell.

2.1. Introduction

The increasing global need for renewable resources is undeniable. In addition to sun and wind energy, soluble organic components in wastewater are a renewable resource. Electroactive microorganisms form the basis of bioelectrochemical systems (BESs), which are a promising technology for the conversion of wastewater into other energy carriers. Electroactive microorganisms catalyze the oxidation of soluble organic components under anaerobic conditions. When they use the anode as electron acceptor, the microorganisms form a biofilm, and the anode becomes a bioanode [117]. The application of a bioanode

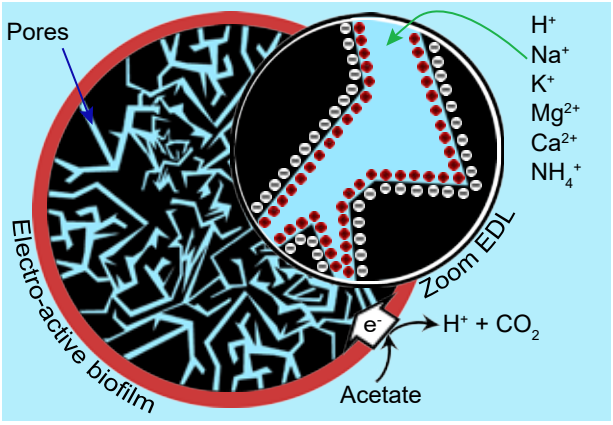

Figure 2.1. The principle of capacitive granules with an electrochemically active biofilm. A faradaic reaction occurs when the biofilm oxidizes acetate and electrons are transferred to the activated carbon granule. This electron transfer, together with cation transport, leads to the formation of an electric double layer inside the pores so that charge is stored: a capacitive process.

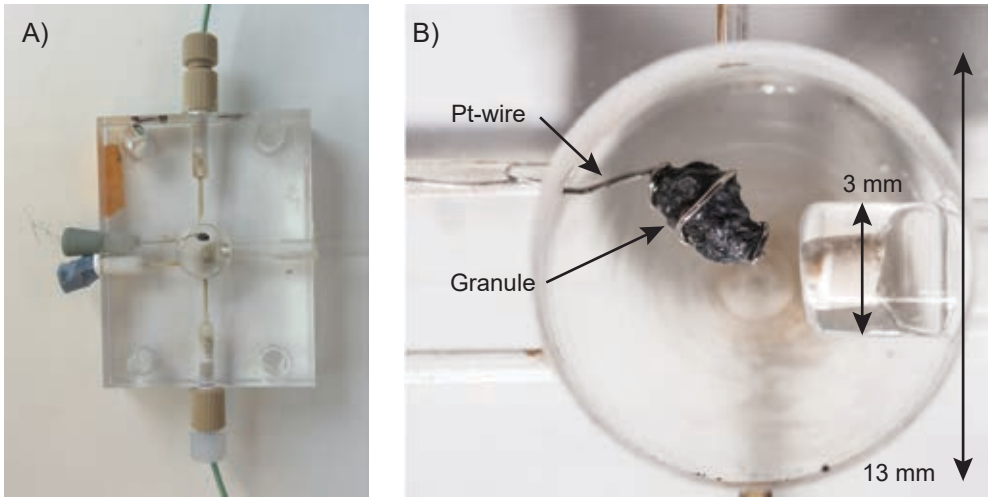

Figure 2.2. A) The anode half-cell contains B) the anode compartment (volume of 1 mL and diameter of 13 mm) with capillary for reference electrode and graphite granule held by a Pt wire.

is found in two types of BESs. The first generates electrical power over an electrical load: a microbial fuel cell (MFC); the second utilizes power in addition to the oxidation of organics, to form products at the cathode, such as H_2, H_2O_2 and NaOH: a microbial electrolysis cell (MEC) [35]. Both systems simultaneously remove the organics from wastewater and produce a useful resource.

Conversion rates and energy recovery in bioanodes are still low when compared to biogas production through anaerobic digestion, even when taking into account significant losses for electricity production from biogas [26,34]. A strategy to enhance the conversion rate at the bioanode is the use of three-dimensional electrodes to provide more surface area for microbial growth per volume of reactor. These electrodes are often made of graphite felt [73,81,82], graphite granules or activated carbon granules [84–86]. An additional property of activated carbon granules is their high specific surface area (SSA), which is the surface area created by the porous structure of the carbon granules. An electric double layer (EDL) can form on this pore surface area in presence of an electrolyte [118]. In this EDL, electricity can be stored, acting as a capacitor, where high SSA generally relates to more charge storage: a property widely used in supercapacitor technologies [119]. Using activated carbon as a bioanode (**Figure 2.1**) allows two processes to occur: (i) the electro-active biofilm releases electrons during the oxidation of organics (faradaic process), and (ii) these electrons are stored at the pore surface in the carbon, while cations are required to maintain the charge balance in the EDL (capacitive process) [120]. Following this concept, activated carbon granules have previously been integrated with the bioanode to form a capacitive bioanode, for in-situ charge storage [104], as well as in a fluidized bed reactor, where the granules are charged and discharged in separate locations [96].

While granular electrodes, both with high surface area (activated carbon granules) and with low surface area (graphite granules), have been applied as bioanodes, it is unknown how much current can actually be produced by one single granule. For this purpose, an MFC was developed to study one single granule. We investigated three types of granules: two types of activated carbon granules with high SSA, and one graphite granule with low SSA. We analyzed the current produced during continuous operation and the performance during intermittent charge and discharge cycles in terms of charge recovery.

2.2. Experimental

Setup of the single granule MFC

The single granule MFC was made of two Plexiglas plates, with a cylindrical chamber (13 mm diameter, 1 mL volume) drilled in each plate for an anode and cathode compartment (**Figure 2.2**). The anode chamber contained the granule, held in place by a Pt wire (300 µm diameter, 17.9 g c/m^3), and a capillary for the reference electrode (3M KCl Ag/AgCl, QM710X, ProSense Qis, Oosterhout, The Netherlands), see **Figure 2.2B**. During assembly, multiple points of contact between wire and granule were ensured and, using a multimeter, the contact resistance was checked between wire and a point on the granule. We ensured the contact resistance was below 5 Ω. A cation exchange membrane (fumasep FKB, FuMa-Tech GmbH, St. Ingbert, Germany) separated the anode and cathode chambers. The cathode consisted of a piece of platinum foil connected to a stainless-steel rod (Austenitic Corrosion Resisting Steel, Material No. 1.4539, ThyssenKrupp Materials International GmbH, Essen, Germany) as the current collector. An overview of the experimental set-up can be found in the supporting information (SI) S1.

Three types of granules were used as anode: two activated carbon granules and one graphite granule. As a control, the Pt wire alone, without granule, was tested throughout the experiment. The activated carbon granules, with high SSA, were GAC830W, hereafter denoted as GAC, and PK1-3, hereafter denoted as PK, both from Cabot Norit Nederland B.V., Amersfoort, The Netherlands. The graphite granule, with low SSA, hereafter denoted as GG, was obtained from enViro-cell Umwelttechnik GmbH, Oberursel, Germany.

Though the current is a surface related process, it is singularly difficult to determine the surface area of a granule as used by the biofilm. As such, it was decided to use the volume as a normalization parameter, because of its usefulness for translating results to reactor performance. Through sieving, granules between 1 and 2 mm (stainless steel Analysensieb, Retsch, Haan, Germany) were obtained. The granules were further visually selected based on their comparable shape. As initial observations of mass and size indicated differences in

Table 2.1. Physical properties of the granules

Granule	Mass (mg)	Density (g/cm^3)	Volume (mm^3)
GAC	6.6±0.1	1.06±0.003	6.2±0.1
PK	10.2±0.1	1.03±0.004	9.9±0.1
GG	15.4±0.1	2.13±0.007	7.2±0.1

density, the granule envelope volume was determined from the weight and envelope density. The envelop volume includes the solid carbon skeletal structure and the volume of the pores of the granule and excludes the inter-granule volume of a granular bed [121]. The envelope volume, density (detailed information for its analysis in S2) of the granules and dry weight (dried for 24h at 105° C) of each granule is shown in Table 2.1.

Inoculum, media and operational strategy

The inoculum originated from a bioanode running on acetate. To obtain an active biofilm, the granules were first operated as a bioanode in a larger cell, completely filled with GAC granules, using a resistor of 1kΩ and a 50 mM PBS buffer (pH 7) and a cathode open to air. After 2 weeks, one granule was transferred to the single granule MFC (GAC 17 days, PK and GG 21 days after inoculation).

The anode medium contained 10mM $NaCH_3COO$, 0.2 g/L NH_4Cl, 10 mL/L Wolfe's Vitamin solution [122], 10 mL/L Wolfe's mineral solution [17] with 10.0 mg/L of Na_2SeO_3, $NiCl_2.6H_2O$ and $Na_2WO_4.2H_2O$ in 50 mM PBS buffer at pH 7 (5.43 g/L $Na_2HPO_4.2H_2O$, 2.65 g/L KH_2PO_4, 0.13 g/L KCl). The catholyte was a 100 mM K_3FeCN_6 solution in 50 mM PBS buffer at pH 7. Temperature of the anolyte recirculation vessel was controlled at 35°C in a water bath. Anaerobic conditions of the anolyte were created by continuous flushing with N_2. The electrolytes were replaced before the start of the electrochemical experiments (GAC 90 days, PK and GG 77 days after inoculation). The recirculation flow rate of anolyte and catholyte was between 0.5 (external resistance) and 2 (anode potential controlled) mL/min.

During the growth phase in the singe granule MFC an external resistance of 1 MΩ was used, which was later decreased to 100 kΩ and 10 kΩ. This high resistance was chosen as not to draw too high currents from the small bioanode and thus damage the biofilm in its growth phase [123]. When the cell voltage stabilized at 10 kΩ, the electrochemical measurements were performed. The Pt wire control was connected via a 2 MΩ resistor to the cathode, during the entire experimental period. We used a higher resistance for the Pt wire than for the granule, because a lower current was expected from the Pt wire alone, because of its low surface area compared to the granules.

The anode potential and cell voltage over the external resistance were measured for each MFC throughout the experimental period and recorded every 60 seconds with LabVIEW and Fieldpoint modules (National Instruments Netherlands BV, Woerden, The Netherlands), except during electrochemical measurements.

Electrochemical experiments

All electrochemical measurements were performed using a potentiostat (Ivium n-Stat with IviumSoft v2.462 (Ivium Technologies BV, Eindhoven, The Netherlands), with the anode as working electrode. All potential values are reported versus Ag/AgCl reference (+205 mV vs. NHE). The measurements were recorded every 0.1 second.

Polarization curves

Polarization curves for granules with biofilm were recorded at anode potentials of -400, -300 and -200 mV for at least 600 seconds, up to 2 hours for GAC and PK because of their higher capacitance, until the current was stable. The average current during the last 60 seconds of each potential was used for the polarization curve.

Constant potential charge and discharge

To determine the charge recovery of the high SSA granules compared to the low SSA granule, charge – discharge experiments were performed on the bioanodes. A single cycle consisted of 60 seconds Open Circuit (OC), followed by a discharge period of 180 seconds at a fixed anode potential. To ensure that each particle was equally discharged before the experiment at -300 mV, in line with previous work [85,86,96], the granules were discharged for 1 hour before each charge – discharge experiment, from which the continuous current for each granule was taken as the average of the last 60 seconds. The stored charge can be determined by subtracting the total continuously produced charge from the total charge measured during discharge (total surface area of the current-time graph) [85]. The relative charge recovery η was calculated (equation 1) over 40 sequential cycles. The relative charge recovery is used to compare the total accumulated volumetric charge (current integrated over total cycle time) of the intermittently operated active carbon bioanodes (PK and GAC) to the volumetric charge accumulated during continuous operation of the GG bioanode, which was considered as a non-capacitive granule because of its low SSA, in the same amount of time [86]: $\eta = Q_{intermittent}/Q_{GG,\ continuous}$ (equation 1).

Porosity characterization

To characterize the porous structure of the carbon granules, N2 adsorption (77K) was measured using Micromeritics Tristar 3000. SSA and pore size distribution (PSD) in the micropore (<2 nm) and mesopore (2-50 nm) range were analyzed using the Carbon-N_2 2D-NLDFT model [124] (Non Local Density Functional Theory). More details on the analysis can be found in SI S3.

2.3. Results and discussion

Current production of a single granule bioanode

After the growth phase, each granule reached a stable current. **Figure 2.3A** shows the currents achieved during polarization curves. The current density per volume of granule at an anode potential of -300 mV, which is the potential used in charge-discharge experiments, was 25 mA/cm^3 (0.16 mA) for GAC, 60 mA/cm^3 (0.59 mA) for PK and 33 mA/cm^3 for GG (0.23 mA). The control experiment with only the Pt wire did not produce more than 0.154 mA/cm^3 wire volume (0.32 μA at E_{an} = -313 mV) throughout the experiment, indicating that the current produced by the Pt wire as bioanode was negligible compared to the current produced by the bioanode granules. After opening the cell at the end of the experiments, a biofilm was observed during visual inspection (**Figure 2.3B**).

Charge recovery of the capacitive bioanodes was higher than that of the graphite granule bioanode.

The relative charge recovery (η) describes the efficiency of the charge transfer of a capacitive system, during charge and discharge cycles, as compared to a non-capacitive system in continuous operation. Previous work by Deeke et al. showed that charging and discharging of a capacitive anode resulted in an η of 1.0 to 1.3 compared to a graphite anode in a flat plate MFC [86], showing the enhanced current production for a capacitive MFC.

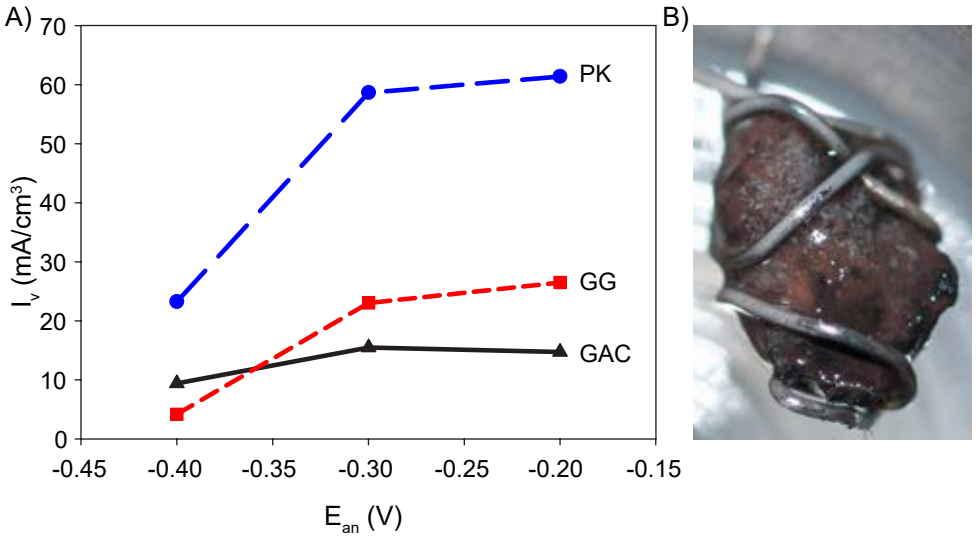

Figure 2.3. A) The current densities, normalized to granule volume, achieved during polarization curves for the three granules. B) The PK granule as bioanode, photographed at the end of the experiment.

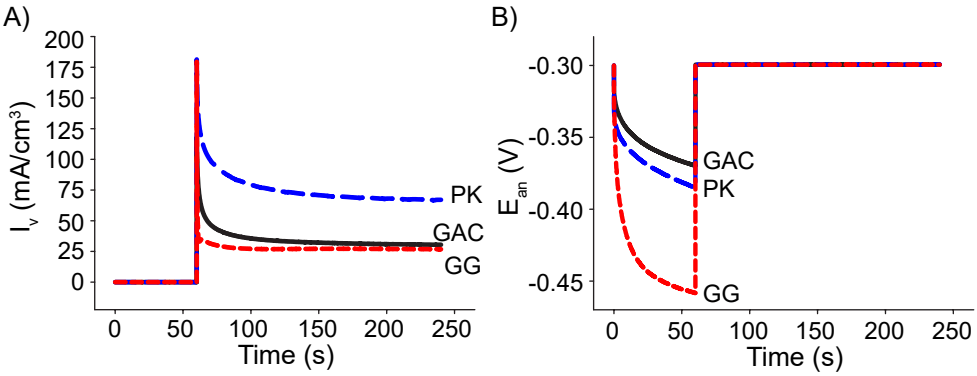

Figure 2.4. One typical charge and discharge cycle, where charging occurred in the first 60 seconds, followed by a 180 second discharge period. A) Volumetric current density in time for the three granules. B) Anode potential in time during the same charging and discharging cycle.

Figure 2.4 shows the current (A) and anode potential (B) in time during a single cycle of charging (60 seconds) and discharging (180 seconds) of the three bioanode granules. During OC conditions, there is no current and electrons are stored in the granule. As a result, the anode potential decreases towards the equilibrium anode potential. During discharge, the anode potential is controlled at -300 mV, and because of the potential difference with the open circuit potential reached during charging, electrons are released from the granule. The current showed a peak, which is a combination of capacitive and faradaic current, after which the current decreased towards a stable value, which is the faradaic current continuously

produced by the biofilm from conversion of acetate (without storage). The stored charge (**Figure 2.4A**) was 9.7 times larger for the PK and 4.1 times larger for GAC granules compared to GG, which implies a higher capacitance compared to GG. The lower capacitance of GG resulted in a lower bioanode potential, while anode potential of GAC and PK decreased more slowly.

After 40 charge and discharge cycles, the accumulated charge over the total timespan was 318 C/cm^3, of which 59 C/cm^3 stored (and discharged) charge, for GAC, 547 C/cm^3, of which 86 C/cm^3 stored charge, for PK and 211 C/cm^3, of which 18 C/cm^3 stored charge, for GG. In the same timespan 269 C/cm^3 for GG was accumulated in continuous operation. This results in a η of 1.2 for GAC and 2.0 for PK, which indicates that both activated carbon granules in intermittent mode outperformed the GG granule in continuous mode. GG itself had an η of 0.8 – meaning that continuous operation results in better performance than intermittent operation. The results show the PK granule has the highest η, while the η of GAC is in the same range as found the capacitive anode by Deeke et al., which also composed of GAC type activated carbon [86].

Influence of porosity characteristics of the granules

N_2 adsorption was used to study the pore structure of the three granule types, in the pore width range 0.3 to 50 nm. The specific surface area (SSA) was 885 m^2/g (940 m^2/cm^3) for GAC, 764 m^2/g (790 m^2/cm^3) for PK and 0.438 m^2/g (0.934 m^2/cm^3) for GG. In **Figure 2.5**, the cumulative pore volume is shown as a function of the pore width. GAC and PK both showed about 250 times higher total pore volume than GG. The pore volume increased until 5 nm for GAC, until 29 nm for PK and for GG the pore volume increased up to the range limit of 50 nm. The microporosity (pore volume < 2 nm) was 80% of total pore volume for GAC, 60% for PK and 4% for GG and the mesoporosity (pore volume between 2 and 50 nm) was 20% of total pore volume for GAC, 40% for PK and 96% for GG. The combination of low SSA and

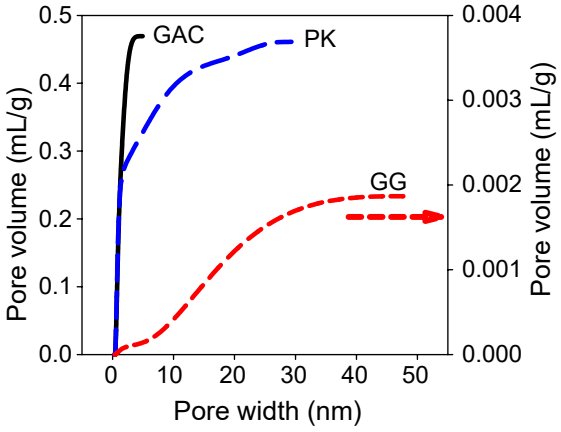

Figure 2.5. Pore size distribution in the range of 0.3 to 50 nm: cumulative pore volume against the pore width for the three carbon granules. The total pore volume in the pore width range is shown.

high density indicates the pores of the GG granule are likely close to the external surface. It should be noted the SSA cannot be used for normalization of current, as the pores <50 nm are smaller than the bacteria themselves (e.g. ***Geobacter sulferreducens*** is about 1.7 µm long by 0.4 wide µm (based on 10 observations in the SEM image of an electrode surface from Bond and Lovely [125]).

From the polarization curve and **Figure 2.4**, it can be seen that the continuous current densities of GAC and GG are similar and thus the biofilm activities are similar on the two granules. During the charge and discharge experiments, however, it is clear that more charge can be stored per cycle in GAC than in GG. As the biofilm activity for both granules is similar, it becomes clear that the physical granule properties, rather than possible capacitive properties of bioanode bacteria [65,66,126–128], are dominant for the charge storage. As the SSA is linked to the charge storage via surface available for EDL formation [118], the differences in NLDFT surface area, which is about 866 times higher for the GAC granule than for GG, can explain the larger storage capacity of GAC compared to GG. However, the 3.2 times higher charge storage cannot be explained by differences in SSA only. One possible explanation could be not all pore surface area is used, as Deeke et al. found increasing thickness of the capacitive layer of a capacitive bioanode decreased the charge stored [86].

The continuous current density of PK was 2.4 times higher than GAC, indicating that the biofilm activity was higher on PK granules. Similarly, PK had 2.3 times higher charge storage during the intermittent experiments compared to GAC. As the SSA of PK is lower than of GAC, the higher charge storage may be due to the higher biofilm activity. While the SSA of PK is lower than of GAC, it does have a higher mesoporosity. Although the higher mesoporosity has been shown to have a positive influence on the capacitance in supercapacitors and capacitive deionization [120,129–131], and could also affect charge storage by the capacitive bioanodes [86], other variables than the pore structure are likely to be of influence as well. Properties such as surface roughness and surface chemistry could be different for each granule and might enhance the biofilm via surface availability (external surface per granule volume), protection from shear forces and biofilm attachment (e.g. hydrophobicity [132]). More investigation is required to identify the determining variables for the performance of granular systems.

Potential for higher performance in larger reactor systems

The volumetric current densities of the single granules have been determined for both the working volume (anode) and for the volume of the granule itself (via weight and envelope density), in order to compare the single granule results to bioelectrochemical granular anode reactors in previous studies. These reactors were either operated using continuous [78,95,133–135] or intermittent [96,104,105] harvesting the current from the granular anode. The results from the previous studies and the current densities of the single granules can be seen in **Table 2.2**.

The volumetric current densities of the single granules are several orders of magnitude higher than those reached by other systems. In continuous systems, current densities between 9 and 1,500 A/m^3 of granules, depending on reactor size and configuration, have been achieved [34,78,95,133–135]. The PK granule produced 43 to 7,200 times higher current density than the currents reported in a granular bed reactor. Especially in larger reactors, the performance of these granules in continuous mode is low.

Table 2.2. Table comparing single granule results to both intermittent and continuously operated systems found in literature.

Granules[a,b]	Cell type	V_{anode} (mL)	$V_{granules}$ (mL)	I_V (mA/cm³ reactor)	I_V (mA/cm³ granules)	Circuit[d]	Cathode	Source
Continuous operation								
GAC 830	Single chamber, packed bed	2,200[c]	1,405	0.006	0.009	100 Ω resistor	n/a	[135]
GG[b1]	Two chamber, packed bed	350	182	0.063	0.121	10 Ω resistor	O_2 reduction	[34,134]
GG[b2]	Two chamber, packed bed, 6 in series	936	576	0.052	0.085	46 Ω resistor	$K_3Fe(CN)_6$	[34,78]
GG[b2]	Two chamber, packed bed	156	111	1.063	1.495	0mV E_{an}	$K_3Fe(CN)_6$	[34,95]
GG[b3]	Two chamber tubular, packed bed	4,900	2,500	0.033	0.066	1 Ω resistor	Biological O_2 reduction	[34,133]
GAC	Two chamber, single granule	1	0.0062	0.155	24.958	-300 mV E_{an}	$K_3Fe(CN)_6$	This study
PK	Two chamber, single granule	1	0.0099	0.586	59.475	-300 mV E_{an}	$K_3Fe(CN)_6$	This study
GG	Two chamber, single granule	1	0.0072	0.231	31.934	-300 mV E_{an}	$K_3Fe(CN)_6$	This study
Intermittent operation								
GAC 1240	Fluidized bed, external discharge	2,102	392	0.001	0.004	-300 mV E_{an}	$K_3Fe(CN)_6$	[96]
GAC 830	Fluidized bed, in situ discharge	3,534	583	0.003	0.020	48 Ω resistor	O_2 reduction	[105]
GAC 3030	Fluidized bed, in situ discharge	7	1.14	0.260	1.603	1000 Ω resistor	O_2 reduction	[104]
GAC	Two chamber, single granule	1	0.0062	0.394	63.462[e]	-300 mV E_{an}	$K_3Fe(CN)_6$	This study
PK	Two chamber, single granule	1	0.0099	0.757	76.765[e]	-300 mV E_{an}	$K_3Fe(CN)_6$	This study
GG	Two chamber, single granule	1	0.0072	0.218	30.202[e]	-300 mV E_{an}	$K_3Fe(CN)_6$	This study

a) GAC: Granular Activated Carbon in mesh size
b) GG: granular graphite with particle size distribution in mm diameter: [b1]2-6, [b2]1.5-5, [b3]average of 10.
c) single chamber system: reactor volume reported
d) E_{an}: anode potential versus Ag/AgCl reference electrode
e) volumetric current density of the single granules during the intermittent operation were taken from the discharge only, as this is most consistent with operation in larger reactor systems where the current generated originates from the discharge of the capacitive granules.

The comparison for granular bioanodes in intermittent operation shows a similar trend: currents between 4 and 1,600 A/m^3 of granules were reported [96,104,105], which are 48 to 21,000 times lower than the current density of the PK granule. Again, a similar trend is seen in that the smaller system performed much better than the large system.

There are several possible explanations for the low performance of both intermittent and continuous granular bioanodes compared to the single granule MFC, related to 1) contact, 2) flow and 3) biofilm damage. First, good contact between the granule and Pt wire was ensured and among the intermittently operated systems, increased collision force resulted in higher current density [104]. The second explanation is related to limited medium flow, where for the highest current density, homogeneity was ensured in the granular bed [95]. Third, the contact and sheer force between the granules and the current collector may damage the biofilm. From this comparison, it becomes apparent that there is much room for improvement in systems using granular bioanodes.

2.4. Conclusions

In this study, three single carbon granules were studied as bioanodes in a MFC. The highest volumetric current density was found using the PK activated carbon granule. In intermittent operation, where the charge storage in electrical double layer capacitance is used, the highest relative charge recovery of 2.0 and charge storage were found for the PK activated carbon as well, which was 4.7 times higher than the graphite granule. In comparison with other granular systems, it was shown that granular bioanodes can achieve much higher current densities than shown so far, especially if capacitive bioanodes are used. We demonstrate here a new test system in which single granules can be studied in detail, under continuous and intermittent operation strategies. This setup opens new opportunities to study bioanodes and to better understand the processes that determine the performance of granular electrodes. More insight in the performance of systems, that use capacitance by operating in intermittent mode, gives essential insights for further development of capacitive bioanodes in microbial fuel cells. If the untapped potential of a single granule can be realized on a larger scale, a big leap can be made towards practical application.

Acknowledgements

The research is supported by the Dutch Technology Foundation STW, which is part of the Netherlands Organization for Scientific Research (NWO), and which is partly funded by the Ministry of Economic Affairs (VENI grant no 13631). The authors would like to thank Anneke Delsing and Miruna Florea, from Eindhoven University of Technology, for their help on the skeletal volume analysis of the carbon granules.

Supporting information chapter 2

S1. Experimental set-up

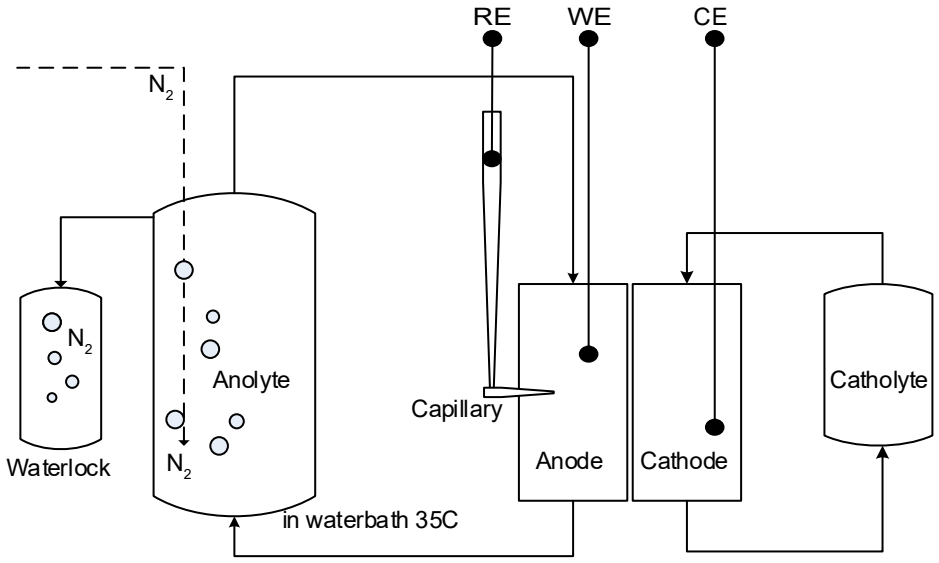

Figure S1. Experimental set-up. Continuous N_2 bubbling in recirculation vessel.

S2. Envelope density

The density of the granule was determined as the envelope density, meaning the mass of the granule divided by sum of the skeletal volume (only carbon) and the total pore volume (TPV (cm^3/g: multiply with mass for volume) (equation S1).

The skeletal volume was determined via helium adsorption using Micrometrics AccuPycII 1340 Pycnometer with a 10 cm^3 sample holder. The total pore volume was determined as the sum of cumulative pore volume found via the NLDFT analysis (from 0.36 nm until the last pore width per granule, see Table S1) and pore volume from the last pore width of NLDFT up to 300 nm pore from analysis of N_2 adsorption data using the Barrett-Joyner-Halenda (BJH) model, as seen in equation S2.

The results are seen in Table S1 and S2. The resulting volumes (Table S3) correspond to the physical size observed in the measurements: GAC and GG granules were approximately the same size, while PK was larger.

$$\rho_{envelope} = m_{sample}/(V_{skeletal} + m_{sample \cdot TPV}) \quad \text{Equation S1}$$

$$TPV = \sum [[\sum \text{Pore volume}_{NLDFT} + \sum \text{Pore volume}_{BJH}] \quad \text{Equation S2}$$

Table S1. Calculation of the total pore volume (TPV).

	BJH			NLDFT for TPV	TPV	
	Range pore width (nm)	∑Pore volume for range	pore width	∑Pore volume	cm^3/g	rel. error
GAC	339.3 – 4.5	0.01	4.50	0.47	0.48	0.2%
PK	245.9 – 24.8	0.04	24.86	0.46	0.49	0.2%
GG	361.3 – 35.8	0.0017	35.84	0.0018	0.0035	0.3%

Table S2. Measurement values from helium pyncometrics and calculated envelope density.

	Weight	error	Skeletal volume	error	Skeletal density	Error	Envelope density	Error
	g	g	cm^3	cm^3	g/cm^3	g/cm^3	g/cm^3	g/cm^3
GAC	2.9643	0.0001	1.363	0.0028	2.175	0.0044	1.062	0.0031
PK	1.958	0.0001	0.930	0.0027	2.106	0.0061	1.034	0.0037
GG	6.1649	0.0001	2.870	0.0032	2.148	0.0024	2.132	0.0065

Table S3. Investigated granules and the resulting volume from the calculated envelope density.

		Mass (mg)	Error (mg)	Volume (mm^3)	Error (mm^3)
biotic	GAC	6.6	0.1	6.2	0.1
	PK	10.2	0.1	9.9	0.1
	GG	15.4	0.1	7.2	0.1

S3. Porous structure characterization

The program SAIEUS [136] was used to analyze the Pressure-Volume data from the N_2 adsorption. The program uses the Carbon-N_2 2D-NLDFT model [124] (Non Local Density Functional Theory). In the program, the adjustment parameter Lambda was chosen as to have a smooth (maximum of two peaks) pore size distribution (PSD) curve and the pore width range from 0.36 nm to the where the change in pore volume reached zero (different for each granule type), as well as to keep close to the isotherm as possible.

The results from the analysis are 1) the specific surface area at the end of the pore range chosen for the granule type (Table S4), 2) the PSD as the cumulative pore volume versus the pore width (**Figure 2.5**), and 3) the cumulative pore volume for the envelope density (Table S1).

Table S4. Specific surface area by weight and by volume via the density.

	SSA (m^2/g)	SSA (m^2/cm^3)
GAC	885	940
PK	764	790
GG	0.438	0.934

Lake Louise, Canada

Chapter 3

The granular capacitive moving bed reactor for the scale up of bioanodes

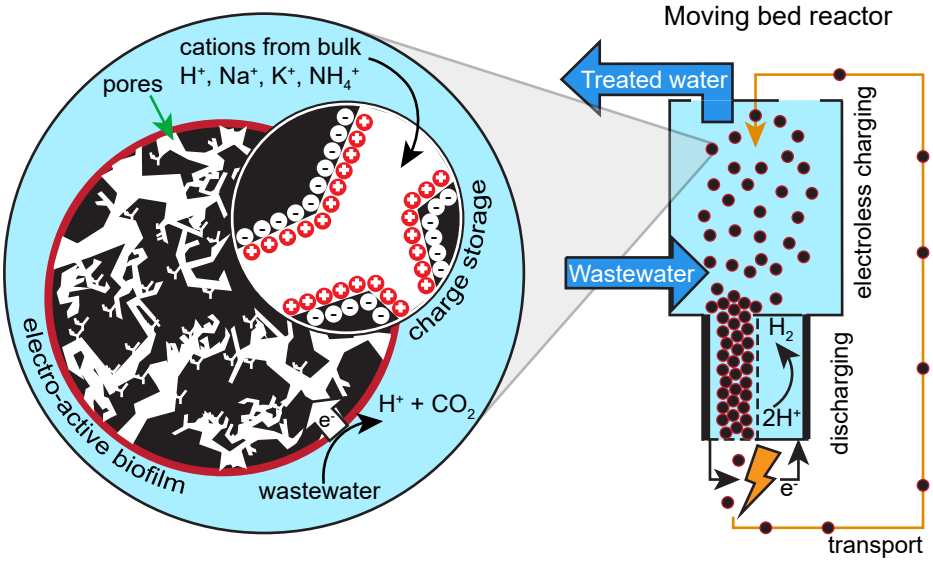

This chapter is published as:

C. Borsje, T. Sleutels, M. Saakes, C.J.N. Buisman, A. ter Heijne, The granular capacitive moving bed reactor for the scale up of bioanodes, J. Chem. Technol. Biotechnol. 94 (2019) 2738–2748. doi:10.1002/jctb.6091.

Abstract

BACKGROUND: Scaling up bioelectrochemical systems for the treatment of wastewater faces challenges. Material costs, low conductivity of wastewater, and clogging are issues that need a novel approach. The granular capacitive moving bed reactor can potentially solve these challenges. In this reactor, capacitive activated carbon granules are used as bioanode material. The charge storage capabilities of these capacitive granules allow for the physical separation of the charging and the discharging process and therefore a separation of the wastewater treatment and energy recovery process.

RESULTS: This study investigates the performance of the granular capacitive moving bed reactor. In this reactor, activated granules were transported from bottom to top of the reactor using a gas lift, and settled on top of the granular bed, which moved downwards through the internal discharge cell. This moving granular bed was applied to increase the contact time with the discharge anode to increase the current density. The capacitive moving bed reactor (total volume 7.7 L) produced a maximum current of 23 A/m^2, normalized to membrane area (257 $A/m^3_{granules}$). Without granules, the current was only 1.4 $A/m^2_{membrane}$. The activity of the biofilm on the granules increased over time, from 436 up to 1259 $A/m^3_{granules}$. A second experiment produced similar areal current density and increase in activity over time.

CONCLUSION: Whereas the produced current density is promising for further scaling up of bioanodes, the main challenges are to improve the discharge of the charged granules, and growth of biofilm on the granules under shear stress.

3.1. Introduction

Scaling up Microbial Electrochemical Technologies

The focus of wastewater treatment is shifting from removal of organic material and pollutants towards the recovery of energy and nutrients. Microbial Electrochemical Technologies (MET) offer opportunities to recover the chemical energy from the dissolved organic material during removal. Electro-active bacteria oxidize these dissolved organics into electrons, protons, and CO_2. When electro-active bacteria grow on an anode, called a bioanode, the electrons from the oxidation can be used to recover electrical energy in Microbial Fuel cells (MFCs), to produce products such as H_2 [38], H_2O_2 [37], hydroxide [137,138], or to recover of nutrients like ammonia [139] and phosphate [44,140] in Microbial Electrolysis Cells (MECs).

Although METs have been successfully operated on laboratory scale for the past decades, scaling up is still a major challenge [141]. Common strategies for scaling-up are to enlarge the cell or the use of multiple stacks of smaller cells [78,97,141–144]. When enlarging and stacking, the material costs increase with the reactor size, as a large part of the material costs can be allocated to the expensive electrodes [145] and ion exchange membranes, which are necessary for high performance and efficiency [71]. In general, the performance of scaled-up reactors decreases compared to lab-scale [89]. One of the reasons is that conductivities of wastewaters are typically low: around 1 mS/cm [76]. The low conductivity results in lower cell voltage, due to the increased resistance of the electrolyte for ion transport [41,76]. Maintaining low distance between anode and cathode in larger reactors is challenging, especially as there is a risk of clogging [65]. Granular capacitive bioanodes have been identified as a possible solution for these challenges [96].

Granular capacitive bioanodes

Granular capacitive bioanodes are granular activated carbon particles with an electro-active biofilm. The use of granular material results in a large available surface area for growth of electro-active bacteria per volume of reactor [73,146]. Activated carbon granules, in addition, contain pores, which results in a large internal surface area, allowing for formation of electrical double layers (EDL) [119]. Using the EDL, the granules can be used to store electrons resulting from the oxidation of substrate by electro-active bacteria [85–87,147–149]. During charging, the potential decreases towards the equilibrium potential of the biocatalyzed oxidation reaction. The charged state of the granules can thus be measured via the potential of the granules. When the equilibrium potential is reached, acetate oxidation and consequent charging of the granule stops [87]. After charging, the capacitive granules can be discharged at a current collector, which is poised at a higher potential than the granules' potential, and power is produced [87,96]. During discharge, as electrons are transferred to the current collector, cations are released to the electrolyte [96] and the potential of the granules increases [85,87]. The produced current is a combination of capacitive and faradaic current [84,96]. The release of ions is expected to increase the conductivity of the solution in the discharge cell, thereby reducing the ohmic losses and allowing for improved performance during treatment of low conductivity wastewaters. At the same time, discharge of the granules is a requirement for growth of electro-active bacteria as they only grow when producing current. During charging this is directly linked to the amount of charge that can be stored in the granules, thus directly linked to the amount of charge discharged.

Fluidized granular bed systems improve mass transport, of both solids and ions, and are thus attractive for MET applications [96,110]. The fluidized capacitive bioanode reactor by Deeke et al. (2015) showed that charging and discharging could be separated by transporting the charged granules from a charging reactor to an external discharge cell. Other studies used fluidization of a granular bed to make contact between capacitive granules and an anode [104–106,114,115,150]. Both approaches resulted in limited current density, likely due to short contact time of the granules with the current collector. Therefore, this study aims to investigate the effect of prolonged contact times on current production. Longer contact times of the capacitive granules with a current collector requires a different reactor type and design. Instead of a fluidized reactor, we therefore designed and operated a moving bed reactor. This reactor type allows for granules to move through a discharge cell in a semi-packed bed, where the granules have longer contact with the current collector compared to a fluidized system [151].

In the moving bed reactor, with a total volume of 7.7 L, capacitive bioanodes granules were circulated using a gas lift and settled down on a moving granular bed. The performance of the moving bed reactor was studied under ideal conditions: non-limiting acetate concentrations, constant pH, and with inhibition of methanogenic activity. Two independent experiments were performed. Granules were harvested regularly to monitor activity of the electro-active biofilm in a separate test cell, as well as to study the presence of biofilm on the electrode with SEM.

3.2. Materials and methods

Reactor

A novel design for a granular capacitive moving bed bioanode was developed, where activated carbon granules circulated using a gas lift and settled through an internal discharge cell. This new reactor design was based on the continuous sand filter reactors [152], which circulate sand particles, commercially known as Dynasand by Nordic Water (Nordic Water (https://www.nordicwater.com/product/dynasand/)), in order to create a moving granular bed.

Reactor design

The reactor consisted of a PVC tube of 138 cm length with a diameter of 95.4 mm. This tube was divided in five sections (**Figure 3.1A**): the top section, the main column, the funnel section with the discharge cell, the conical bottom, and the gas lift tube. The total reactor had an anode volume of 7.7 L (both liquid and granules) and a cathode volume of 300 mL, both excluding the recirculation volumes (470 and 250 mL respectively). A scaled drawing of the design with associated recirculation volumes and flows can be found in Supporting information (SI).

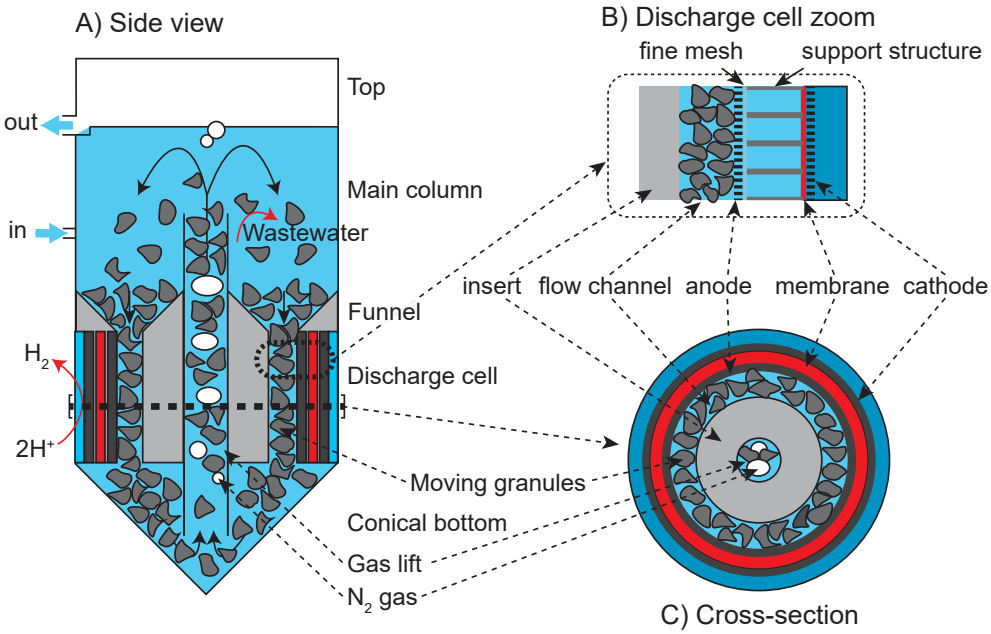

Figure 3.1. (A) Schematic overview of the reactor with its 5 sections. The red arrows indicate the oxidation and reduction reactions, while the solid black arrows indicate the flow of the granules. (B) Detail of the discharge cell (C) Cross-section of the discharge cell.

The main column held the bulk of the liquid and allowed the granules to settle down towards the funneled section, which narrowed the flow path, in radius, from 39.7 mm (between outer tube and gas lift of 16 mm) to 8 mm in the discharge cell. The discharge cell consisted of five concentric parts, which are from inside to outside: the flow channel, the discharge anode, the membrane on its support structure, the cathode, and the cathode compartment. **Figure 3.1B** shows a zoom to the discharge cell construction and **Figure 3.1C** shows a cross-section of the discharge cell.

The flow channel was created by an insert, made from PVC, and the discharge anode. The discharge anode (2 mm thick titanium mesh 1.4 coated with Pt/Ir Mixed metal oxide, Magneto Special Anodes B.V., Netherlands) had a mesh structure of 10 cm long (1/14th of the total reactor length), which allowed anolyte access to the membrane for ionic contact. The volume in the flow channel, for the moving granule bed, next to the mesh part of the discharge anode was 163 cm^3. The Cation Exchange Membrane (Ralex CM-PP, MEGA a.s., Czechia) was fixed on an open-structured PVC support (121 holes), which resulted in 137 cm^2 effective membrane area.

The cathode (same make as anode discharge anode) was on the outside of the membrane. An injectable gasket (Repliset F5, Streurer GmbH Nederland, Netherlands) was used to seal the membrane and electrodes.

Below the discharge cell, the reactor was shaped as a funnel (95.4 mm to 20 mm diameter). A Luggin capillary was inserted into the reactor here to connect a reference electrode. The bottom of the funnel led to the opening of the gas lift, which has an inner diameter of 9 mm. The gas lift ended just below the water level at the top of the reactor. The top section facilitated separation of solids, gas and liquid. The anolyte overflowed into the recirculation volume, where the gas and liquid effluent were separated.

The reactor contained 1200 mL (584 g dry weight, in the first experiment) and 2415 mL (1174 g dry weight, in the second experiment) of activated carbon granules (density 0.486 g/cm^3, coconut shell based HR5, Eurocarb, United Kingdom), sieved to size between 0.5 and 0.8 mm (Stainless steel sieves, VWR, Netherlands). The porosity was measured at 1100 m2/g specific surface area for pore width range 0.3 to 50 nm (2D-NLDFT (Non-Local Density Functional Theory) model applied to N_2 adsorption measurements at 77 K using Micromeritics Tristar 3000). At the bottom of the reactor, anolyte and granules were transported up by the gas lift. After exiting the gas lift tube, the granules settled down in the main volume, on top of the granule bed. This way, a moving bed of capacitive granules was created that moved downward through the discharge cell. This continuously settling bed of granules moved through the 8 mm wide channel, resulting in a particle bed in contact with the discharge anode. The circulation cycle was completed as the granules settle towards the bottom of the gas lift, where the conical shape of the bottom centers the granule flow to the gas lift.

N_2 flow to the gas lift was supplied via a mass flow controller (Mass-stream, Bronkhorst Nederland B.V., Netherlands) to provide a steady flow of granules. The use of N_2 also ensured an anoxic environment. Granule flow measurements from the top of the gas lift showed that the residence time of the granules in the discharge cell was between 27 and 52 seconds for 500 to 300 mL/min of N_2 flow (see SI section S2). Change in flow rate was not observed to affect the current density on long-term.

Measurements in the reactor

DO (dissolved oxygen, SE 715, Knick, Germany) and pH (CPS71 and CPS11D, Endress+Hauser B.V., Netherlands) were measured online in the anolyte recirculation. The anolyte pH was controlled at 6.9±0.3 (Liquiline, Endress+Hauser B.V., Netherlands) through NaOH dosing into the circulation, which was pumped at 150 mL/min (same rate for the catholyte). A heating jacket around the main tube heated the anolyte to 28°C using a water bath (Immersion circulator DC10, Thermo Fisher Scientific, Netherlands).

The charged state of local granules (see section 1.2), before entering the discharge cell, was measured as the $E_{granules}$ potential using a Pt/Ir wire (0.25 mm diameter, 80/20 ratio Pt/Ir, Advent-RM, England) and a reference electrode in close proximity. The potential of the wire represented the potential of the granules, as the wire takes the same potential as granules when they collided with the wire. The wire was removed for regular cleaning from biofilm growth.

Granular activity test cell

To determine the change in activity of the electro-active bacteria growing on the granules, a small volume of granules from the reactor was taken regularly with three replicates per day. These granules were placed in a small test cell. **Figure 3.2A** shows a schematic view of the granules in the test cell and **Figure 3.2B** a photo of the test assembly. The activity test cell consisted of a 6 mm diameter titanium electrode (contact surface coated with Pt/Ir MMO, Magneto Special Anodes B.V., Netherlands), which was screwed against the granules at 40 N.cm (TorqueVario-S 36849, Wiha, Germany) in a PMMA housing. The cathode was a Pt/Ir wire in the electrolyte. The electrolyte and experimental conditions were the same as in the anode side of the reactor.

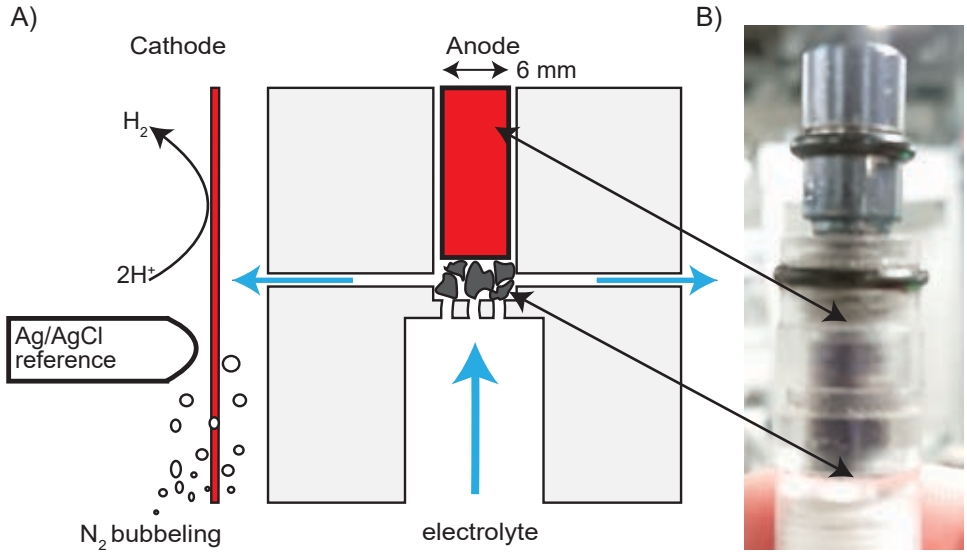

Figure 3.2. (A) Schematic of the granular activity test cell where a small batch of granules could be tested for bioanode activity. The granules were pressed between the cell and the anode (blue arrows indicate electrolyte flow) and (B) photo of the test assembly.

Inoculum and medium

As inoculum, a mixed electro-active community was taken from a microbial electrolysis cell in our laboratory. This cell was running on acetate, used methanogen inhibitor (Na 2-bromoethanesulfonate; Na 2-BES), and operated at a controlled anode potential of -0.35 V vs Ag/AgCl [153].

The granules were used with inoculum during the testing phase of the reactor, which will have resulted in an initial activity by biofilm on the granules.

The influent was continuously supplied in the middle of the main column to the reactor, resulting in a hydraulic retention time (HRT) of 35±3 hours (volume for HRT includes recirculation volume). The influent was fed through mixing (1:1) of carbon source and nutrients source from two different vessels preventing microbial growth in the influent. The carbon source vessel contained potassium phosphate buffer (20 mM), acetate (the first experiment had 20 mM in the start-up phase and 40 mM day 14, the second experiment was started with 40 mM), and 20 mM Na 2-BES. Acetate was measured using Ion Chromatography (761 Compact IC, Metrohm, Switzerland with column 00G-4375-E0, phenomenex, Netherlands). The nutrients source contained 20 mM KCl, 20 mM NaCl, 10.4 mM NH4Cl, 1.4 mM CaCl2, 80 µM MgSO4 and 0.2 mL/L trace metal solution [154]. The chemical compounds were obtained from VWR. The influent solutions were continuously sparged with N2. The catholyte consisted of a 40 mM phosphate buffer solution and was continuously supplied to keep the catholyte pH below 12. This prevented degradation of the sealing gaskets.

Electrolyte for the activity test cell was the same as the influent for the reactor and used for all measurements during 1 day.

Electrochemical methods

All electrochemical methods were performed using potentiostats in a 3-electrode setup (IviumStat for the reactor and Ivium-n-Stat for the test cell, Ivium Technologies, Netherlands). All potentials were controlled or measured against an Ag/AgCl/3M KCl reference electrode (+205 mV vs SHE, QM711X/GEL, Q-I-S, Netherlands). Reference electrodes for the reactor were connected using Haber-Luggin capillaries (3M KCl), while for the activity test cell the reference electrode was placed directly in the main volume.

Current and potentials were measured every 60 seconds for the reactor and every second for the activity test cell. To prevent oscillation in the potentiostat control, due to the capacitive character of the reactor, a high frequency shunt (3 times 100 µF in series, MCCB1E107M2FCB, Multicomp) was attached between reference and counter electrode.

Control of the discharge anode in the reactor

The discharge anode was controlled at an applied anode potential followed by a period of applied current. The anode potential control was used to harvest the electrons at constant energy level (common procedure in MFC operation), while applied (forced) current was used to force discharge of the capacitive granules, as increased discharge of the granules will increase both the capacitive current and biological activity of the reactor (see section 1.2 for more details). **Figure 3.3** shows examples of the control method for the discharge cell. The discharge anode potential was controlled at 0 V vs Ag/AgCl for 1 hour, followed by current control for 1 hour or until +0.15 V vs Ag/AgCl was reached. During the experimental procedure, the current was controlled at three different levels, depending on the performance of the reactor: +7.3, +10.9 and +14.6 A/m^2 on top of the last measured current. The applied current

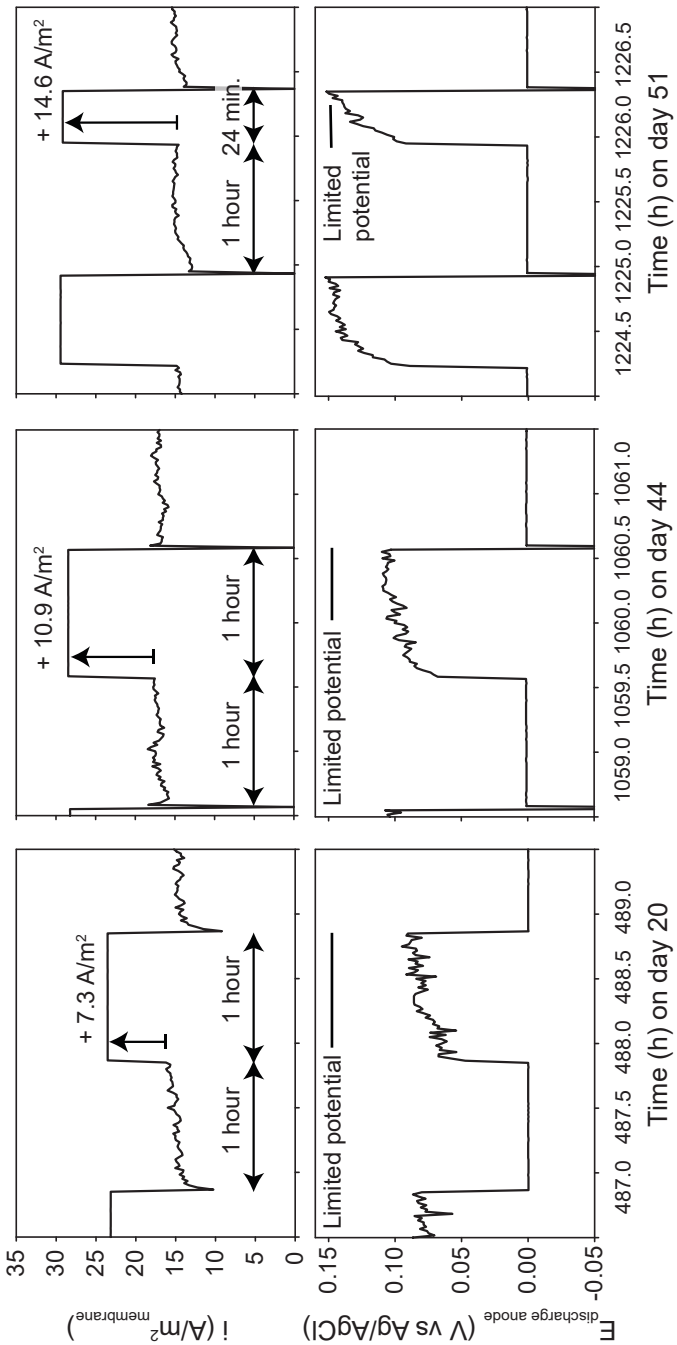

Figure 3.3. The discharge cell was controlled by controlling the anode potential at 0 V vs Ag/AgCl for 1 hour and then controlling the current at an applied current, lasting either 1 hour or until an anode potential of +0.15V was reached. In this figure, examples are shown for the three applied current controls used in the first experiment.

resulted in an increase in anode potential. The current control period was aborted when the anode potential increased past +0.15 V vs Ag/AgCl, to prevent unwanted electrochemical reactions, or maintained for a maximum period of 1 hour if the anode potential remained below +0.15 V vs Ag/AgCl. This sequence was performed throughout the whole experiment (unless stated otherwise).

Activity test control

The activity of the capacitive granules was measured in a polarization curve, as the current produced at -0.1, -0.2 and -0.3 V vs Ag/AgCl. For one data point the last 10 seconds of 10 minutes applied potential were averaged and the current was normalized to the volume of dry granules (via the bulk density and the dry weight, after washing 3 times with milliQ and drying overnight at 105°C). To ensure positive currents only, the granules were charged to -0.4 V vs Ag/AgCl or lower (except where notes differently). For activity tests, the faradaic charging current decreased the potential at open cell potential (OCP) (see section 3.1.2).

Scanning electron microscopy

A sample of granules was taken from the reactor, at the point where they were settling in the main column. Fixation for Scanning Electron Microscopy (SEM) analysis (JSM-6480LV, JEOL, Netherlands) was performed with 24 hours at 4°C in 6.25% glutaraldehyde in PBS, filtered over 0.22 µm. The granules were then washed 3 times for 15 minutes with PBS (filtered over 0.22 µm), 20 minutes with 30, 50, 70 and 90% ethanol, twice for 30 minutes with 96% ethanol, dried at 40°C for a minimum of 1 hour and stored in closed bottles at room temperature.

3.3. Results and discussion

The reactor showed stable performance

Figure 3.4 and **Figure 3.5** shows the current density of the reactor per membrane area in the discharge cell of the first (**Figure 3.4**) and second (**Figure 3.5**) experiment. The behavior of the current over time will be discussed in combination with the results of the granule activity (section 3.3.2). In the first experimental run, the average daily current density ranged between 10 and 23 $A/m^2_{membrane}$ during 66 days of reactor operation. During the first 8 days, the daily average current density increased from 10 A/m^2 to 19 A/m^2. From day 33 on, the controlled current was increased to +10.9 A/m^2 (see section 2.4.1 for more details on the potential-current control cycle). Over the course of the following 12 days, the daily average current increased to a stable maximum of 23 A/m^2 (day 44), with a maximum 17 A/m^2 during potential control. Further increasing of the controlled current to +14.6 A/m^2 (day 45 to 54) resulted in the highest daily average current of 25 A/m^2 on day 46, after which, the current density decreased to 20 A/m^2. At an applied current of +10.9 A/m^2 from day 54 onward, the daily average current increased again to 21 A/m^2. After 66 days, the acetate feed was stopped: the results of which will be shown and discussed in more detail in the last section of the results.

The experiment was concluded by removing the granules (day 73), to investigate if the current was indeed produced from the granules. The daily average current produced by the discharge anode without granules (and 16 mM acetate) was 1.4 $A/m^2_{membrane}$: as this current is only 9% of the current obtained with granules, at the same discharge anode potential, the granules contributed to most of the current in the moving bed reactor.

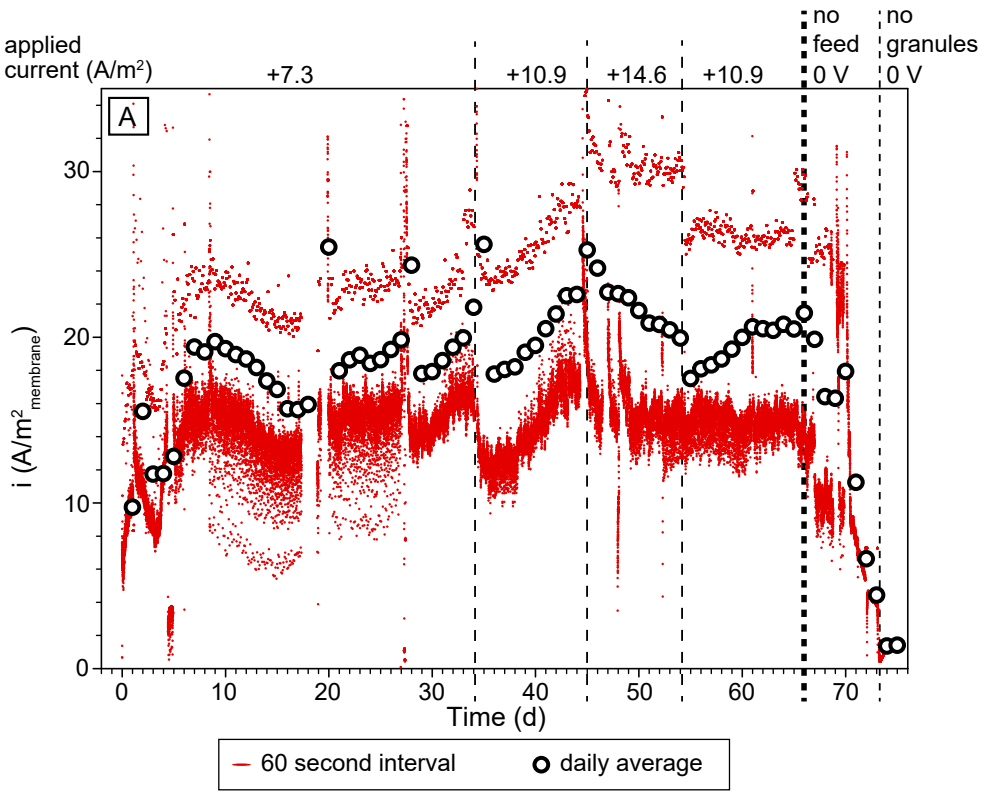

Figure 3.4. The current density per membrane area in the reactor during the first experiment The different periods of control are indicated with the dashed lines. On top of the figure are the different the applied currents in the potential-current control cycles, where the e.g. +10.9 A/m² was applied on top of the last measured current at controlled potential. Thin dashed lines indicate the change in applied current. Open circuit data is not displayed for clarity of the figure.

A second experiment was performed for 33 days under similar conditions, though with 2415 mL of unused granules (as compared to the pre-used granules used in the first experiment, see section 2.3), and resulted in comparable current densities to the first experiment, with a maximum of daily average of 21 A/m² and 17 A/m² under potentiostatic control. The current increased rapidly to 10 A/m² in the first 5 days, as the unused granules started up as a bioanode, after which the maximum of 21 A/m² was reached on day 16. Afterwards, there was trouble in controlling the system. The current density never increased to previous levels and the experiment was terminated. Due to the troubles with the system, the applied current did not exceed +7.3 A/m².

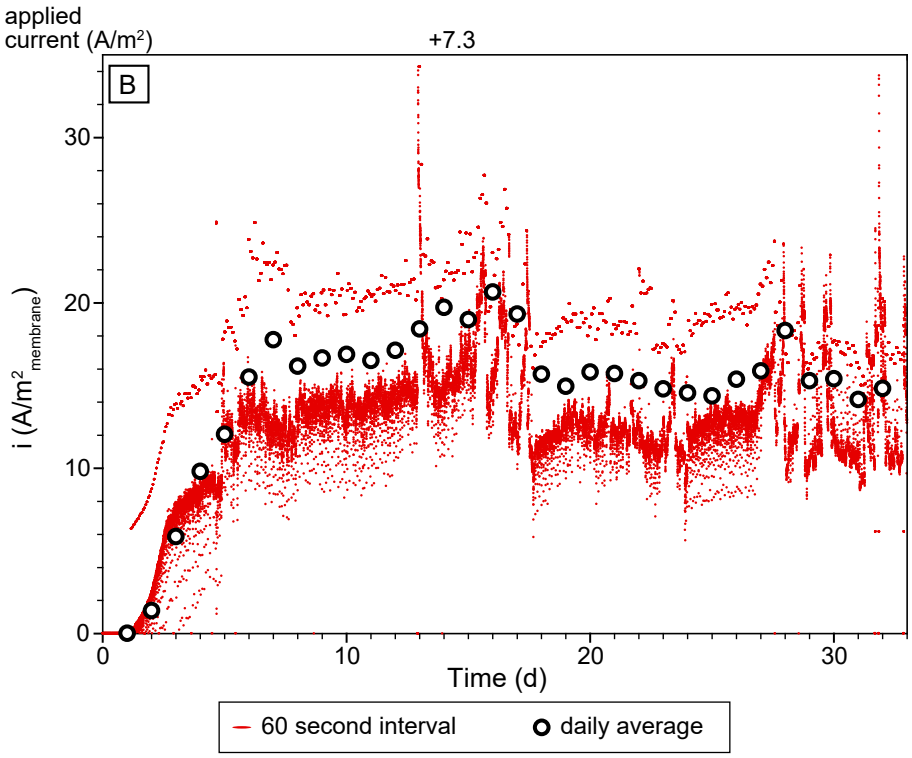

Figure 3.5. The current density per membrane area in the reactor during the second experiment. The small red dots show the data per minute, open circles show the daily average. On top of the figure is the applied current in the potential-current control cycles, where in the second experiment only 7.3 A/m2 was used, applied on top of the last measured current at controlled potential. Thin dashed lines indicate the change in applied current. Open circuit data is not displayed for clarity of the figure.

The current data recorded per minute show a large variation. This variation is the result of the discharge method of sequential potential control and current control: the current measured during controlled potential is always lower than the applied current, which was controlled at a higher value to force higher rates (see methodology). A second reason for the variation is the intermittent contact of granules with the discharge anode, releasing a varying amount of charge per minute. Peaks, such as on day 2, 20, 28, 35, 45 and 47 (first experiment) and day 13 (second experiment) are due to maintenance, where a capacitive peak occurred after a short OCP period. Other peaks after day 16 in the second experiment were due to continued trouble in the system.

Although the current density per membrane area is similar for both experiments, the second experiment was performed with double the volume of granules of the first experiment. This means that the areal current density (A/m^2) remained the same while the granular current density ($A/m^3_{granules}$) halved. This indicates there is an optimum ratio of granules to the discharge anode surface area. This optimum is related to earlier studied ratio of charging to discharging time [85,86,155,156]: the charging time is the time the granules are outside the discharge cell, which increases with more granules, and the discharging time is the time the granules are in contact with the discharge anode.

The activity of the granules increased over time

The activity of the electro-active bacteria on the granules was measured throughout the experimental periods. A small volume of granules (16±5 mg) was taken from the reactor regularly. **Figure 3.6** shows the current density of the granules over time, normalized to granule volume at three controlled potentials used in the polarization curve for the first (**Figure 3.6A**) and second (**Figure 3.6B**) experiment.

For both experiments, there is a clear increase in the activity. For the first experiment, at an anode potential of -0.1 V vs Ag/AgCl, the current increased from 436 $A/m^3_{granules}$ (averaged over the first 10 days) to 1259 $A/m^3_{granules}$ (average last 2 measurement days) showing 2.9 times increase in current density over the experimental period. During the first 3 days, the negative current at -0.3 V vs Ag/AgCl during this time shows the anode potential in the test cell was lower than the granule potential of the sample: the granules in the reactor had not been fully charged yet. The increase in activity with time is in line with the reactor performance: the current density of the granules in the test cell and in the reactor increased until around day 45 and stagnated after that time until the end of the first experiment. In the second experiment, the activity increased by 1.6 times until day 25. After day 25, the activity stagnated, similar to the reactor performance and similar to the behavior in the first experiment.

As both reactors show stagnating activity over time simultaneous with a stagnating current density in the reactor, the stagnating current density is likely the result of limited coverage of granule by electro-active biofilm. We propose two mechanisms occurring simultaneously: (i) shear stress on the biofilm, and (ii) insufficient discharging of the granules, which is directly linked to growth (see section 3.1.).

Shear stress on the biofilm

The shear stress on the outer surface of the granules was caused by the constant movement of the granular bed. SEM images, taken of granules from the reactor, indeed show limited growth on the granule surface. **Figure 3.6** shows SEM images of granules, from the first experiment, in three different states of growth: clean, day 17 and day 60. Three important observations can be made based on these images: 1) Biofilm is formed in the large pores on the granule surface and 2) biofilm development increased in the period in which activity of the biofilm on the granules increased. 3) The outer surface of the granules was devoid of microorganisms, probably because of shear stress. Thus, the shear stress affected the total amount of biofilm present on the granules, which limits the faradaic contribution to the total current produced by the granules during discharging.

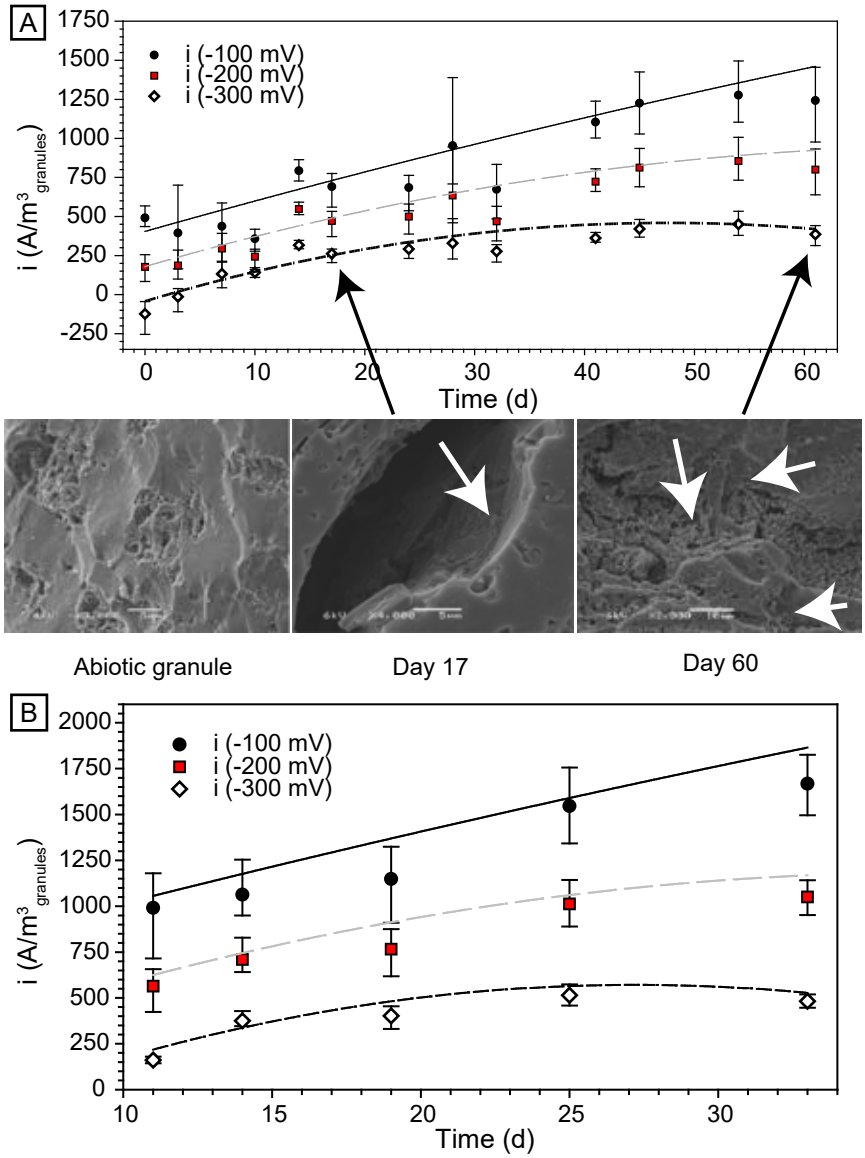

Figure 3.6. Activity of the granules in the test cell at 3 anode potentials: black circles -100 mV vs Ag/AgCl, red squares -200 mV vs Ag/AgCl, open diamonds -300 mV vs Ag/AgCl. A) The first experiment and B) the second experiment. The current density is expressed as volume of granules at the discharge anode in the test cell (dry weight into volume of granules). The lines are added to guide the eye. The SEM images show the increased amount of biofilm on the granules over time, with the white arrows pointing to concentrations of microorganisms.

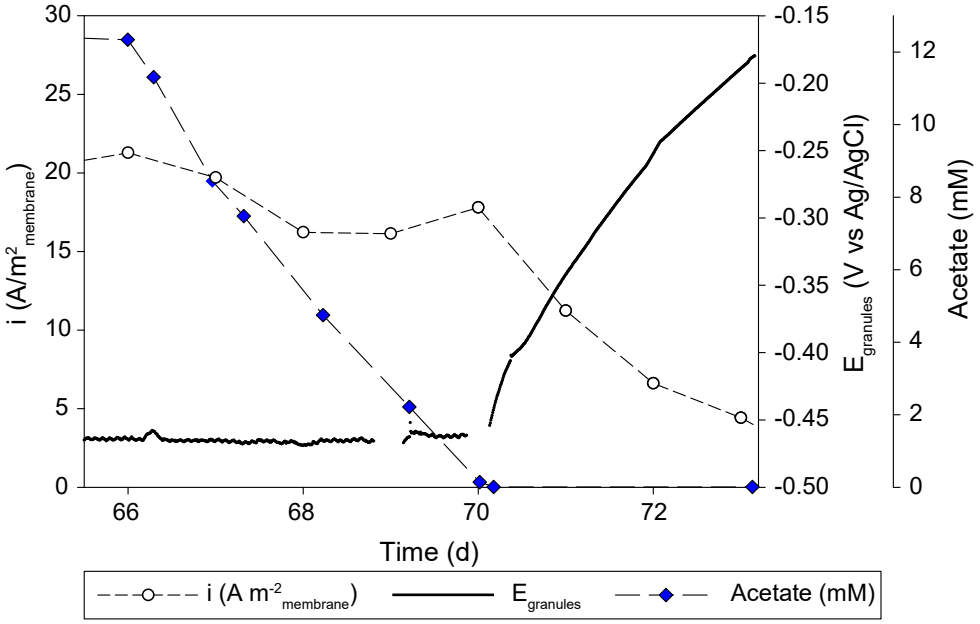

Figure 3.7. The current density (short, dashed line with open circles) of the reactor in the period without feeding the system. The increase in the potential $E_{granules}$ (solid black line) shows the discharging process when the charging process is limited by the low acetate concentration (long dashed line with blue diamonds).

Insufficient discharging of the granules

Figure 3.7 shows the measured current, open circuit granule potential and acetate concentration after feeding of the system was stopped at the end of the first experiment. When the acetate concentration decreased below the detection limit of 0.01 mM, the current decreased. At the same time, the granule potential ($E_{granules}$), measured above the discharge cell, increased. Since the potential of the granules is linked to the stored charge (see section 3.1.2), the increase in granule potential shows that the granules were slowly releasing electrons to the discharge anode. The discharging period in the reactor is equal to the residence time of the granules in the discharge cell, which is between 27 and 52 seconds (see methodology). This is many times shorter than the multiple days that were required here to discharge, without acetate feeding, and a clear indication that the discharging is limiting the current produced by the reactor.

Improving the discharging will not only improve the growth and activity of the biofilm, but also increase the total current as more charge is transferred during discharge. Thus, improving the discharge of the granules is essential to exploit the reactor's maximum performance.

Perspectives for application of the granular capacitive moving bed reactor

Comparison with other granular bioanode systems

Table 3.1 shows the results of the current density of the moving bed reactor in comparison with other experimental studies using granular bioanode systems. Here we present the current density normalized to granule volume, to compare with the other granular bioanodes. The current density per projected membrane area or projected cathode area is also shown in order to compare the current density of the discharge cell to other systems' cell designs.

The moving bed reactor produced a maximum of 257 $A/m^3_{granules}$ (daily average), during the first experiment. If normalized to the volume of the discharge cell, this is 1891 $A/m^3_{granules}$ or 7 times higher than when normalized to the total volume of granules in the reactor. The granules from the reactor produced 1667 $A/m^3_{granules}$ at -0.1 V vs Ag/AgCl as a fixed bed in the activity test cell during the second experiment. These results are comparable to the 1495 $A/m^3_{granules}$ produced by a non-capacitive granular packed bed at 0 V vs Ag/AgCl [95]. The comparison between current density per total volume of granules in the reactor and

Table 3.1. An overview of previously studied granular bioanode systems for comparison with the granular capacitive moving bed reactor.

	A (cm^2)	V (mL)	$V_{granules}$ (mL)	i (A/m^2)	i ($A/m^3_{granules}$)	i ($A/m^3_{reactor}$)	Reference
Non-capacitive bioanodes							
packed bed cell	a)	156	111	a)	1495	1063	[95]
Capacitive bioanodes							
fixed single granule	1.3[b)]	1	0.01	5.7	76765	757	[87]
fluidized bed cell	0.8[c)]	40	2.3	2.6	89	5	[114]
fluidized bed cell [d)]	7[c)]	7	1.1	2.6	1603	260	[104]
fluidized bed reactor [d)]	719[b)]	1000	300	0.2	37	11.1	[105]
fluidized bed reactor [d)]	3.1[c)]	1000	177	1.3	2.3	0.4	[115]
fluidized bed reactor	11[b)]	2102	392	1.3	3.6	0.7	[96]
fluidized bed reactor	70[c)]	680	80	2.4	214	25.2	[106]
moving bed reactor [e)]	137[b)]	7700	1200	22.6	257	40.1	This study
moving bed discharge cell [e)]	137[b)]	163	163	22.6	1891	1891	This study
fixed bed activity [f)]	a)	a)	0.024	a)	1667	a)	This study

a) Unknown or not determined.
b) Projected surface area of the membrane
c) Projected surface area of the cathode
d) Current density for maximum power
e) First experiment
f) Second experiment

granule volume in the discharge cell shows again that there is an optimum ratio of granules to discharge anode surface (see section 3.3.1). Still, compared to the best performing capacitive bioanode, at -0.3 V vs Ag/AgCl, the performance in the test cell (482 $A/m^3_{granules}$, in the second experiment) was 159 times lower than measured for a single activated carbon granule, fixed to a Pt wire, (76765 $A/m^3_{granule}$) at the same potential [87].

Other capacitive bioanodes with intermittent contact were either fluidized for contact with the discharge anode [104–106,114,115,150] or were fluidized before flowing through an external discharge cell [96]. The fluidization by stirring the granular activated carbon in the study by Liu et al. (2014) produced 1603 $A/m^3_{granules}$ [104], similar to the moving granules in the discharge cell of the moving bed reactor, however this system was several times smaller. Compared to the fluidized bed reactor with an external discharge cell [96], the moving bed through the discharge cell increased the areal current density 17 times.

The fluidized capacitive bioanode studied by Tejedor-Sanz et al. (2017) produced the highest current density per granule volume so far: 214 $A/m^3_{granules}$ at +0.2 V vs Ag/AgCl [106]. The moving bed reactor produced a maximum of 257 $A/m^3_{granules}$ (daily average over the potential-current control cycles). If only the periods of potential control are considered, the reactor produced a maximum of 215 $A/m^3_{granules}$ at 0 V vs Ag/AgCl. It is generally considered that increased scale leads to lower current density. So, it is interesting to notice that in the moving bed reactor the result was achieved with 1200 mL of granules, as compared to 80 mL of granules in the fluidized bed of Tejedor-Sanz et al.: comparable granular current density using more granules. Normalization to the projected surface area shows our reactor had a 10 times higher areal current density, therefore a higher current density was produced using less materials. These results are promising for scale up of bioanodes using moving bed capacitive bioanodes.

Conclusions and strategies for improving the reactor towards application

In this paper, we focused on improving the contact time of the granules with the discharge anode. The granular capacitive moving bed reactor has shown promising results with regards to scaling up bioanodes. The granular capacitive moving bed reactor produced 23 $A/m^2_{membrane}$ (257 $A/m^3_{granules}$) showing stable performance for 66 days and an increase in activity on the granules over time. The granular current density is similar to smaller scale fluidized capacitive bioanodes, which is promising for scale up of bioanodes.

Analysis of the results show the limitations of the reactor: 1) the shear stress, on the biofilm on the granule surface, imposed limitations on the faradaic current, and 2) the capacitive current is limited in the reactor, as evident from the slow discharging without recharging. Aside from this, the results show there is an optimum ratio of granules per discharge anode surface area: the areal current density was similar between the two experiments but normalization to the granule volume halved the current density.

The same conclusion was drawn via normalization of the produced current to the discharge cell granule volume, which showed 1891 $A/m^3_{granules}$: 7 times higher than 257 $A/m^3_{granules}$ in the reactor.

Strategies to tackle the main challenges, limited capacitive current and limited biofilm coverage on the granules, are necessary to increase the current density. To increase coverage of the biofilm, granules should be chosen or engineered to provide protection from shear stress. However, some application of shear might be beneficial for removal of methanogenic bacteria which often grow on the outside of bioanode biofilms [74]. Optimizing the available

surface for biofilm growth, protected from shear stress but still allowing removal, would allow for higher faradaic current to add to the capacitive current. The capacitive current depends on the material properties of the activated carbon granules, as previous experiments have shown [87]. Material properties, such as porosity [120,129–131], surface roughness [157–160], surface chemistry [132,161] and material conductivity all play a role on the produced current. Material conductivity is an important factor, as decreasing the resistance of the granules will improve the charge transfer of highly capacitive granules. Choosing granules with the right properties, or engineering granules for reduced resistance will change the optimum volume of granules in the reactor.

After engineering granules for lower resistance and improved protection against shear stress for the biofilm, a study into the optimal ratio of granules to discharge anode surface area should be performed. Finally, the results presented in this study were obtained in ideal conditions i.e. acetate as substrate, pH control and sufficient buffer capacity. Therefore, the moving bed reactor should be studied in real conditions such as real wastewater, limited buffer capacity and minimum addition of chemicals. The improvements and experience with real conditions are needed to realize the full potential of the granular capacitive moving bed reactor.

Acknowledgements

This work was performed in the cooperation framework of Wetsus, European Centre of Excellence for Sustainable Water Technology (www.wetsus.eu). Wetsus is co-funded by the Dutch Ministry of Economic Affairs and Ministry of Infrastructure and Environment, the European Union Regional Development Fund, the Province of Fryslân and the Northern Netherlands Provinces. The authors thank the participants of the research theme 'Resource Recovery' for the fruitful discussions and their financial support.

Supporting information chapter 3

S1. Experimental set-up of the reactor and associated equipment

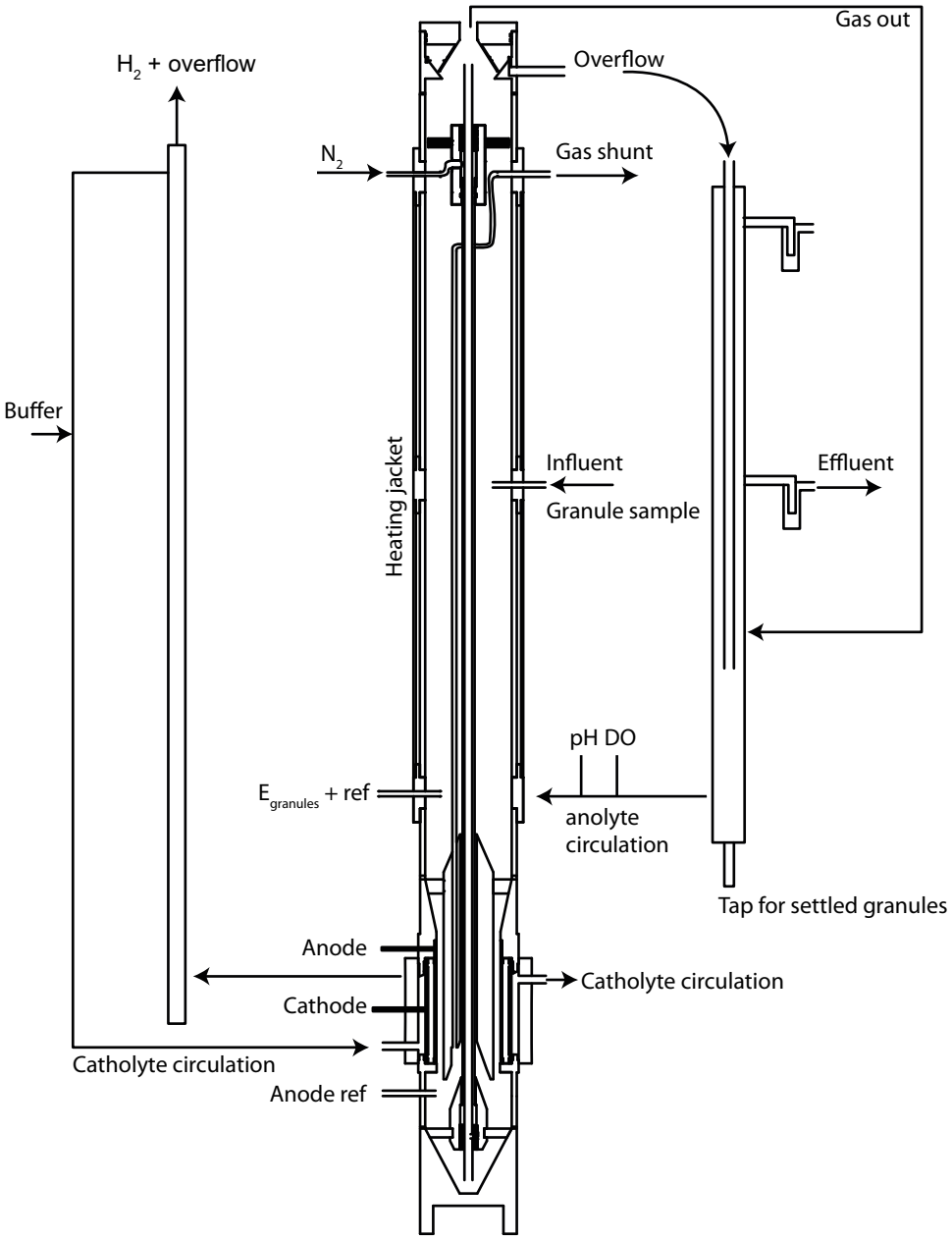

Figure S2. A scaled drawing of the reactor design with associated circulation vessels and flows.

S2. Granule flow measurements

The flow of the granular material was measured by extending the gas lift by 20 cm and capturing the granular flow externally in a graduated cylinder. Figure B1 shows the results in the range of 200 to 500 mL/min. The linear regression line in Figure B1 results in Equation S1. R^2 is 0.8695.

Granule flow = 0.015 × N_2 gas flow - 1.35 Equation S1

The mass balance of granule flow can be written with the vertical velocity and the cross-sectional area of this flow (Equation B2). As the granule flow from the gas lift (Equation B1) is equal to a vertical flow multiplied with the flow area of the gas lift at 0.63 cm^2 and using the area of the discharge cell at 16.34 cm^2 and the length of the discharge anode at 10 cm, Equation B3 gives the time in the discharge cell as dependence of the granule flow from the gas lift.

Area1 x vertical velocity1 = Area2 x vertical velocity2 Equation S2

Time in discharge cell = (length of discharge anode × Area discharge cell) / (Granule flow from the gas lift) Equation S3

The time in the discharge cell for the used flow rates is 52 to 27 seconds for 300 to 500 mL/min.

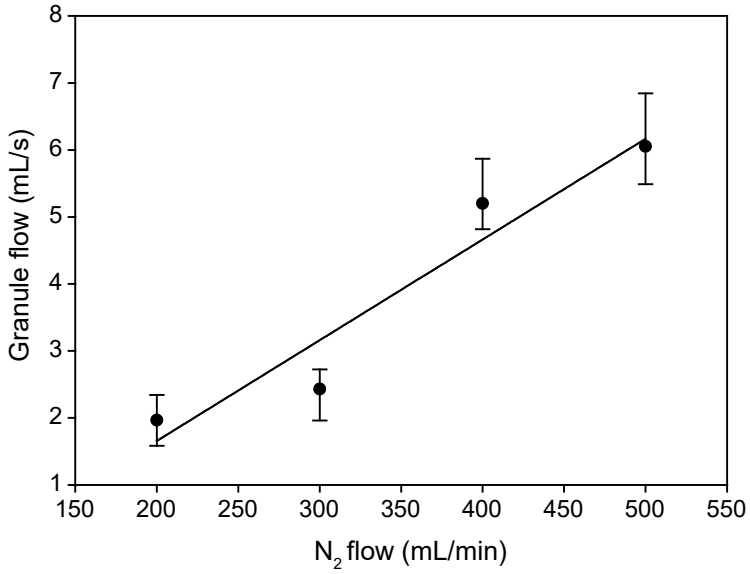

Figure S3. Granule flow from the gas lift resulting from changes in the N_2 gas flow into the gas lift.

Dettifoss, Iceland

Chapter 4

Making the best use of capacitive current: comparison between fixed and moving granular bioanodes

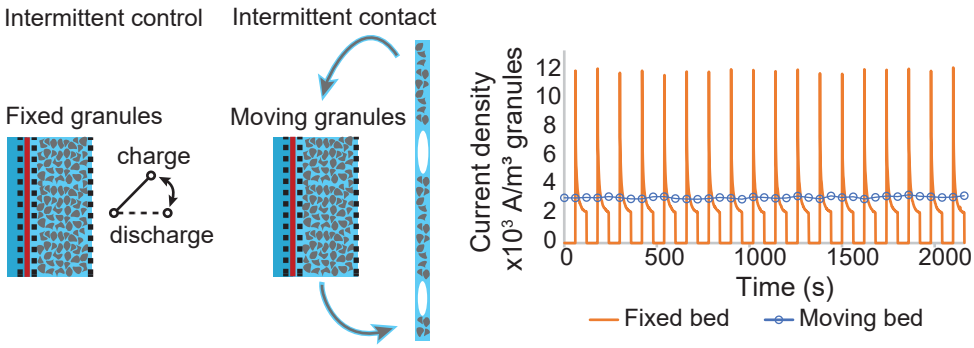

This chapter is published as:

C. Borsje, T. Sleutels, W. Zhang, W. Feng, C.J.N. Buisman, A. ter Heijne, Making the best use of capacitive current: Comparison between fixed and moving granular bioanodes, J. Power Sources. 489 (2021) 229453. doi: 10.1016/j.jpowsour.2021.229453.

Abstract

Capacitive bioanodes can be used to improve current production in bioelectrochemical systems. Capacitive bioanodes can be used to improve current production in bioelectrochemical systems for combination of energy recovery and wastewater treatment. Here, we compared current production in fixed and moving bed capacitive bioanodes. For fixed bed bioanodes, the recovered charge was studied as a function of the discharge current collector position and the thickness of the granule bed. The most capacitive charge was recovered from the current collector closest to the membrane. Increasing bed thickness from 5 mm to 10 mm resulted in a 1.6 times higher current density per membrane area. These findings were used to improve the design of a moving bed reactor, where granules moved through a discharge cell and were recirculated using a gas lift. The moving bed produced a current of 43 A/m^2, about 2 times the fixed bed current over the full charging and discharging cycles. The relatively short discharge time and long charging time of the moving bed as compared to the fixed bed bioanodes led to higher capacitive currents. The design of the discharge cell and the ratio between charge and discharge times can be further optimized to make better use of stored charge of the granular capacitive bioanodes.

4.1. Introduction

A sustainable approach to wastewater treatment should allow for recovery of energy and nutrients [162]. Energy can be recovered using bioanodes in bioelectrochemical systems (BESs), to directly produce an electrical current from the biological oxidation of dissolved organic matter in wastewater. Bioanodes are anodes in a BES on which an electroactive biofilm grows [163]. The current can be used to produce electrical power in a microbial fuel cell [36], to produce valuable products, like hydrogen [38,137] and hydroxide [137,138], or to drive separation processes such as desalination [164], recovery of ammonia [43,139,144] and recovery of phosphate [44,140], in a microbial electrolysis cell. Scaling up these systems, however, is still a challenge [89], since it often involves energy losses and contact resistance, which reduce current densities and conversion efficiency compared to lab-scale systems [100]. Research and development has focused on electrode materials [165–168], microbial communities [92,169–176] and reactor design [72,96,110,141,177–179], but has yet to lead to a scalable and efficient cell or stack design [89,116,165,176,180] whereas small-scale stacked MFCs have been demonstrated [181].

High surface area for biofilm attachment has been shown to improve current densities compared to low surface area electrodes [182,183]. This attribute was used to form packed bed electrodes with high current and power densities using graphite [78,184,185] or activated carbon granules [186]. Activated carbon has a large surface area because of a high porosity. On this large surface area (in the order of 1000 m^2/g) an electrical double layer can be formed, which can be used to store electrical and ionic charge [100]. This charge storage property of activated carbon enables intermittent operation of capacitive bioanodes as charge, produced by the bioanode, is stored when the anode is disconnected from the electrical circuit. When the capacitive bioanode is then connected to the electrical circuit, the stored charge produces a capacitive current, on top of the faradaic current from acetate oxidation at the bioanode, resulting in a high (peak) discharge current.

The implementation of capacitive bioanodes has followed two directions [100]: a bioanode with an internal or external capacitor [84–88,101,128,147,148,187–194], or fluidized capacitive granules [96,104–107,114,115,150,195–197]. The main difference between the two is that the bioanode with a capacitor is used with intermittent control, which requires a period without producing an electrical current in the circuit [85], whereas the fluidized granules are in intermittent contact, where the capacitive granules only discharge when they are in contact with the current collector [96]. Fixed capacitive bioanodes allow improved stability for scale up using stacked MFCs [192,198,199] and use of temporary operation for applications like robots and remote sensors [149]. The main advantage of the fluidized bed capacitive bioanodes compared to fixed capacitive bioanodes, is the ability to continuously produce a current [96,107]. The fluidized bed bioanode continuously produces a capacitive current on top of the faradaic current as charged particles pass the discharge cell. The fluidization also improves access to substrate [196] and promises to decrease clogging issues related to wastewater treatment since it allows for physical separation of the charging and discharging process [107].

Several types of fluidized bed bioanode reactors have been developed [116]. Mechanical stirring [104,196], liquid [105–107,114,127,150,195–197] and gas [96,107] have been used to move the charged granules to induce intermittent contact with the discharge anode, which generated an electrical current. A moving granular bed reactor has been developed, in which the granules were fluidized in a gas lift and recirculated through settling on top of a moving granular bed. The granules were discharged in an internal discharge cell through which the granular bed moved [107]. When normalized to the volume of the discharge cell, this moving bed reactor had a higher current than a fixed granular bed, however, per total volume of granules, the current was lower. The current was limited by incomplete discharge of the capacitive granules by an inadequate total granule volume to discharge surface area ratio [107]. To further develop the moving granular bed system, it is crucial to understand what are the factors that influence its performance. One aspect that needs further study is how the current of the moving granular bed compares to a fixed granular bed. Although fixed and fluidized capacitive bioanodes have been studied separately, a comparison between the two systems is lacking. In addition, it is not known how the thickness of the granule bed and the position of the current collector affect the performance of the capacitive bioanode. This information is important to assess which system is most attractive to recover current from capacitive bioanodes. The aim of this study was therefore to investigate and compare the capacitive and faradaic charge transfer in fixed and moving bed capacitive bioanodes using a discharge cell with similar design.

4.2. Materials and methods

Reactor setups

Discharge cell

The fixed and moving granular bed bioanode setup used a similarly designed electrochemical discharge cell [200]. **Figure 4.1** shows a schematic view on the fixed and moving bed discharge cells in three different configurations. The fixed bed cells with 5 and 10 mm bed width had two (inner, outer) or three (inner, middle, outer) electrodes serving as current collectors respectively. The moving bed cell was operated with only one

(inner) electrode operating as current collector and used the second (outer) electrode for measurements instead of discharge. The cathode flow compartment (10 mL) was filled with carbon felt. The electrodes were titanium with Pt/Ir mixed metal oxide coating (Magneto Special Anodes BV, Schiedam, Netherlands). The effective cation exchange membrane area was 22.3 cm^2 (Ralex CMH-PP, Mega c.z., Stráž pod Ralskem, Czech Republic).

Fixed bed setup

The anode flow compartments of the fixed bed systems were 3D printed structures (PLA, printed using Ultimaker 2+, Ultimaker, Utrecht, Netherlands) modeled after previous cell designs [75] (see CAD images in the supporting information (SI), Figure S1). The anode was formed by granular activated carbon granules, which filled the anode compartment. The granules were kept in the flow channel using a fine plastic mesh which was glued on the entrance and exit of the 3D structure. On the other side of the inner current collector, the cation exchange membrane separated the bioanode from the cathode compartment. To ensure a watertight seal, injectable gasket (Repliset F5, Streurer GmbH Nederland, Maassluis, Netherlands) was used between the anode current collectors and the 3D printed structure. The rest of the cell was sealed using gaskets and O-rings [200]. The total anode volume, including the recirculation volume was 100 mL. The total catholyte volume was 67 mL and the catholyte was continuously sparged with N_2, just before entering the cell. Additional 10 mL flow channels were added to the outside of the cell and used to maintain the cell at 30° C using a heating bath (Immersion circulator DC10, Thermo Fisher Scientific, Breda, Netherlands).

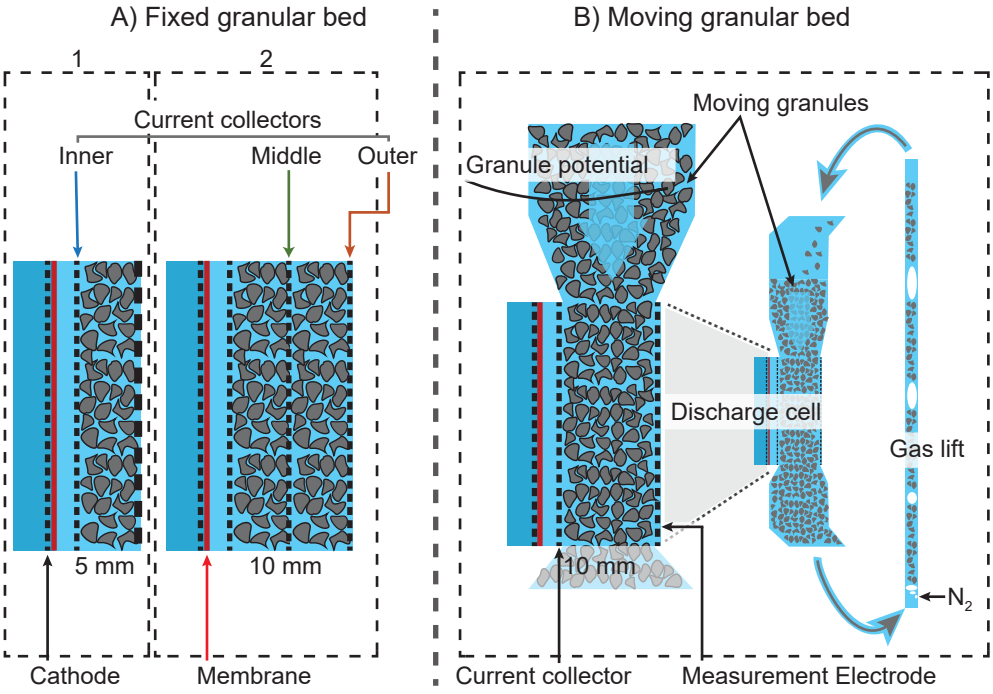

Figure 4.1. A schematic overview of the three different cell configurations. The fixed granular bed cells were (A1) 5 mm and (A2) 10 mm thick, with 2 respectively 3 anodes in the bioanode compartment. The moving granular bed (B) had 1 current collector in the discharge cell.

Moving bed setup

The moving granular capacitive bed bioanode setup, an adaption from previous design [107], consisted of 2 main parts: the discharge cell and a two-part glass flow volume (produced by Laboratory Glass Specialists B.V, Assen, Netherlands). The setup was designed after the previous moving bed reactor. **Figure 4.1B** shows the moving bed reactor, with the discharge cell and recirculation of granules. In the supporting information, CAD images of the reactor and discharge cell are shown in Figure S2. The discharge cell had an anode flow channel for the moving granular bed, which was formed by two 15.8 cm long transparent PMMA parts with a thickness of 10 mm. The distance between anode current collector and cathode current collector was 5 mm.

This 5 mm space contained the cation exchange membrane and plastic mesh, to prevent membrane movement and to prevent granules from filling the space. For normalization of the current, the exposed membrane area of 22.3 cm^2 and a granule volume of 22.3 cm^3 (in the 10 mm width next to the membrane) were used. The parts of the current collectors not in contact with the granules were coated with a non-conductive paint to prevent biofilm formation. The discharge cell was connected to the rest of the reactor by two PMMA funnels, above and below the cell. The granules were circulated through the system and moved through the discharge cell into the bottom part of the reactor. At its lowest point, the granules were transported up to the top of the flow volume via a gas lift using N_2 gas. From the top of the gas lift, a PVC tube with 9 mm inner diameter, the granules settled down through the next part of the reactor. Above the discharge cell, the granules settled on the top of the moving granular bed. The gas flow was controlled at 140 mL/min and monitored using a mass flow controller (Massstream D-6311 with ±1% accuracy, Bronkhorst Nederland B.V., Veenendaal, Netherlands). At the top of the reactor, the gas was separated from the liquid and granules. Further up, a narrow opening prevented the granules from flowing out, but allowed the electrolyte to overflow into a recirculation bottle. The anode had a total volume of 1458 mL, of which 1083 mL was anolyte and the rest were granules. The catholyte circulated through a similar recirculation volume.

Medium, inoculum, and granules

The medium for the bioanodes was mixed from carbon source and nutrient feed bottles. The carbon feed contained 40 mM acetate, 10 mM KH_2PO_4 and 10 mM K_2HPO_4 and 10 mM sodium 2-bromoethanesulfonate (2-BES). The nutrient feed contained 20 mM KCl, 20 mM NaCl, 10.4 mM NH_4Cl, 1.4 mM $CaCl_2$, 0.08 mM $MgSO_4$ and trace elements solution 0.2 mL/L [154]. The catholyte was a 50 mM phosphate buffer. Both the anolyte, after mixing, and the catholyte pH were 6.9. The anolyte feed bottles were constantly flushed with N_2 gas and the solutions were fed at a 1:1 ratio into the recirculation volume at 0.084 and 1.8 mL/min (fixed resp. moving bed) to reach a hydraulic retention time of 10 hours. For both systems, the pH was controlled at 6.9 in the recirculation of the anolyte through NaOH dosing. The recirculation was set to 80 mL/min for both anode and cathode. The catholyte was continuously sparged with N_2 gas just before entering the cell, to limit H_2 crossover over the membrane. The inoculum was taken from acetate-fed bioanodes that were operated with 2-BES to suppress methanogenic growth [153].

Table 4.1. Setup parameters in the experiments.

Cell	Bed width (mm)	Granule volume (mL)	Charging time (s)	Discharging time (s)	Discharge potential (V)
Fixed bed replicate 1	5	17.8	60	60	-0.3 V
Fixed bed replicate 2	5	16.4	60	60	-0.3 V
Fixed bed	10	27.8	60	60	-0.3 V
Moving bed 1	10	375	363±32	23±2	-0.2 V & 0V
Moving bed 2	10	375	320±18	20±1	-0.2 V & 0V

The activated carbon granules (HR5, Eurocarb, UK) were washed and wet sieved between 0.5 and 0.8 mm sieves (stainless steel sieves, VWR, Netherlands). The granules had a bulk density of 0.486 g/cm^3 and surface area of 1100 m^2/g between 0.3 and 50 nm pore width [107]. **Table 4.1** shows the volumes of the granules as used in the experiments. The volume of the granules in the fixed bed was calculated from the dry weight and bulk density. The volume of the granules in the moving bed was measured in a measurement cylinder.

Electrochemical control and measurements

The electrochemical cells were controlled using a potentiostat (n-Stat with sModules, Ivium Technologies B.V., Eindhoven, Netherlands), where the potentials were measured against an Ag/AgCl/3M KCl reference electrode (+205 mV vs SHE)(QM711X/Gel, ProSense, Oosterhout, Netherlands). All further potentials are reported referenced to the Ag/AgCl reference electrode potential. The reference electrodes in the fixed bed reactor were connected via a 3M KCl salt bridge to a capillary (4 mm diameter, Prosense, Oosterhout, Netherlands), which was placed in anolyte flow before entering the anode flow compartment.

In the moving bed reactor, the capillaries were placed in the granular bed: one in the middle of the discharge cell, and one close to the granule potential probe at the top of the granular bed [107]. This probe was a Pt/Ir wire (Pt/Ir 80:20, Advent-RM, Oxford, United Kingdom) placed in the granular bed before the granules entered the discharge cell.

Fixed bed operation

The fixed bed bioanodes were first controlled at -0.3 V, using all current collectors combined to allow the biofilm to grow over the whole granular bed. After the continuous current was stable, the intermittent experiments were performed.

The multiple current collectors in the fixed bed setups allowed multiple combinations of current collectors to control. The 5 mm cell had three control options (inner, outer and both combined) and the 10 mm cell had seven control options.

Each experiment consisted of a continuous control phase of 1000 seconds at -0.3 V, followed by 150 cycles of 60 seconds open circuit charging, followed by 60 seconds discharging at -0.3 V. After the intermittent cycles, a second 1000 seconds of continuous control at -0.3 V ended the experiment. The faradaic current produced by each current collector was calculated as the average of the last 100 seconds of continuous potential control after the intermittent experiment. The faradaic current was used to calculate the faradaic charge transferred over 20 cycles by multiplication by 20 (the number of cycles) and 60 (the discharging time per cycle). The faradaic charge was then used to determine the capacitive

charge by subtracting it from the total recovered charge over the same 20 cycles [85]. The current and the potential of all current collectors were measured every second. The average charge per cycle was calculated using the last 20 cycles. A representative cycle was calculated by averaging the current over 20 cycles for every time point. The results of the replicate 5 mm reactors were averaged.

Moving bed operation

The current collector in the moving granular bed was continuously controlled at -0.2 V in the first 27 days for Moving bed 1 and in the first 40 days for Moving bed 2. The current became positive after 10 days, which was taken as the start of the intermittent experiment. The anode potential was changed from -0.2 V to 0 V on day 27 and 40, when the granule activity test (see 4.2.) seemed to stabilize, to study the effect of anode potential on the produced current. The potential was controlled at 0 V until for the rest of the experiment. The potential of the measurement electrode in the discharge cell (see SI Figure S3) and the potential of the granules were collected every 60 seconds, together with the anode current collector potential and current. The measurement electrode was further used in combination with the current collector to measure the resistance over the granular bed. During these resistance measurements, the current collector potential was not controlled and electrochemical impedance spectroscopy (PGSTAT302N with FRA32M, Metrohm Autolab, Utrecht, Netherlands) was used to scan 100 times at controlled current of 0±1 mA and 5 kHz, after an open circuit period of 5 minutes. The real part of the impedance represented the granular bed resistance.

The capacitive granules were charged and discharged in the moving bed through intermittent contact with the current collector by recirculating the granules through the discharge cell. The granule velocity was determined using video analysis of the granular flow in the discharge cell (see 4.2.). The retention time of the granules was 23±2 seconds in the discharge cell (discharging) and 363±32 seconds outside the discharge cell (charging) for Moving bed 1 (20±1 seconds resp. 320±18 seconds for Moving bed 2).

Other analyses

Moving bed granule flow velocity

The moving bed flow velocity was used to determine the charging and discharging time. Videos (1080p, 60 fps using Nikon D750 and Sigma 105 mm F2.8 EX DG at F11) were recorded of the moving particles in the discharge cell. A graduated scale (5 mm intervals) was drawn on the transparent side through which the granular flow was observed (see example still image with flow path in SI Figure S4). For each video, the scale was determined in pixels/cm. Using Fiji ImageJ2 [201], flow paths were determined for 5 granules per video, on days 10, 17 (Moving bed 2), 28, 47 and 66 (Moving bed 1). The recorded length and timestamps for the first and last frame of the path were used to determine the superficial flow velocity (cm/s). The volumetric flow was calculated by multiplying the flow velocity with the discharge area (22.3 cm^2). The recirculation time of the granules was calculated by dividing the total volume of the granules by the volumetric flow. The discharging time was calculated by dividing the length of the discharge cell (exposed to the membrane area for 10 cm) by the superficial flow velocity. The charging time was calculated by subtracting the discharge time from the recirculation time.

Bioanode activity of moving bed granules

An external test cell, developed in our previous study [107], was used to measure the bioanode activity of a small sample of granules taken from the reactors (minimum of 3 times on 1 day, per setup). The bioanode granules were first allowed to charge in open circuit until -0.45 V and then discharged at -0.2 and 0 V for 600 seconds per step, with the current and potential logged every second. The activity of the granules was determined as the average current over the last 60 seconds, normalized to the volume using the dry weight and bulk density. The electrolyte had the same composition as the influent of the moving bed systems.

Chemical analyses

The precipitates on the current collectors of the moving bed were identified using X-ray diffraction (XRD) and Energy Dispersive X-ray spectrometry (EDS) to confirm elemental composition. XRD was performed using a Bruker D8 advanced diffractometer with a Cu source. Analysis was performed over a range of 10 to 60 degrees in 4 degrees per minute. EDS was performed using a scanning electron microscope (JSM-6480LV, JEOL (Europe) B.V., Nieuw-Vennep, Netherlands) and EDX spectrometer (Oxford Instruments x-act SDD energy dispersive x-ray spectrometer, Oxford Instruments NanoAnalysis, Halifax, United Kingdom).

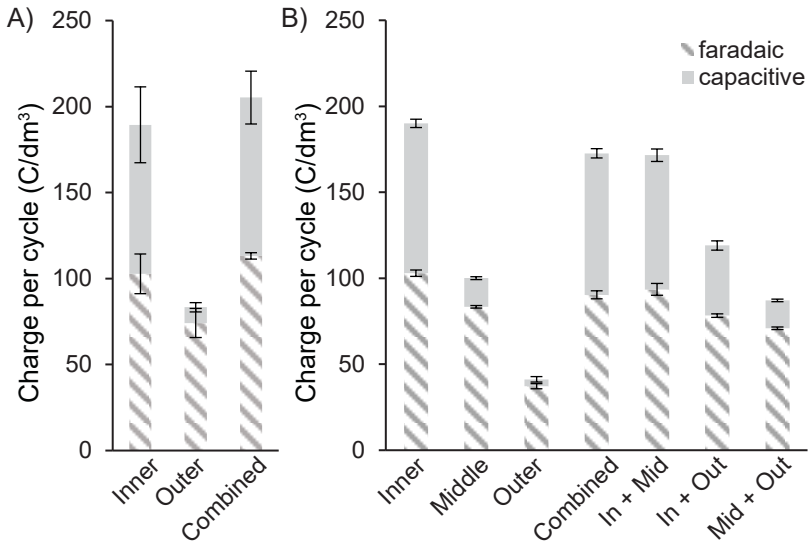

Figure 4.2. The average charge produced in 1 cycle of charging and discharging, normalized to the volume of granules in the granular bed. A) for 5 mm granular bed width, averaged over the replicates, and B) for 10 mm bed width. The Combined current collector combined all current collectors, and In + Mid (and similar in B) indicate a combination of controlling the inner and middle current collector simultaneously.

4.3. Results and discussion

Fixed bed: discharging closest to the membrane is most efficient to recover stored charge

The fixed bed granules were charged and discharged in intermittent operation to investigate the effect of the position of the anode current collector and the width of the granular bed on the recovered charge. The produced current was recorded and analyzed for each anode current collector and for each combination of anode current collectors in the granular beds. Before the start of the intermittent experiments, the reactors produced an average 14 A/m^2 in the 5 mm cells and 33 A/m^2 in the 10 mm cell using all current collectors combined. The average charge produced in one discharge cycle, normalized to volume of granules (see **Table 4.1**), is shown in **Figure 4.2**, where the total charge is the sum of the faradaic and capacitive charge (see section 4.2.). For both bed thicknesses, the inner current collector produced higher total charge than the current collectors further away from the membrane. When the inner current collector was combined with one of the other current collectors, the produced charge was similar or lower compared to the inner electrode alone.

The total charge per cycle was on average 2.3 times higher when the inner current collector was used compared to the outer current collector in the 5 mm cells. For the 10 mm granular bed, the total charge was 4.6 times higher for the inner current collector compared to the outer current collector.

The total charge was separated into faradaic and capacitive charge (see also section 3.2). When the inner current collector was used, the contribution of capacitive charge to total charge was considerable and constituted about 34-48% of the total charge. At increasing distance from the membrane, the contribution of the capacitive charge decreased strongly, whereas the faradaic charge showed a less strong decrease. The inner current collector is thus crucial to produce a high capacitive current.

The wider discharge cell produced more overall charge

In the previous section the total charge was normalized to the membrane surface area. This normalization gives insight in the performance of the additional granules in the thicker bed compared to the thinner bed. In this section the total charge is normalized to the granule volume, which gives insight in the activity per granule. In **Figure 4.3**, the current and charge produced during a single cycle is shown for the inner current collector of the 5 mm and 10 mm granule bed. **Figure 4.3A and B** show the current and charge normalized to the volume of the granules in the granular bed and **Figure 4.3C and D** show the current and charge normalized to the membrane surface area. **Figure 4.3A and 18C** show a representative charge-discharge cycle for the inner anodes of both cells, which is characteristic for capacitive bioanodes [85,86]. During the open circuit period, no current was released to the anode and charge is stored in the granules [85,87]. During discharging, the stored charged was released in a capacitive peak current, which decreased towards the faradaic current. The striped area in **Figure 4.3C and D** shows the charge from the faradaic current of the granular bed (13 A/m^2 for 5 mm, and 21 A/m^2 for 10 mm), and the grey area corresponds to the capacitive charge in **Figure 4.3C and D**. Looking at **Figure 4.3D** we can see that the 10 mm granular bed produced 1.6 times more overall charge than the 5 mm granular bed when normalized to membrane area. At the same time, the charge per volume of granules (**Figure 4.3B**) was similar in the 5 and 10 mm bioanodes. Therefore, the additional granules in the wider granule bed added to the overall charge recovered, while the charge per granule was the same regardless of bed width.

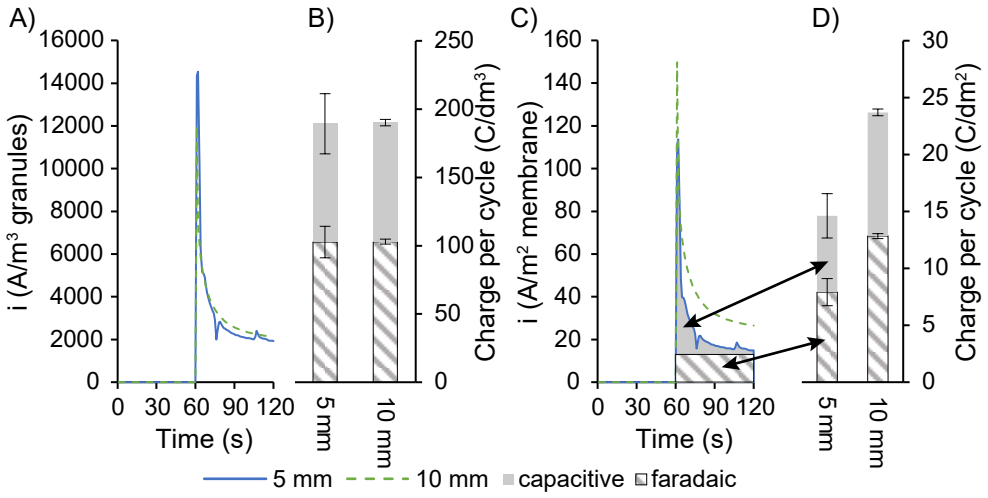

Figure 4.3. The charge and current produced in 1 representative cycle of charging and discharging, averaged over 20 cycles, for the inner anode for the 5 mm, averaged over the replicates, and 10 mm granular bed width. A) and B) Current and charge density normalized to volume of granules in the discharge cell. C) and D) Current and charge density normalized to exposed membrane area. The striped area under the graph shows to the recovered faradaic charge in the cycle of the 5 mm cell, the grey area shows the recovered capacitive charge.

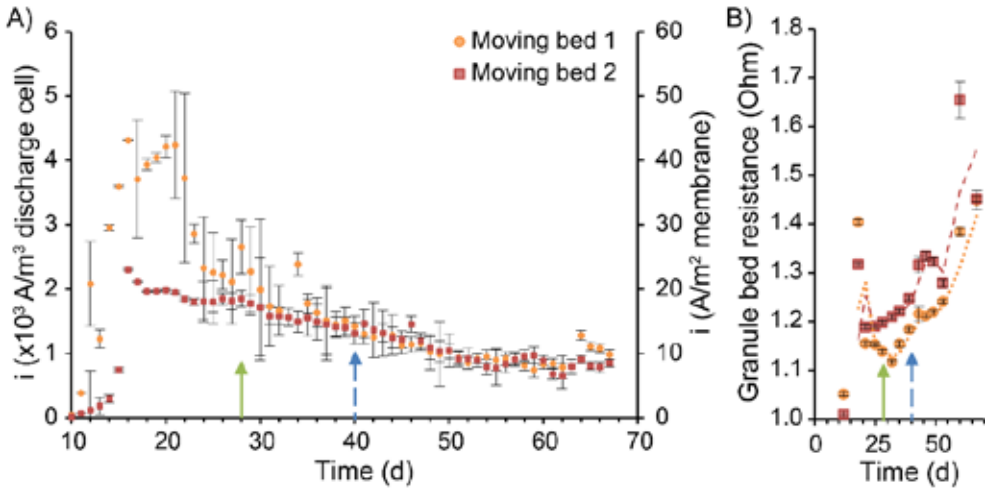

Figure 4.4. A) Daily average of the produced current, after the current became positive, normalized to the volume of granules in the discharge cell, and to the exposed membrane area. B) The resistance over the granular bed, as measured between the discharge anode and the second electrode in the discharge cell using impedance spectroscopy at 5 kHz. The arrows show when the discharge anode potential was changed from -0.2V to 0V (straight for moving bed 1, dashed for moving bed 2). The error bars are the standard deviation over the day.

Moving bed bioanode reached a high current, which decreased with time due to increasing granular bed resistance

Since the fixed bed bioanodes showed that the inner current collector resulted in the highest charge, the two moving bed bioanodes were discharged using the current collector closest to the membrane. The bed width of the moving bed bioanodes was 10 mm, which was required to obtain granular flow with the size of the granules used [202].

In contrast to the fixed bed intermittent control, the discharge electrode control in the granule bed was continuous, while the capacitive granules were moving between the discharge cell (where they released charge) and the rest of the reactor (where they were charged). The granules moved down in the bed through the discharge cell and were recirculated using a gas lift, which resulted in an average discharging time of 23 seconds and charging time of 363 seconds for Moving bed 1 (see **Table 4.1**). **Figure 4.4** shows the current density of the replicate moving bed bioanodes, which were operated for 67 days. The current density is normalized to the volume of granules in the discharge cell and to the membrane area in the discharge cell. The current density of both systems increased quickly during the first 16 days, after which the current density reached a maximum. At the same time the potential of the granules, as measured before entering the discharge cell, reached a potential close to thermodynamic equilibrium of acetate oxidation (-0.49 V), indicating fully charged granules [107](see SI Figure S3). Moving bed 1 reached a maximum current density of $4.3x10^3$ $A/m^3_{granules}$ (257 A/m_3 total volume of granules). The current of Moving bed 2 was always lower than the current in Moving bed 1 and reached a maximum of $2.3x10^3$ $A/m^3_{granules}$. During the experiment, the discharge potential was increased from -0.2 V to 0 V (see Methodology), on day 27 for Moving bed 1 and on day 40 on Moving bed 2, but no effect on the current density was observed. After the high current density, the current decreased over the rest of the experimental time.

To identify if the current was related to the resistance of the granule bed, we measured the ohmic resistance over the moving granular bed between the two electrodes on each side of the moving bed in the discharge cell. **Figure 4.4B** shows the ohmic resistance during the experiment. The resistance increased over time, as the current decreased. The resistance for Moving bed 1 was lower than for Moving bed 2, which matches with the higher current of Moving bed 1. At the end of the experiment, the cells were opened to identify potential causes for the increase in resistance. We observed that the mesh openings in the discharge anodes were partially filled with hydroxyapatite, $Ca_5(PO_4)_3(OH)$, which are solids (identified using XRD and EDS measurements) in which the activated carbon granules were trapped (see SI, Figures S5, S6 and S7). The increasing resistance over the granular bed may thus be caused by these precipitates.

The activity of the granules increased but the moving bed current did not

To measure the biological activity of the granules in an external test cell, granules were taken from the moving bed reactors: in triplicate per reactor per sampling day. The activity was measured at a constant potential as an indicator of the performance of the biofilm on the granules [61]. **Figure 4.5A and B** show the activity of the granules of Moving bed 1 and 2 for the discharge potentials of -0.2 V and 0 V. Activity is expressed as current normalized to the volume of granules in the sample (see section 4.2.). The activity of the granules from both moving beds increased over time, where Moving bed 1 showed higher activity than

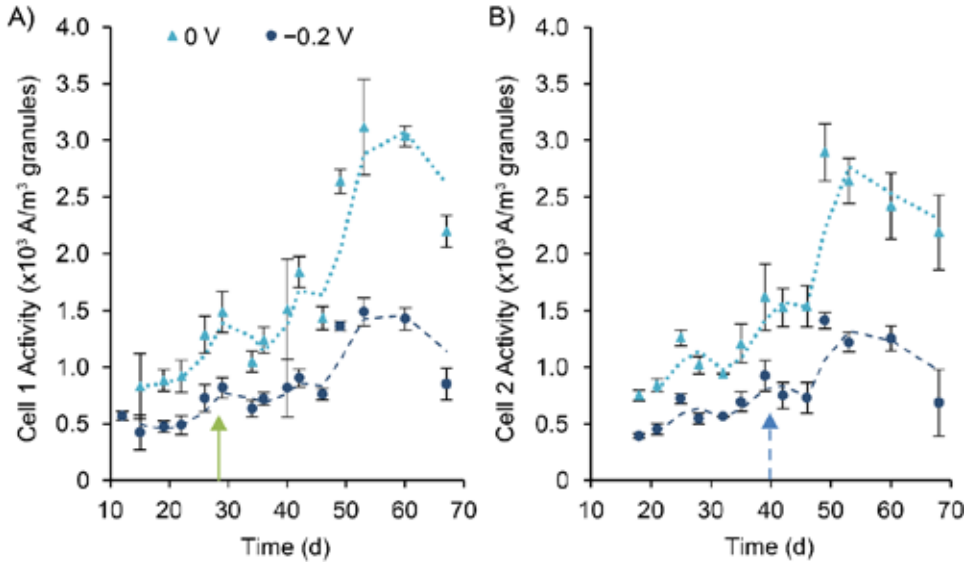

Figure 4.5. The daily activity of the granules in the moving bed, as measured in the external test cell for (A) Moving bed 1 and (B) Moving bed 2. The values are averaged over 3 samples, with the error bars showing the standard deviation. The line shows the moving average between 2 points to guide the eye. The arrows show the time of change in anode potential (green for cell 1, dashed blue for cell 2).

Moving bed 2 over the whole experiment, which is in line with the higher current observed for Moving bed 1. In our previous study, we correlated an increased activity with increased amounts of biofilm on the granules [107]. The increasing activity of the biofilm on the moving bed granules in this study, however, did not correspond to an increased current density in the reactors, most likely due to the increase in internal resistance of these reactors (**Figure 4.4B**).

Discharge cell current density in the moving bed was higher than in the fixed bed

We investigated the performance of the moving bed bioanode as compared to the fixed bed bioanode operated in intermittent mode. **Table 4.2** shows an overview of the best performance and operational parameters for the 10 mm fixed granular bed bioanode, operated for 24 days, and the moving granular bed bioanode, 16 days after start.

The discharge current density of the moving bed was slightly higher than that of the fixed bed. In the moving bed, there is a high contribution of the capacitive current to the total current, as the moving bed continuously discharged fully charged capacitive granules.

Table 4.2. Comparison between the 10 mm fixed granular bed, discharged at the inner current collector, and best performing moving granular bed. The discharge and capacitive current densities are the average current calculated from the charge per cycle, divided by 60 seconds of discharging.

	Fixed bed		Moving bed	
Volume of granules (mL)	27.8		22.3	
Growth time (days)	24		16	
Charging time (s)	60		363	
Discharging time (s)	60		23	
Potential difference (mV)	[a] 66		[b] 271	
Current density	[c] x10^3 A/ m$^3_{granules}$	[c] A/ m$^2_{membrane}$	x10^3 A/ m$^3_{granules}$	A / m$^2_{membrane}$
- Discharge (60 seconds)	3.2±0.0	39±0.3	[d] 4.3±0.6	[d] 43±6
- 1 cycle (120 seconds)	1.6±0.0	20±0.2	-	-
- Faradaic	1.7±0.0	21±0.4	-	-
- Capacitive	1.5±0.0	18±0.4	-	-

a) Calculated using the potential measured at the end of the charging time, averaged over the last 20 cycles of the intermittent experiment, and the discharge anode potential.
b) Calculated using the daily average of the potential of the granules before entering the discharge cell and the discharge anode potential.
c) Calculated from the average charge per cycle, over the last 20 cycles of the intermittent experiment.
d) Highest daily average current density in the discharge cell of Moving bed 1.

The potential difference between charged granules and the current collector, is the driving force behind the capacitive current [88]. The high capacitive current in the moving bed, compared to in the fixed bed, was the result of the high potential difference due to the fully charged granules that continuously entered the discharge cell for discharging. In the fixed bed, the potential difference, determined from lowest potential before discharging, was 66 mV: 4 times lower than in the moving bed.

The granules in the moving bed were always fully charged because the charging time was 6 times longer and the discharging time 3 times shorter. A short discharge time, though resulting in a high contribution of capacitive current, does not allow for large amounts of stored charge to be harvested [88]: the granules were likely already fully charged again shortly after being discharged. Thus, the ratio between charging and discharging time can be further improved. In the fixed bed, the low potential difference between granules and current collector indicates that the short charging time in the fixed bed was a limiting factor for the capacitive current since the granules were not fully charged.

Thus, the short discharge time and the long charging time in the moving bed thus resulted in a high capacitive current and thus in a higher discharge current density compared to the fixed bed bioanode. Of course, on top of this effect, the current from the moving bed reactor is continuous, in contrast to the intermittent discharging of the fixed bed, where current is only produced half of the time. The average current over the total charging and discharging cycle was therefore only half of the current density during discharge alone (see graph in graphical abstract). This shows how a moving bed can make the best use of the capacitive properties of bioanode granules.

4.4. Conclusions and outlook

We showed that the moving granular bed used properties of the capacitive bioanodes granules better than a fixed granular bed, since in the moving bed, the fully charged granules produced a continuous high capacitive current. In the fixed bed reactor, study of the position of the discharge electrode, showed that only the electrode closest to the membrane was effective in recovering the stored (capacitive) charge. Regarding bed thickness, an increasing thickness from 5 to 10 mm resulted in higher current density (normalized to membrane area), at similar volumetric activity. These results were used to design the discharge cell of the moving bed reactor. From the comparison between the fixed and moving bed, it was found that the short discharge time (~23 s) together with the long charging time (~363 s) in the moving bed resulted in a high capacitive current, though the granules were not discharged well. The design of the discharge cell and the ratio between charge and discharge times can be further optimized to make better use of stored charge of the granular capacitive bioanodes. In terms of design of the discharge cell, a better understanding of the discharge process is needed and how it depends on contact resistance and mass transfer processes.

Improving the discharging will also affect the charging process: a high capacitive discharge current would transfer more stored charge, making more charge storage capacity available to be charged again. The charging time of the moving bed is dependent on the volume of granules outside of the discharge cell, the recirculation rate, and the length and contact area for discharge. Improving the discharge process is thus important to optimize current production. These parameters can be further optimized to effectively charge and discharge the granules in the moving bed reactor to further improve the use of capacitive current from granular bed bioanodes.

Acknowledgements

This work was performed in the cooperation framework of Wetsus, European Centre of Excellence for Sustainable Water Technology (www.wetsus.nl). Wetsus is co-funded by the Dutch Ministry of Economic Affairs and Ministry of Infrastructure and Environment, the European Union Regional Development Fund, the Province of Fryslân and the Northern Netherlands Provinces. The authors thank the participants of the research theme 'Resource Recovery' for the fruitful discussions and their financial support.

Supporting information chapter 4

S1. CAD drawing of the fixed bed anode compartment

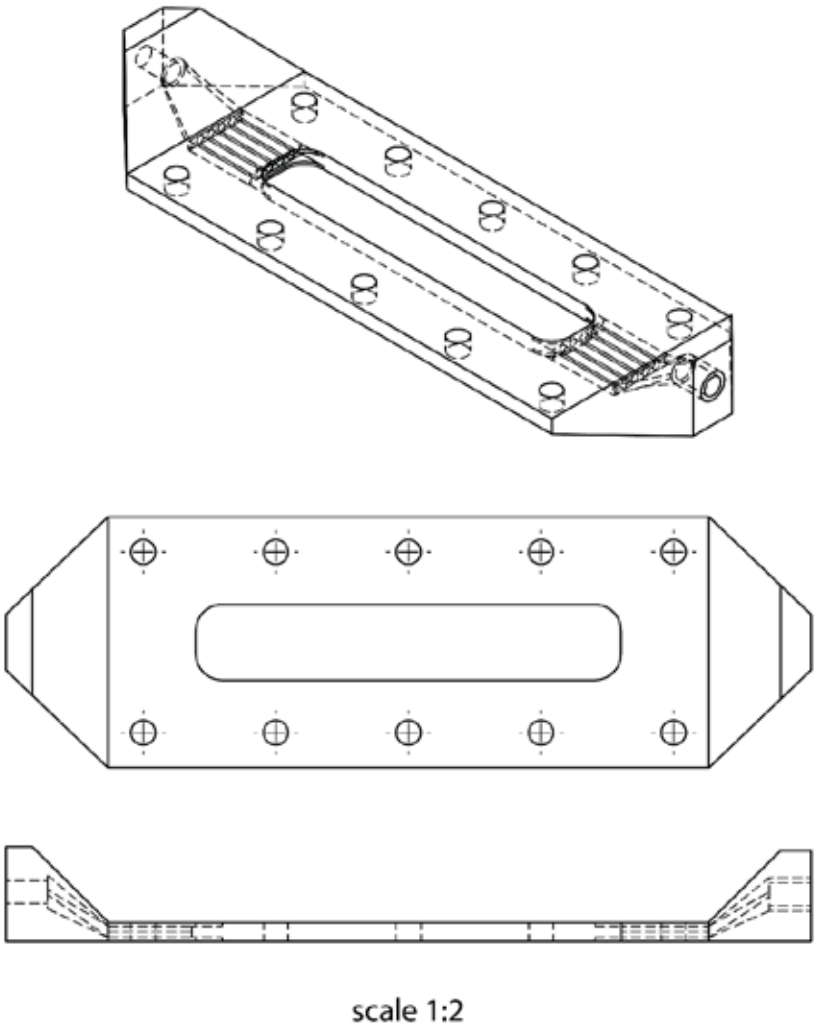

Figure S1. Anode compartment of the fixed bed setups. For the 5 mm bed, one of these was used, and for the 10 mm bed, two were attached with a current collector in between.

S2. CAD drawing of the reactor and discharge cell of the moving bed setup

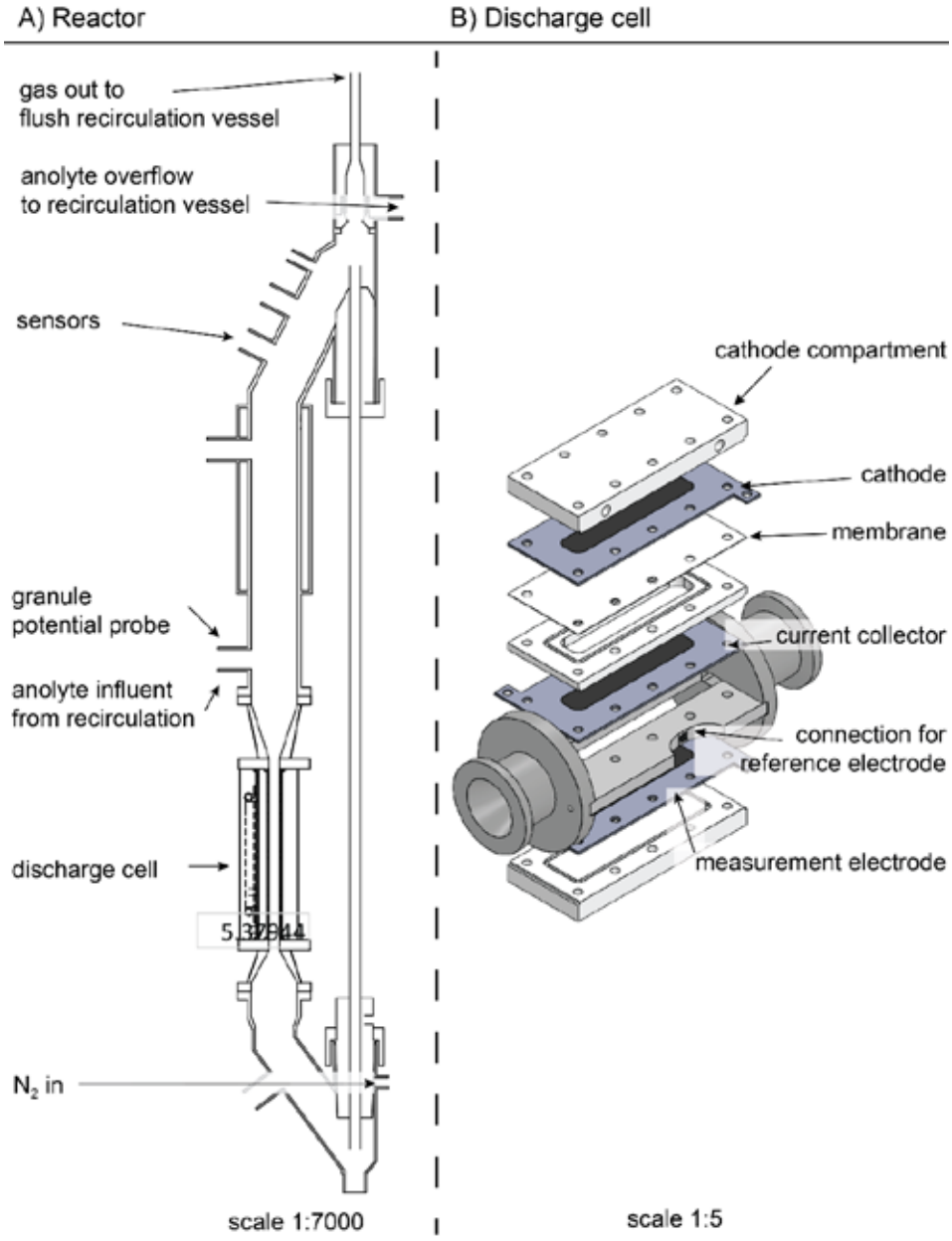

Figure S2. A) A CAD drawing of the moving bed setup. The discharge cell (B) was attached between two glass volumes. The granular bed started just above the discharge cell.

S3. Potentials in the moving bed reactor

In the moving bed setups, three potentials were measured: the current collector potential (as controlled by the potentiostat), the measurement electrode potential (on the other side of the 10 mm flow channel), and the granule potential (as the potential of a Pt/Ir wire with which the granules collided in the moving granular bed.

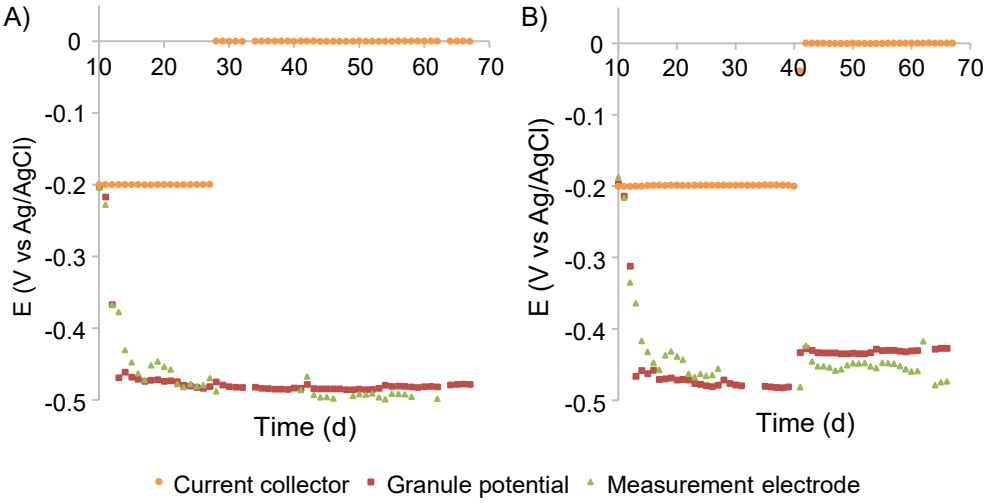

Figure S3. Measured potentials in A) Moving bed 1 and B) Moving bed 2.

S4. Flow analysis

The granules were tracked for an average of 190 frames. In Figure S1, the circled granule is an example of how the tracked granules were selected, and the arrow shows the path length. On the side of the granular flow, the graduated scale can be seen.

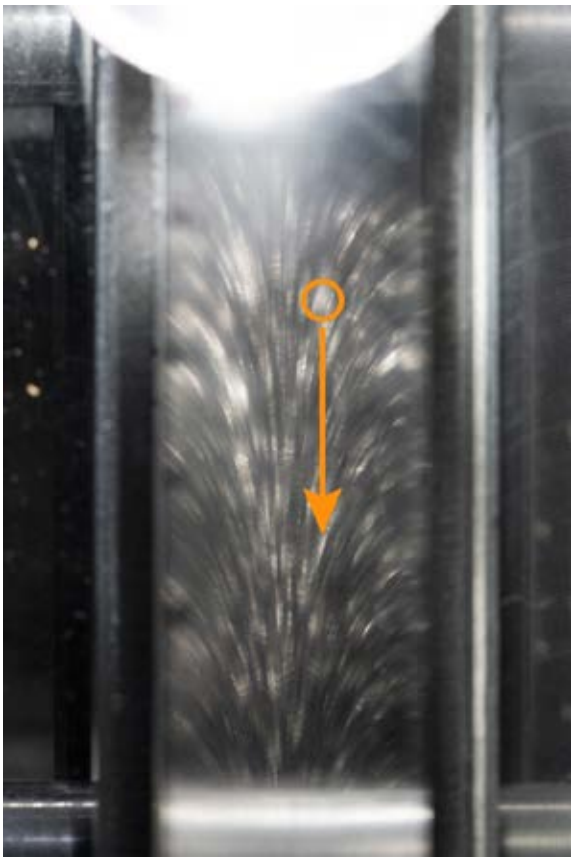

Figure S4. Single frame from a video used for analysis of granule flow.

S5. Trapped granules in hydroxyapatite

After opening the moving bed discharge cells, the current collector was washed. The mesh openings of the current collector contained precipitates, in which activated carbon granules were trapped. Figure S5A shows a photo of one of the current collectors, both of the Moving bed systems had similarly trapped granules. The precipitates were extracted and analyzed using X-ray diffraction (XRD) and Energy dispersive X-ray spectrometry (EDS) (see methodology). The EDS analysis was used to confirm the elemental spectrum used to determine the crystal structure. Figure S5B shows a scanning electron microscope image of the precipitates (2000x magnification), with the EDS spectrum of the same spot in Figure S6 and the weight and atomic mass percentage of the sample. The source of carbon in the EDS spectrum was likely from the support sticker used to hold the sample in the scanning electron microscope. The XRD spectrum, shown in Figure S7, shows the precipitates to be calcium hydroxyapatite: $Ca_5(PO_4)_3(OH)$. The sample was also analyzed for calcite ($CaCO_3$), which was an alternative explanation for the carbon in the EDS spectrum, but the XRD spectrum did not match.

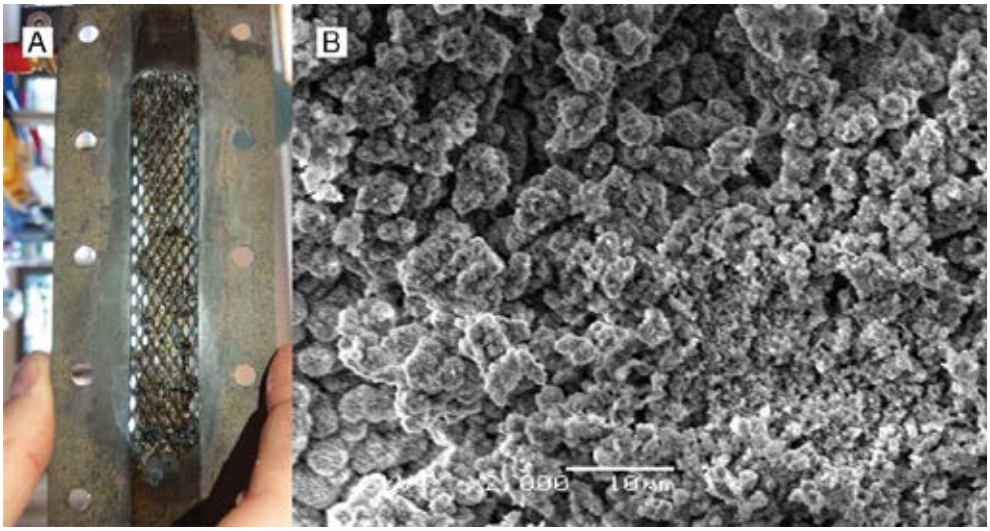

Figure S5. A) Current collector of the moving bed, after washing. Visible precipitates and trapped granules in and on the mesh electrode structure. B) Scanning electron microscope image of the precipitates, 2000x magnification.

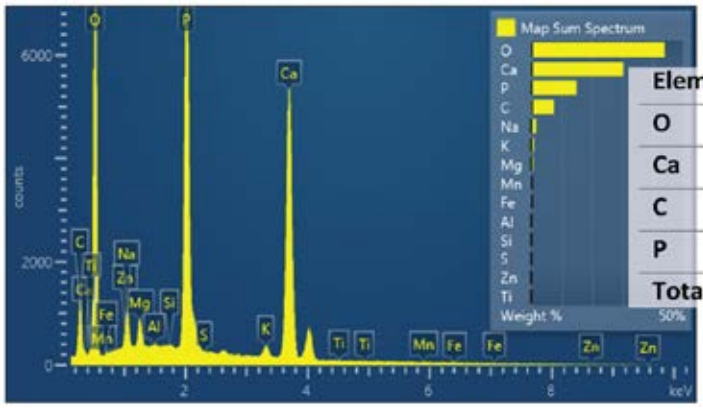

Element	Wt%	Atomic %
O	43.77	57.94
Ca	30.16	15.94
C	7.42	13.08
P	14.87	10.17
Total		97.13

Figure S6. Results of the Energy Dispersive X-ray spectrometry analysis of the precipitates. Insert table shows the largest contributors to the elemental spectrum of the precipitates.

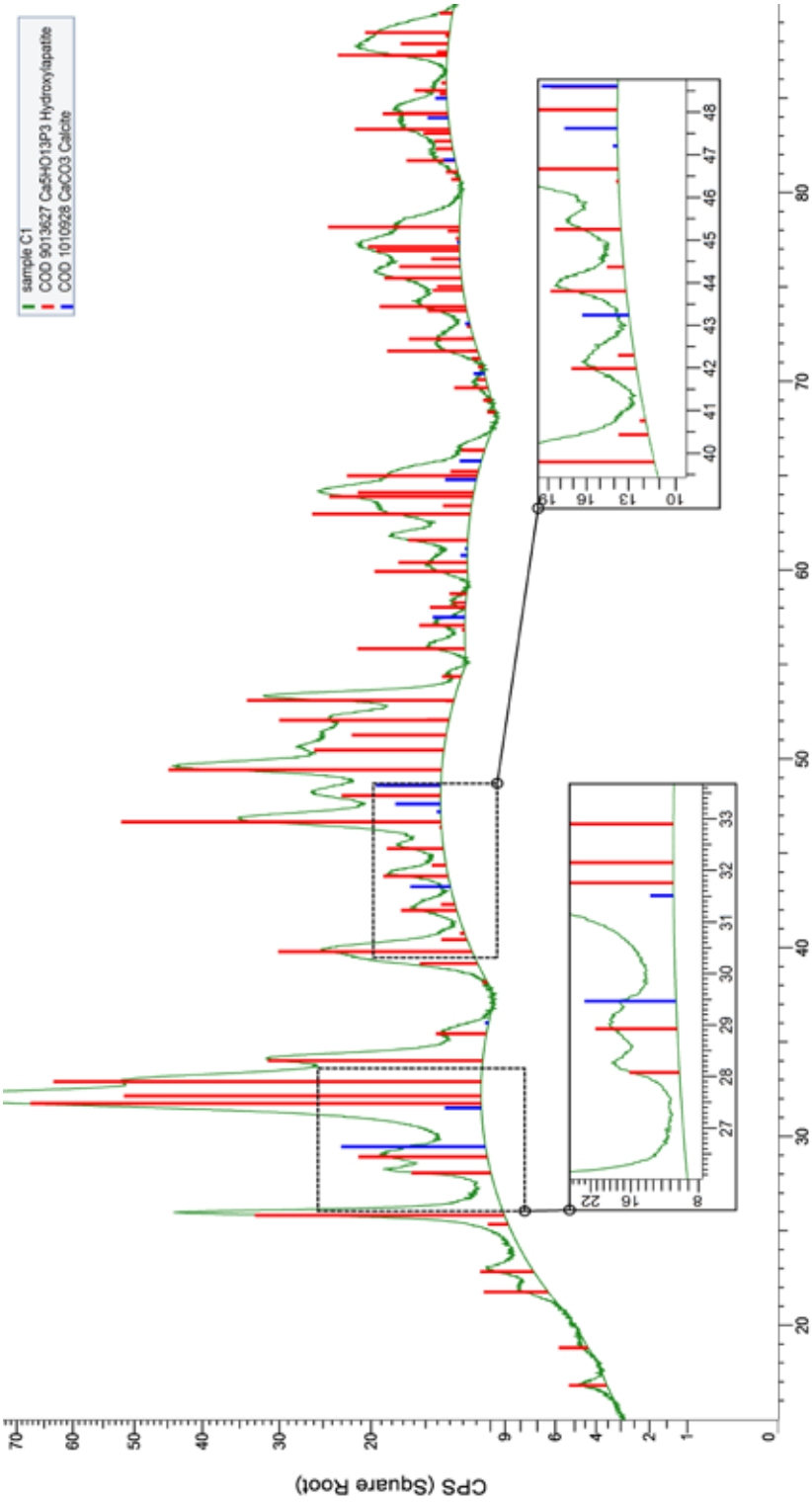

Figure S7. XRD spectrum of the precipitates in Moving bed 1. Green line is the sample, the red bars denote hydroxyapatite, blue bars denote calcite.

Svartifoss, Iceland

Chapter 5

Improving the discharge of capacitive granules in a moving bed reactor

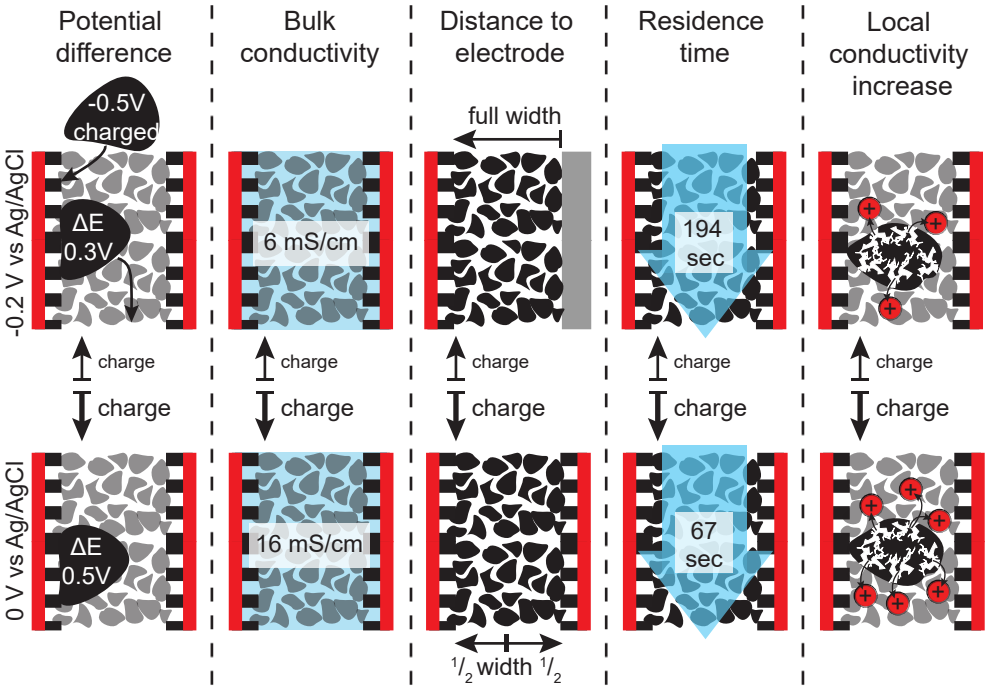

This chapter was submitted as:
C. Borsje, T. Sleutels, C.J.N. Buisman, A ter Heijne, Improving the discharge of capacitive granules in a moving bed reactor, J. Environ. Chem. Eng. (submitted 2021)

Abstract

Bioanodes can be used to recover the energy and nutrients from wastewater in bioelectrochemical systems. The use of capacitive electrodes can improve the current density produced by these bioanodes. Moving bed reactors are studied to produce high current densities, by using capacitive granules for charge storage and with a high bioanode surface area. The bioanodes store charge in the granules, which are intermittently discharged at a current collector. In principle, this allows for more current density in the electrochemical cell, because both faradaic and capacitive currents are harvested. One of the limiting factors of this technology is the capacitive discharge rate. In abiotic tests, the capacitive discharging was most improved by changes in potential difference between the current collector and charged granules (ΔE 0.3 and 0.5 V). Increasing the bulk electrolyte conductivity also increased the transferred charge, which could originate from the increased capacitance – as measured in a separate setup. Discharging from both sides of the granular bed, as compared to discharging from one side, reduced the maximum distance to the current collector, which increased the transferred charge, irrespective of an increase in bulk electrolyte conductivity. This showed the electrical resistance was more important in determining the transferred charge than the ionic resistance. Further analysis of the discharging process showed that discharging increased the local conductivity through the release of ions from the granules. This offers opportunities for the treatment of low conductivity wastewaters. These results provide new insights to further improve capacitive bioanodes.

5.1. Introduction

Recovery of energy and nutrients from waste streams is a necessity for a sustainable society. Municipal wastewater alone contains considerable amounts of nitrogen (14%), phosphorus (7%) and potassium (19%) required in agriculture [1]. Globally, wastewater contains enough energy to provide electrical power to 158 million households [1]. Bioelectrochemical systems (BESs) can be used to recover the energy and nutrients from wastewater [162]. An electrical current can be generated by electroactive bacteria growing on the anode of BESs. These bacteria oxidize dissolved organics in wastewater and release electrons to the electrode. The current can be used to generate electrical power in Microbial Fuel Cells [36] or produce H_2 [38,137], NaOH [137,138], H_2O_2 [37] or separate NH_3 [43,139,144], PO_4^{3-} [44,140] and NaCl [164] from wastewater. Low current densities have thus far limited the implementation of BESs [89,96]. Capacitive bioanodes have been shown to produce more charge than non-capacitive bioanodes by using intermittent charging and discharging [85,86]. Capacitive bioanodes are a special configuration of BESs, that use capacitive electrodes, which can store and release charge [100] in the pores of activated carbon [88]. The charge, stored during charging by the electroactive bacteria, is released as a capacitive current during discharging. This capacitive current is produced on top of the faradaic current produced directly by the bioanode [85]. The charge is stored by the formation of an electrical double layer: electrons are stored at the surface of the pores [100], and cations from the electrolyte are attracted, or anions are expelled, to balance the negative charge [120]. These cations are released during discharging, which is expected to increase the local conductivity of the electrolyte [96].

To be able to use large amounts of activated carbon granules, and thus a large specific surface area of electrode surface, as capacitive bioanodes, fluidized bed bioanode reactors have been developed [96,104–108,114,127,196,197,203]. The granules function as charge carrier as well as biofilm carrier, and are discharged at a current collector to produce a continuous current [108]. These granules are fluidized to make intermittent contact with a current collector, by stirring [104,196], liquid [105,106,114,127,196,197,203] and gas [96,107,108]. The reactors make use of intermittent charge storage of the capacitive bioanode granules by using the large ratio of external surface area per volume of granules for the biofilm to produce charge. The stored charge is then harvested by discharging to a relatively small surface area electrode [107], which is the most expensive part of a bioelectrochemical system [145]. Thus, the costs per active volume of reactor are decreased. The current produced in these types of reactors, however, is still several orders of magnitudes lower (257 $A/m^3_{granules}$) [107] than the maximum current that could be achieved when a single granule is used as bioanode (76.8×10^3 $A/m^3_{granule}$) [87].

In a moving bed reactor, the granules move as a moving granular bed through an internal discharge cell, using a gas lift to fluidize and transport the granules back to the top of the reactor [107,108,113]. To increase the volumetric current from this moving capacitive bed, a better understanding of the discharging process of the granules is required.

The discharge rate is determined by the potential difference between the charged granules and current collector [88,107,108]. Both the capacitance and the resistance over the granular bed affect the potential difference between the granules and current collector [204,205]. For a bed of capacitive granules this resistance consists of: contact between the granules, between the granules and the current collector, the resistance of the granular material itself

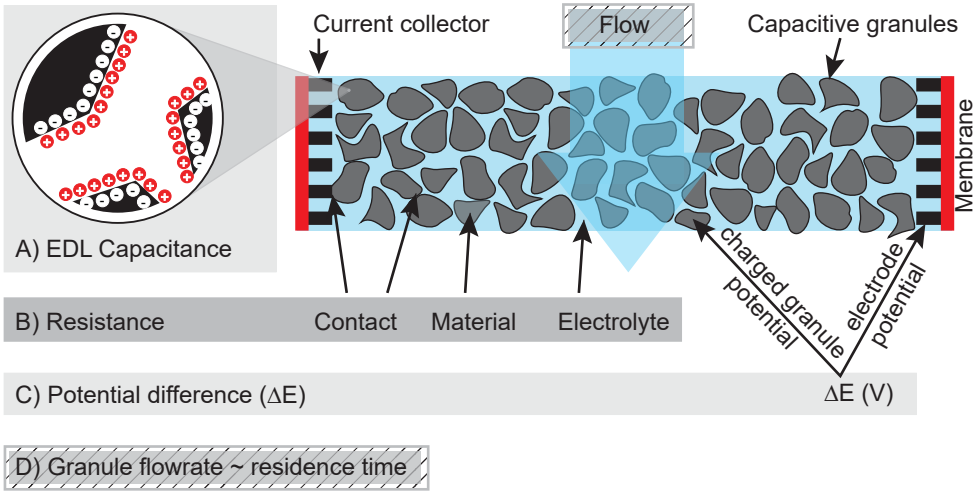

Figure 5.1. Factors influencing the capacitive discharge from a moving bed electrode. The capacitance is formed by the electrical double layer (EDL) on the surface of the porosity. The resistance of the granular bed consists of contact resistance, material resistance of the granules and the ionic resistance of the electrolyte. The potential difference (ΔE) is the difference between the electrode potential and the potential of the charged granules. The flowrate of the granules through the cell influences the residence time of the granules in the discharge cell.

[206] and the resistance of the electrolyte. The conductivity of the electrolyte also affects the capacitance of the granules. The residence time in the discharge cell is determined by the granule flowrate, which in turn affects the time the granules are in contact with the current collector [107,108]. The residence time therefore affects how much charge is transferred per granule, when it is in the discharge cell.

The aim of this study therefore is to optimize process parameters for discharge of capacitive granules under abiotic conditions. We investigated the discharging of charged granules as a function of 1) the potential difference between current collector and granules 2) the conductivity of the bulk electrolyte, 3) the distance between granules and current collector, 4) the flowrate of the granular bed.

5.2. Materials and methods

Moving bed reactor

The moving bed reactor was constructed similar to the gas lift reactor in our previous study [108]. The granules were recirculated in the reactor, using a gas lift, which consisted of a top and bottom glass volume, with a PMMA electrochemical cell attached in between. The electrochemical cell was used to charge and discharge the granules.

The N_2 flow for the gas lift was controlled using a mass flow controller (Mass-stream D-6311 with ±1% accuracy, Bronkhorst Nederland B.V., Veenendaal, Netherlands). The reactor volume in which the granules circulated was 1.2 L. The electrolyte recirculated at 80 mL/min via a recirculation bottle with 0.3 L liquid volume, where the gas effluent from the gas lift was sparged through and separated from the electrolyte. This ensured an anaerobic environment. The counter electrode had a volume of 2.3 L, including the flow compartments in the electrochemical cell and the recirculation bottle.

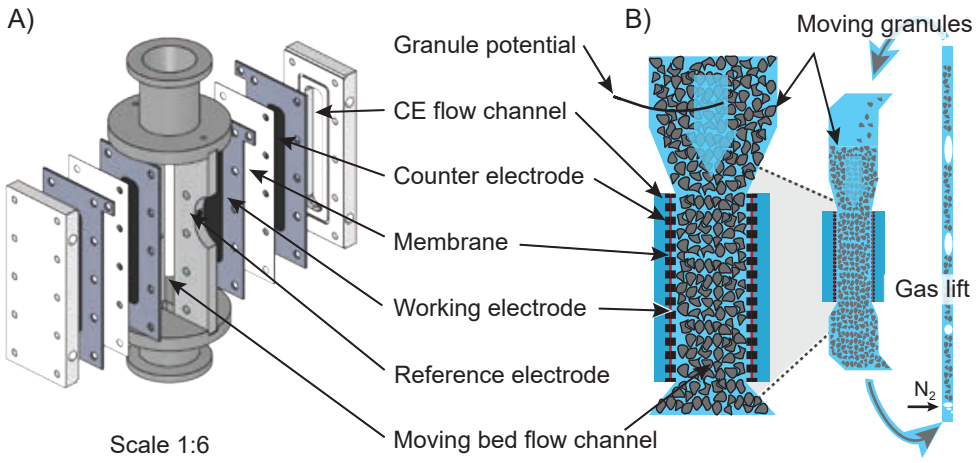

Figure 5.2. A) A CAD drawing of the electrochemical cell, with vertical cross sections. B) A schematic view of the cell, perpendicular to the electrode surfaces showing the 10 mm separation between the working electrodes, and its position in the gas lift reactor (modified from Ref [108]).

The electrochemical cell, also called the discharge cell, was constructed with two pairs of working electrodes and counter electrodes (**Figure 5.2**), to be able to connect the granule bed to the working electrode on both sides. The electrodes consisted of titanium with a mesh insert coated with Pt/Ir (Magneto Special Anodes B.V., Schiedam, Netherlands). The electrodes were separated by a cation exchange membrane (Ralex CMH-PP, Mega c.z., Stráž pod Ralskem, Czech Republic). The working electrodes were separated by 10 mm thick transparent PMMA pieces and exposed to the membrane by 22.3 cm^2. The 10 mm separation created a space for the moving bed of granules. A capillary, attached to a 3M KCl salt bridge and a reference electrode, was inserted in the cell between the working electrodes.

The granules were transported from the bottom to the top of the reactor by the gas lift. From the top, the granules settled down on top of the granular bed slightly above the electrochemical cell. The granules moved as a bed through the cell and back into the bottom part of the reactor. A Pt/Ir wire (80:20 w%, 0.25 mm, Advent-RM, Oxford, United Kingdom) was placed in the granular bed above the electrochemical cell, to measure the potential of the granules against a locally placed reference electrode, before they were charged or discharged. The granular material (bulk density 0.486 g/cm^3, coconut based HR5, Eurocarb) was sieved between 0.5 – 0.8 mm (stainless steel sieves, VWR). The system was filled with 176 g of granules (weight after washing and overnight drying at 105° C).

The electrolytes were prepared from demineralized water and Na_2SO_4, under constant mixing, until the conductivity reached 5.5 and 15 mS/cm (pH/Cond 340i, WTW, Weilheim, Germany). Na2SO4 was chosen to avoid unwanted electrochemical reactions such as chlorine formation [207]. The electrolyte was chosen as a simple salt solution to avoid introducing extraneous variables that may arise from the complex composition of (synthetic) wastewater. The 5.5 mS/cm solution was chosen to match the conductivity of the synthetic medium used previously [107], and was increased to study the effect of higher bulk electrolyte conductivity. The same solutions were used as electrolyte in the capacitance measurements. The electrolyte for the counter electrode was a 50 mS/cm Na_2SO_4 solution. The influent for the reactor was constantly flushed with N_2, and the recirculation vessel was flushed with N_2 as well. The solutions were added to the reactor at 1.3 mL/min.

Table 5.1. Overview of performed experiments.

Charge – discharge cycle (working electrode potential)	Cell configuration (# working electrodes)	Electrolyte conductivity	Flowrate	Discharge time	Figure #
Charging -0.5 V Discharging -0.2; 0 V	2WE	Low & High	Low	Long	3
Charging -0.5 V Discharging 0 V	1WE and 2WE	Low & High	Low	Long	4
Residence time Charging -0.5 V Discharging 0 V	2WE	High	Low & High	Long	5

Experimental strategy

The performance of the moving bed was determined from the charge transferred during discharging. The granules were first charged at -0.5 V vs Ag/AgCl, until they reached about -0.49V vs Ag/AgCl, which is close to the (open circuit) potential of acetate oxidation by bioanodes [116]. The discharging was studied for four different factors (**Table 5.1**): A) discharge potential, leading to a potential difference with the charged granules, B) bulk electrolyte conductivity, C) 1 or 2 working electrodes (WE), reducing the maximum distance between granules and current collector by a factor of two, and D) low and high flowrate of the moving granular bed.

The concentration of the bulk electrolyte affects the capacitance of the granules [204]. This means more charge can be stored and discharged for the same potential difference. Therefore, the capacitance of the granules was studied in the same electrolyte as used in the moving bed experiments.

Electrochemical measurements and control

The electrochemical cells were controlled by potentiostats (nStat, Ivium Technologies B.V., Eindhoven, Netherlands), with the working electrodes controlled against Ag/AgCl/3M KCl reference electrodes (+203 mV vs SHE, QM711X/Gel, ProSense, Oosterhout, Netherlands). All further potentials are referenced to the Ag/AgCl reference electrode.

The reference electrodes were attached to 3M KCl salt bridges and capillaries (4 mm diameter, Prosense, Oosterhout, Netherlands). One potentiostat was used to control either one or both working electrodes, together with the matching counter electrodes, against the reference electrode. Another potentiostat was used to measure the potential of the second working electrode and the potential of the granules. The channels were synchronized and set to floating mode (measured against common ground) using Iviumsoft (Iviumsoft version 4.946, Ivium Technologies B.V., Netherlands).

The granules were charged during initial experiments. Before the start of the experiments in **Table 5.1**, the granules had a potential of -0.47 V. Each discharge experiments had four phases: 1) pre-charging, 2) self-discharge monitoring, 3) discharging and charging cycles, 4) charging after. In the pre-charging phase, the granules were charged for 12 cycles of 50 minutes at -0.5V, followed by 10 minutes open circuit (OC): this allowed for fully charging and monitoring of the intermediate charging process (at OC). The pre-charging was followed by 2 hours of OC to monitor the self-discharge process (for example parasitic faradaic processes such as oxygen reduction, from oxygen crossover from the counter electrode over the membrane) [208]. After charging, the experiment was performed by discharging and charging the granules for 10 sequential cycles. Discharging was done at -0.2V and 0V, for 20 minutes (long discharging) (or short discharging using 5 minutes, see Supporting Information 1.2), and followed by 1 hour of charging at -0.5V. The difference in potential between the charged granules and the current collector thus became about 0.3 and 0.5 V. After the cycles, the next experiment was prepared for by charging the granular bed again for 6 cycles of -0.5V for 50 minutes and 10 minutes of OC. The whole program was run 3 times, to obtain 30 cycles of discharging and charging.

The cumulative charge, calculated by Iviumsoft from the current over time, was used to differentially determine the charge per discharge cycle. The potential difference (ΔE) for each cycle was calculated by subtracting the measured potential of the granules, at the start of the cycle, from the working electrode potential. The resistance during discharging was calculated by dividing the ΔE by the current. The average resistance and associated standard deviation were calculated for each cycle.

Since discharging of electrons leads to release of ions, both from the charge stored in the electrical double layers, we estimated the increase in conductivity as a result of discharge. The ions released during the discharging were calculated by multiplying the charge, from the current, with 1.04×10^{-5} mol/Coulomb Na^+ (as Q/(n×F), with n = 1 and F = 96485 C/mol e^-). The ions were released into the electrolyte in the discharge cell with a volume of 1–bulk density of granules, or 0.514 mL electrolyte per mL discharge cell, during the discharge time. The concentration of released ions, that adds to the bulk concentration, was calculated by multiplying the concentration of ions released per second by the residence time in the discharge cell (see **Table 5.2**). The concentration of Na^+-ions released was converted to a Na_2SO_4 solution, which assumed SO_4^{2-} as the counter ion in the local solution. The solution conductivity was determined by using regression on reported concentration to conductivity values for a Na_2SO_4 solution. The concentration to conductivity values were calculated by methodology described in [209] for concentrations below 56 mM [209], and regression on concentration to conductivity values from tabular data [210] for concentrations above 56 mM. See Supporting information S3 for the data and regression results.

The ohmic resistance over the granular bed was measured as the real component of high frequency impedance scans (PGSTAT302N with FRA32M, Metrohm Autolab, Utrecht, Netherlands) at constant current (5 kHz, 0±1mA, 100 repetitions) between the two working electrodes, with a 5-minute OC period before the impedance scans. The impedance scans were performed in between the discharging experiments. The resistance of the granular bed was determined using the cell constant, which was determined as 0.045 1/cm by multiplying the ohmic resistance of the cell in an electrolyte with an known conductivity (no granules) [211]. The ohmic resistance was measured together with the bulk electrolyte solution. A linear regression analysis (see supporting information S4 for the data and regression results) was used to determine the ohmic resistance for each experiment, as the bulk conductivity varied slightly for each experiment. The ohmic resistance was further adapted to match the cell configuration: for the 2WE configuration, the ohmic resistance was assumed to be over half of the width of the granular bed (5 mm), as compared to ohmic resistance for the 1WE configuration, which was over the full width of the granular bed (10 mm).

Measurements of granule capacitance were performed on small volumes of granules (9 – 20 mg) in an electrochemical cell developed in a previous study [107], where the granules were pressed against the working electrode. The counter electrode was Pt/Ir wire. The reference electrode was placed directly in the electrolyte. The electrolyte was flushed constantly with N_2 under constant stirring.

Table 5.2. The residence time and recirculation time of the granular bed resulting from the low and high granule flowrate experiments.

	Residence time cell (s)	Circulation time (s)
Low flowrate	194±23	3186±386
High flowrate	67±17	1096±272

The capacitance was measured by charging first in cycles of -0.5V and OC, until the OC potential was lower than -0.45V. The granules were then sequentially discharged and charged at 20 uA and -20 uA respectively, for 10,000 seconds each, until the potential was 0V. The measurement was repeated until at least 7 discharge cycles were available for analysis. To determine the capacitance of the sample of granules, the charge transferred was divided by the change in potential during discharging. During discharging, the potential increased. The change in potential was determined as the difference in potential between the end of the cycle and after 5000 seconds in the cycle. The capacitance was then normalized to the weight of the sample of granules (washed 3 times in ultrapure water and dried overnight at 105° C).

Granule flowrate

The flowrate of the granules moving through the electrochemical cell was determined from videos (1080p, 60 fps, Nikon D750 with Sigma 105 mm macrolens at f/11) taken through the transparent sides of the cell. The focus area was illuminated [108]. The videos were analyzed using Fiji [212] ImageJ2 [201]. The granular flow velocity was determined 10 times per video, by measuring the distance travelled and dividing it by the time between the first and last frame for the granule. The residence time in the discharge cell (volume 22 mL) was calculated by dividing the 11 cm length, over which the membrane was exposed, by the granular flow velocity.

The circulation time, which includes the residence time, was calculated by dividing the total granule volume (362 mL) by the granular flow velocity, multiplied by the horizontal cross section of the cell: 2 cm^2. See supporting information Figure S1 for an example of the measurement. During the experiments, the flow of the granular bed was changed by controlling the gas flow in the gas lift: an increase in gas flow from 140 to 200 mL/min of N_2 resulted in a 2.9 times higher granular flow of the granular bed in the discharge cell: **Table 5.2** shows the average and standard deviations for the residence time and recirculation time at the low and high flowrate.

5.3. Results and discussion

Charge transfer increased with higher potential difference and with higher electrolyte conductivity.

First, we studied how total charge transferred from granules to current collector was affected by the potential difference (ΔE) between the current collector and the charged granules, and by solution conductivity. The granules were pre-charged at -0.5V and then subjected to discharge – charge regimes, in which they were discharged for 20 min and charged at -0.5 V for 60 min, for a total of 30 cycles. The granules were discharged at -0.2 V and 0 V, which resulted in a ΔE of about 0.3 and 0.5 V. In **Figure 5.3**, the produced charge during discharging, in both low and high conductivity electrolyte, is shown against the measured ΔE. The transferred charge increased as expected at higher ΔE.

At low conductivity, the charge increased 2.5 times from 175 C to 429 C when ΔE was increased from 0.3 to 0.5 V. At high conductivity, the charge increased 2.0 times from 257 C to 507 C when ΔE was increased from 0.3 to 0.5 V. The higher ΔE increased the transferred charge on average 2.3 times, which was not proportional to the increase in ΔE (on average 1.6 times). This is likely related to the total resistance during discharging, which we will discuss later.

The bulk conductivity was increased from 6 mS/cm to 16 mS/cm, thereby reducing the ionic resistance of the electrolyte. With the change to high conductivity electrolyte, the ohmic resistance decreased from 0.70±0.02 Ohm to 0.32±0.02 Ohm. The change in ohmic resistance (2.3 times) was thus very close to the change in electrolyte conductivity (2.5 times). The discharge experiments in **Figure 5.3** show that at high bulk electrolyte conductivity, the average discharge was 1.5 times higher compared to at low conductivity, at a potential difference of 0.3 V, and 1.2 times higher for discharging at a potential difference of 0.5 V. Therefore, the increase in bulk electrolyte conductivity resulted in more transferred charge, which was however, not proportional to the increase in electrolyte conductivity or the decrease in ohmic resistance over the granular bed.

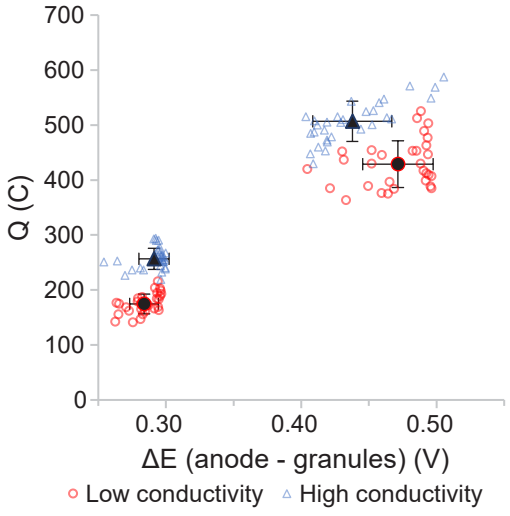

Figure 5.3. Charge from granules discharged at different applied ΔE (0.3 V and 0.5 V) and at low and high conductivity (6 and 16 mS/cm). The black filled markers are the average values. The error bars show the standard deviation of the produced charge and the measured ΔE.

Aside from the bulk electrolyte, the electrolyte in the pores of the granules was also affected by changing from low to high conductivity, which affects the formation of electrical double layers that form the capacitance [213]. The capacitance of the granules was measured by charge – discharge experiments on small volumes of granules in a separate test cell, in the two electrolytes. There was an effect of the bulk electrolyte conductivity on the capacitance of the granules: the gravimetric capacitance increased from 75±15 F/g to 106±10 F/g. This increase is in line with the findings of Zhao and colleagues, where the capacitance was reduced at low molarity compared to high molarity NaCl solution [213]. The increased capacitance could be one of the reasons for the increased charge in the higher concentrated electrolyte and may result from the lower ion transport resistance in the porosity.

In most experiments, the measured ΔE differed slightly from the applied ΔE. This was caused by less efficient charging than discharging. As the granules were discharged, the granule potential increased. Especially at the high applied ΔE and high conductivity electrolyte, when more charge was transferred, the granule potential increased more during discharge than it decreased during charge, resulting in a lower measured ΔE than applied ΔE. To see if this shift in ΔE was indeed due to a difference in charging and discharging, the effect of discharging and charging time was studied further, by applying cycles with a shorter discharge time of 5 minutes, compared to the 20 minutes used in the other experiments, while charging time was unchanged. The results, shown in the supplementary information Figure S2, show that in this case, the measured ΔE indeed stayed closer to the applied ΔE, meaning that charge and discharge were more in balance.

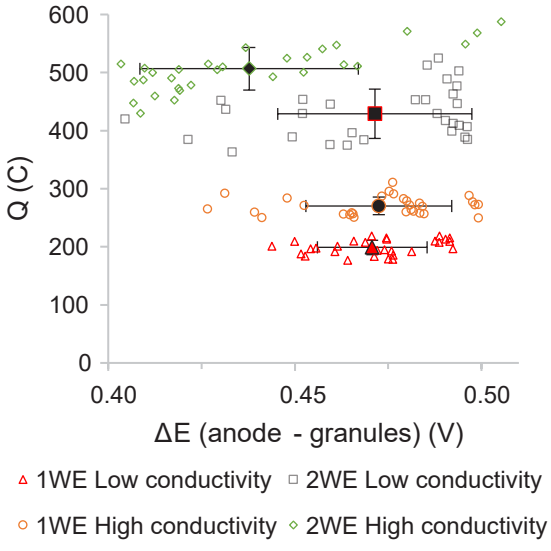

Figure 5.4. The charge from granules, discharged at 1 or 2 working electrodes (WEs), versus measured ΔE. The black filled markers are the average values, and the error bars show the standard deviation.

Charge transfer increased when the bed was discharged on both sides

To study if the transferred charge was affected by electrical resistance or by ionic resistance in the granular bed, the granules were discharged at 1 or 2 WEs, in low and high conductivity electrolyte at a ΔE of 0.5 V. We previously showed that discharging with the electrode closest to the membrane was more efficient than an electrode on the other side of the granular bed [108]. For this study, the electrochemical cell was built using WEs on both sides of the granular bed, that had a thickness of 10 mm, together with a membrane and counter electrode on both outer sides of the system. Using both WEs, instead of one WE, reduced the maximum distance from the granules to the current collector by a factor 2, and thus reduced both electrical and ionic resistance by a factor 2. Aside from the distance, the second working electrode also provided additional surface area (also doubling the surface area of the membrane and cathode). **Figure 5.4** shows the charge from discharging at 1 and 2 working electrodes, in the two electrolytes, for all cycles and the average per experiment. With the additional current collector, the transferred charge increased: in the high conductivity electrolyte, the average charge increased from 270 C to 507 C, and in low conductivity the average charge increased from 199 to 429 C. Thus, by discharging on both sides of the granular bed the transferred charge increased on average 2.1 times. During these experiments, the change from low to high salinity resulted on average in 1.3 times higher charge. From this we conclude that the effect of the bulk electrolyte conductivity on the average charge was less pronounced than the increase in charge from using an additional current collector, and therefore that the electrical resistance is more important in determining the transferred charge during discharging than the ionic resistance. In suspension flow capacitive deionization (FCDI) systems, where an activated carbon powder slurry is charged in an electrochemical cell to desalinate the feed stream [205,214–230], higher carbon content was used to decrease the electrical resistance [220,231]. By simultaneously varying the salt concentration, it was found that the voltage drop was reduced by 72% by the higher carbon content, in contrast to 36% due to increased electrolyte conductivity [231]. Thus, the electrical resistance is more important than ionic resistance for the performance of FCDI systems. These results support our conclusions.

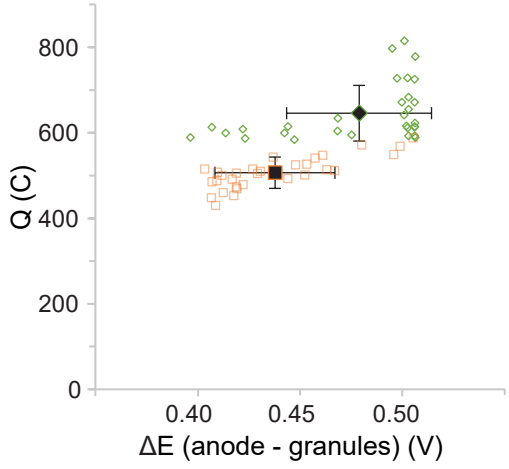

Figure 5.5. Charge produced at different granular flowrates (0.6 and 1.7 mm/s).

Charge transfer increased at higher flowrate

To study the effect of the residence time in the discharge cell, the flowrate of the granules was varied. The residence time determined the time for discharging the granules that passed through the discharge cell in the 20 minutes of discharging (in the charge and discharge cycles). Through the circulation speed of the granules via the gas lift, the residence time of the granules in the discharge cell changed. At high flow rate the residence time was 67 seconds, with a circulation time of 18 minutes, compared to 194 seconds, with a circulation time of 53 minutes, at low flow rate (see **Table 4.2**). **Figure 5.5** shows that with a shorter residence time, 1.3 times more charge was produced, than with a longer residence time. The capacitive current decreases while discharging the stored charge [88]. A shorter residence time will have resulted in more charged granules in the discharge cell during discharging (seen as a higher average ΔE in **Figure 5.5**). This means the charge per time increased and thus resulted in a higher average current. This is in accordance with our findings of the performance of a moving bed bioanode, where a long charging time ensured fully charged bioanode granules which resulted in a high discharge current [108].

The beneficial effect of the higher flowrate was also observed in FCDI systems. Similar to the moving bed, the slurry of suspended powder particles forms a flowing capacitive electrode. A "convective current" [220,223] or "hydraulic current" [226,232] was used to describe the effect of charge entering [226] and leaving [220,223,226,232,233] the cell via the capacitive particles. This current increased with increased slurry flow velocity, up to the point the slurry was thinned due to larger shear effects at the highest flowrates [205]. This is unlikely an issue for the moving bed, where the carbon content is 48.6 wt% (for a bulk density of 0.486 g/cm^3) compared to the carbon content of 10 – 20wt% [221,230,232] of slurry electrodes. The moving granular bed thus has a denser, and therefore a better connected particle network, and if operated equally (potential, electrolyte conductivity and capacitance), a higher charge density per volume, compared to the carbon slurry.

The discharge resistance decreased due release of ions in the local electrolyte

The maximum resistance during discharging was calculated from the measured ΔE and the current. The discharge resistance is the maximum as it is calculated from the ΔE, with the potential of the charged granules before discharging in the discharge cell, and the current. **Figure 5.6A** shows the average discharge resistance and the ohmic resistance for each of the experiments. The ohmic resistance was measured in open circuit, and not during the discharging experiments. The discharge resistance inside the discharge cell is difficult to determine, as there will be a gradient in ΔE over the discharge cell due to the increased granule potential (over the length, due to the time spent discharging [88]) and due to the ohmic resistance (over the width of the cell). The ΔE inside the discharge will therefore be lower than the maximum ΔE, and therefore the resistance during discharging will be lower than the maximum as well.

For the studied factors: applied ΔE, bulk electrolyte conductivity, the maximum distance between granules and the current collector(s), and residence time in the discharge cell due to the flowrate, the resistance matches the earlier conclusions: the discharging resistance was lowest at the higher ΔE, short residence time, high bulk electrolyte conductivity, and a short distance to the current collectors. The lowest discharge resistances were found for the short

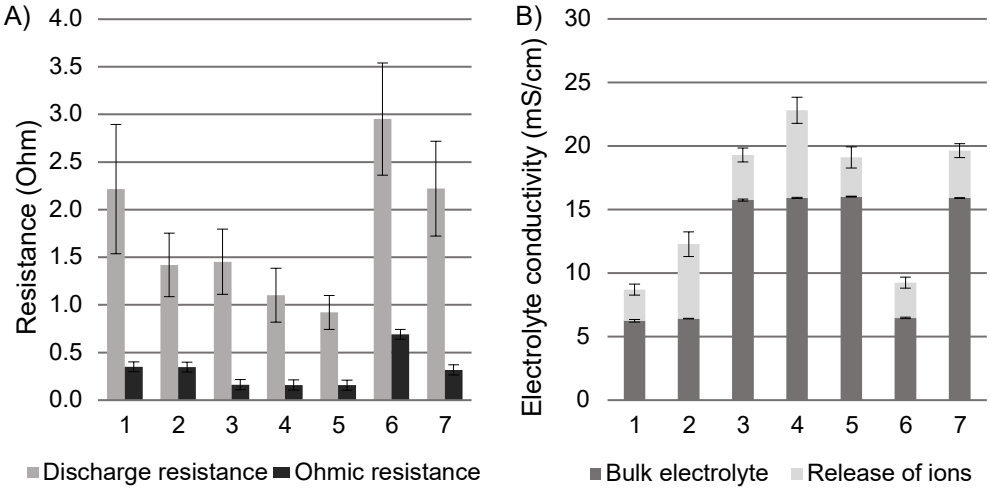

Figure 5.6. A) The discharge and ohmic resistance for each of the experiments. The discharge resistance was calculated using the ΔE and current at each measurement interval. The ohmic resistance was measured without ΔE control. B) The measured bulk conductivity and increase in conductivity, calculated from the charge transferred and the residence time, combine to a local increased electrolyte conductivity in the discharge cell. The average and standard deviation over 30 discharge cycles per experiment, are shown for the experiments in Figures 5.3 to 5.5.

discharge experiment (see SI, S2). As lower discharging resistance means the ΔE inside the discharge cell was closer to the maximum ΔE, this increased the driving force for discharging and therefore increased the transferred charge for the experiment. The experiments varying the applied ΔE show an average 1.4 times lower discharge resistance when discharged at 0.5 V compared to 0.3 V.

This is surprising, as neither the electrical resistance (the ΔE experiments were performed with the 2WE configuration) nor the bulk conductivity were changed (in comparing 0.3 to 0.5 V). The decrease in resistance by using higher applied ΔE can be the result of an increase in local ionic conductivity by ions released during discharging [234]. Capacitive deionization studies using fixed [235], suspension [231] and fluidized bed [236] capacitive electrodes, have shown that the ions, released from the porosity during discharging, increase the concentrations of ions in the effluent [231,235,236]. It was shown that in the fluidized bed system, the charged capacitive carbon beads carried the ions until they were discharged and increased the ion concentration in the bulk solution [236]. In our study, the discharge step takes place at the current collector(s), thus locally releasing ions in solution in the discharge cell. As more charge is recovered, more ions are released from the pores of the granules [231,235], creating a self-strengthening effect of improving the discharging due to a higher discharge.

At the higher applied ΔE, more charge was harvested from the moving bed. From this charge, we can calculate the concentration of ions released. For instance, the 507 C recovered with the high bulk electrolyte conductivity at 0.5 V would translate to 229 mM of salt released in the discharge cell, compared to 79 mM of salt released for the 175 C in the low bulk electrolyte conductivity experiment at 0.3 V. The bulk conductivity was 6 mS/cm (34 mM) for the low conductivity experiments and 16 mS/cm (115 mM) for the high conductivity experiments. Assuming the electrolyte flow equaled the granular flow, the electrolyte concentration increased in the cell, because of the ions released in the discharge cell. **Figure 5.6B** shows the calculated increase in conductivity, on top of the conductivity of the bulk solution, during each of the experiments. The calculated local conductivity increased to an average of 10±2 mS/cm at low bulk conductivity, 1.6 times increase, and to 20±2 mS/cm at high bulk conductivity, 1.3 times increase compared to the bulk alone. At low bulk electrolyte conductivity, the release of ions lead to a stronger increase in local conductivity than at high bulk electrolyte conductivity. This is due to the non-linear behavior of concentration to conductivity at high concentrations [209].

The discharge resistance was lower for the short residence time experiments, compared to the longer residence time, with a higher discharge as a result. Interestingly, the increase in local conductivity due to ion release was less for the short discharge time than the long discharge time, indicating that the driving force outweighs the electrolyte conductivity in determining the discharging. The effect of the residence time on the dilution of released ions in the discharge cell is more relevant for the moving bed bioanode reactor, where the driving force is determined by sufficient charging as well.

The release of ions would decrease the ohmic resistance during discharging, but as the discharge process is also influenced by other factors, more study is required to elucidate the self-strengthening effect on the discharging process. This self-strengthening process is especially interesting for BESs, because at low bulk conductivity, such as wastewater conductivity (~1 mS/cm) [76], the local conductivity at the electrode is increased, resulting in lower losses.

5.4. Conclusion and outlook for application of moving bed reactors

We have studied how four factors influenced the discharging of capacitive granules in a moving granular bed reactor by 1) increasing the potential difference, between the current collector and the granules from 0.3 to 0.5 V, 2) increasing the bulk electrolyte conductivity from 6 to 16 mS/cm, 3) decreasing the maximum distance between the granules and the current collector by a factor of 2, and 4) decreasing residence time in the discharge cell by a factor of 3.

The largest increase in recovered charge was due to the increase in ΔE. Analysis of the resistance during discharging, with the change in ΔE, indicated the discharging itself increases the charge transfer by an increase in local electrolyte conductivity in the discharge cell. A higher ΔE means both a higher charge recovery and a higher electrode potential. For bioanodes, a high anode potential results in an applied high cell voltage when hydrogen is produced at the cathode [71]. This means there will be an optimum between the recovered charge and the choice of electrode potential, for optimal use of energy recovered from oxidation of organics to produce hydrogen.

Increasing the bulk electrolyte conductivity increased the charge, though less than the ohmic resistance was decreased. The capacitance of the granules, clamped in an external test cell, also increased in higher electrolyte conductivity, and may be the reason behind the higher transferred charge in higher conductivity electrolyte. For bioanodes, the electrolyte conductivity will depend on the choice of wastewater. How the composition of wastewater, as well as the influence of the biofilm, affect the discharging process requires more study.

The transferred charge increased by discharging from both sides of the granular bed. The reduced maximum distance to the current collector, at the two different bulk electrolytes, showed that the electrical conductivity of the moving bed is more important in determining the transferred charge than the ionic conductivity. Taken together with the increased local electrolyte conductivity, due to the released ions during discharging of the electrons, it can therefore be concluded that, for capacitive bioanodes, improving the electrical conductivity of the moving bed will improve the discharge regardless of the bulk ionic conductivity.

For capacitive bioanodes, the activity in the charging volume is determined by the amount of charge recovered in the discharge cell [107]. For future operation of moving bed bioanodes, we therefore recommend studying the effect of residence time, in the discharge time, on the long-term operation of the bioanode, and to improve the electrical resistance over the granular bed to help to make the driving force more effective in discharging the stored charge in the granules.

Acknowledgements

This work was performed in the cooperation framework of Wetsus, European Centre of Excellence for Sustainable Water Technology (www.wetsus.nl). Wetsus is co-funded by the Dutch Ministry of Economic Affairs and Ministry of Infrastructure and Environment, the European Union Regional Development Fund, the Province of Fryslân, and the Northern Netherlands Provinces. The authors thank the participants of the research theme "Resource Recovery" for the fruitful discussions and their financial support.

Supporting information chapter 5

S1. Particle tracking for granule flow velocity determination

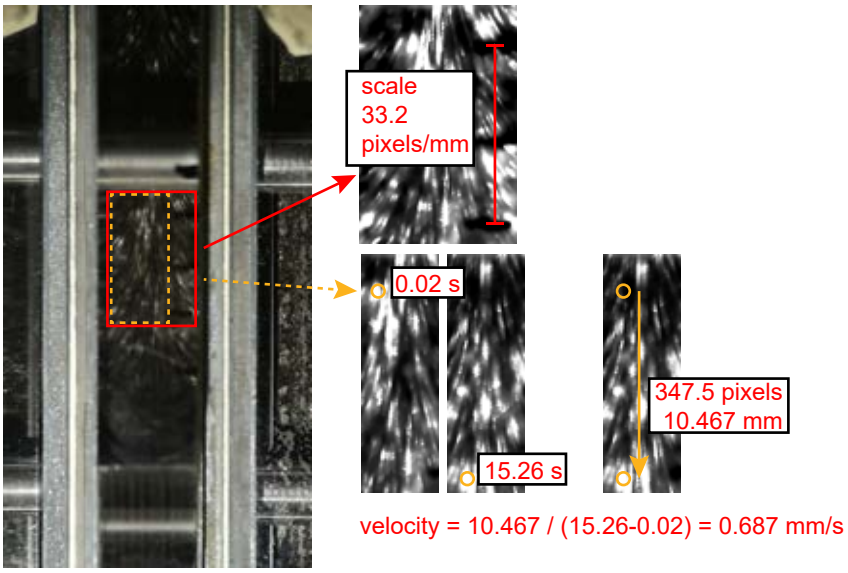

Figure S1. Example of particle tracking using analysis of movies taken of the superficial flow in the discharge cell.

Using Fiji [212] ImageJ2 [201], the scale was set for each movie file. For 10 granules per file, the start and end times were recorded, along with the distance travelled. From this the superficial flow velocity was calculated.

S2. Charging and discharging ratio – (in)efficiency of charging

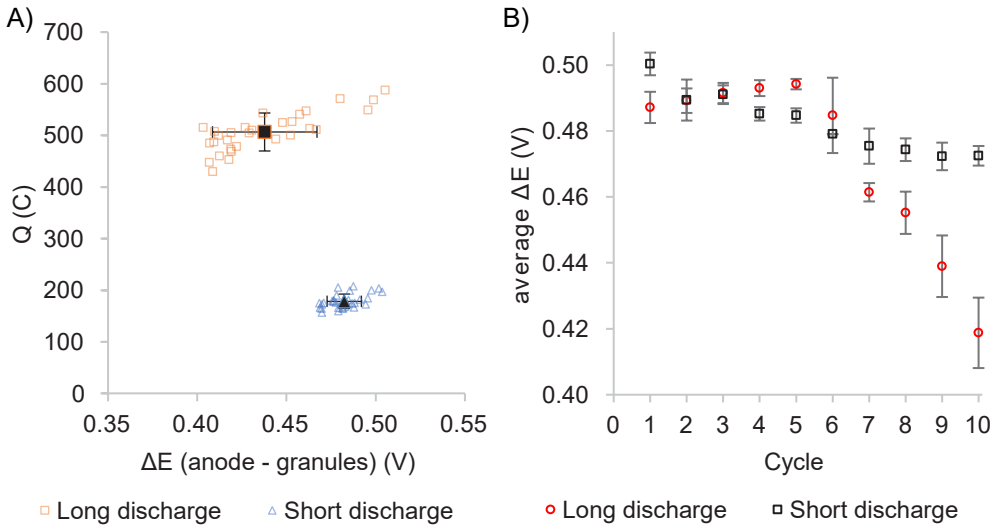

Figure S2. A) Charge vs ΔE for long (20 min) and short (5 min) discharge times. Charging time, after discharging, was 1 hour for both. B) The ΔE over the 10 cycles, averaged for 3 measurements per cycle. Error bars are the standard deviation.

The short discharge experiments were performed by discharging for 5 minutes instead of 20 minutes, in the intermittent charging and discharging cycles. The charging time was the same for each experiment. The experiments were performed in the high conductivity bulk electrolyte and the granules were discharged at ΔE 0.5V

Figure S2A shows the experimental data and the calculated average and standard deviations for the charge and ΔE. The average ΔE, over the 30 discharge cycles, was 0.44V for the long discharge time experiments, and 0.48 V for the short discharge time experiments. **Figure S2B** shows the change in ΔE per cycle (averaged per 3 cycles, as the 30 cycles were performed in 3 sets of 10 cycles). The results show that the average ΔE decreased significantly after the 6th cycle in the long discharge experiments, while remaining relatively stable for the short discharge experiments.

The results show that the short discharge time allowed a more stable ΔE, which can be explained by a better balance between charging and discharging of the granular bed. The charging is evidently not as efficient as the discharging and can be better matched by using a shorter discharge time. The short discharge time did produce 2.8 times less charge on average (179 C vs 507 C), resulting in an average current density that was 1.4 times higher for the short discharge time compared to the long discharge time.

The explanation for this result is similar to the results produced by discharging with a short and long residence time in the discharge cell due to the change in flowrate (see main manuscript), where the discharge was higher as a result of on average more charged granules that were present in the discharge cell during the programmed discharge time.

S3. Release of ions during discharging

Table S1. Electrical conductivity of aqueous Na2SO4 solutions between 7 and 8000 mg/L [209].

conductivity (mS/cm)	conductivity (uS/cm)	mM	mol/L	mg/L
0.012541	12.54114708	0.049281892	4.92819E-05	7
0.024941	24.94069715	0.098563785	9.85638E-05	14
0.049485	49.48530217	0.19712757	0.000197128	28
0.097868	97.86790537	0.394255139	0.000394255	56
0.192687	192.6873821	0.788510279	0.00078851	112
0.377034	377.0344057	1.577020558	0.001577021	224
0.731606	731.6063152	3.154041115	0.003154041	448
1.404189	1404.189496	6.30808223	0.006308082	896
2.659478	2659.477954	12.61616446	0.012616164	1792
4.969967	4969.966559	25.23232892	0.025232329	3584
6.691474	6691.473552	35.20135173	0.035201352	5000
10.20735	10207.34541	56.32216277	0.056322163	8000

Table S2. Electrical conductivity of aqueous Na_2SO_4 solutions [210] (142.04 g/mol Na_2SO_4, water 1 g/L).

%mass	k	g/L	mM
0.5	5.7	5	35
1	11.2	10	70
2	19.8	20	141
5	42.7	50	352

SUMMARY OUTPUT

Regression Statistics	
Multiple R	0.99899659
R Square	0.99799418
Adjusted R Square	0.9977936
Standard Error	0.15565428
Observations	12

mS/cm = mM * a + b		stdev
b	0.114797	0.188643
a	0.183467	0.00901

ANOVA

	df	SS	MS	F	Significance F
Regression	1	120.5475363	120.5475	4975.494	8E-15
Residual	10	0.242282545	0.024228		
Total	11	120.7898188			

	Coefficients	Standard Error	t Stat	P-value
Intercept	0.11479666	0.054456557	2.108041	0.061244
X Variable 1	0.18346667	0.002600992	70.53718	8E-15

Figure S3. Regression analysis on Table S1, y = Ohmic resistance, x = bulk electrolyte conductivity.

SUMMARY OUTPUT

Regression Statistics	
Multiple R	0.998556484
R Square	0.997115051
Adjusted R Square	0.995672576
Standard Error	1.072332708
Observations	4

mS/cm = mM * a + b

	coeff	stdev
b	2.688718	1.689409
a	0.11471	0.008726

ANOVA

	df	SS	MS	F	Significance F
Regression	1	794.8702051	794.8702	691.2531	0.001444
Residual	2	2.299794872	1.149897		
Total	3	797.17			

	Coefficients	Standard Error	t Stat	P-value
Intercept	2.688717949	0.844704742	3.183027	0.086139
X Variable 1	0.114710047	0.004362977	26.29169	0.001444

Figure S4. Regression analysis on Table S1, y = mS/cm, x = mM.Regression analysis on Table S2, y = mS/cm, x = mM.

S4. Regression analysis for ohmic resistance versus bulk electrolyte conductivity

Table S3. Ohmic resistance, as real component of 5 kHz impedance measurements, and bulk electrolyte conductivity during said measurements.

Ohmic resistance (Ohm)	Bulk electrolyte (mS/cm)
0.90	5.62
0.74	5.77
0.67	6.58
0.34	15.33
0.34	15.95
0.31	15.87
0.30	16.06
0.30	16.06

SUMMARY OUTPUT

Regression Statistics	
Multiple R	0.9967427
R Square	0.99349602
Adjusted R Square	0.99219522
Standard Error	0.01656513
Observations	7

y = EIS, x = cond

Ohmic resistance = a * bulk electrolyte + b

	coeff	stdev
b	0.944955	0.052146
a	-0.03946	0.003778

ANOVA

	df	SS	MS	F	Significance F
Regression	1	0.209578189	0.209578	763.7595	1.16E-06
Residual	5	0.001372017	0.000274		
Total	6	0.210950206			

	Coefficients	Standard Error	t Stat	P-value
Intercept	0.94495497	0.019709513	47.94411	7.46E-08
X Variable 1	-0.0394623	0.00142792	-27.6362	1.16E-06

Figure S5. Regression analysis on Table S3, y = Ohmic resistance, x = bulk electrolyte conductivity.

Nijmegen, The Netherlands

Chapter 6

General discussion

6.1. Introduction

The main aim of this thesis was to recover electrical energy from dissolved organics in wastewater with a bioelectrochemical system, by using a bioanode. To match the same volumetric rate as anaerobic digestion (AD), an organic loading rate of 25 kgCOD/m^3.d (25 mgCOD/cm^3.d), converted to power at a voltage efficiency of 40% [22], should be converted in a volumetric current density of 3.5 mA/cm^3 (3500 A/m^3) [34]. For bioanodes, both voltage and coulombic efficiency determine the total efficiency, where a high coulombic efficiency can compensate for a lower voltage efficiency [74]. Selective pressure of the microbial community, which contains both electroactive bacteria (EAB) and methanogenic archaea, is in favor of EAB under low substrate concentrations, such as a low organic loading rate such as 1 mgCOD/cm^3.d (or 0.14 mA/cm^3) [74]. High loading rate, high efficiency, and high volumetric current density will also achieve low substrate concentrations in the reactor. This requires large surface area, for the EAB, per volume of reactor [74]. Capacitive bioanode reactors potentially allow for high current densities, by using intermittent charge storage and large volumes of granules to provide a large surface area for EAB, but high currents have yet to be realized [87,96,107,116]. The main challenge in this thesis was to increase the current density from discharging fluidized capacitive bioanode granules, which combines the large surface area for EAB growth and charge storage capacity of activated carbon granules [87].

Capacitive bioanodes have been studied in multiple configurations, both described in this thesis and in literature [96,104–108,114,127,196,197,203]. **Figure 6.1** shows an overview of the granular capacitive bioanode systems, from fixed bed to fluidized bed and to moving bed reactors. The various reactor designs have their advantages and disadvantages: a full overview can be found in Ref [116]. In general, a division is made between fixed single granules and fixed bed systems (**Figure 6.1a**), which use intermittent control of the anode potential – resulting in an intermittent current, and intermittent contact systems, with a continuously polarized anode – resulting in a continuous current, which use various methods of fluidization to bring the capacitive granules in contact with the anode (**Figure 6.1b-e**).

In this thesis, capacitive bioanodes were studied in four configurations: i) single carbon granules (SG), ii) fixed granular bed cells (FB), iii) small moving bed reactors (SMB, 0.4 L granules), and iv) a large moving bed reactor (LMB, 1.2 L granules). In **Chapter 2,** the maximum achievable current density was established, using single granular bioanodes with fixed to a Pt- wire as current collector. The study showed the potential of larger reactor setups to produce high current density using capacitive bioanode granules [87]. A reflection on the interaction between charged granules and the anode of the capacitive MFCs [116], and the importance of the discharge time per granule [85,86], resulted in the development of the moving bed reactor concept (**Chapter 3**). This new reactor design used physical separation between charging and discharging capacitive bioanode granules [96], and combined it with a moving packed bed of granules to enable increased contact time with the anode current collector, compared to fluidized bed bioanodes [107]. In **Chapter 4**, a moving bed reactor was constructed using a discharge cell design that enabled direct comparison with a fixed bed discharge cell. The aim was to find how the stored charge could be harvested optimally, through the configuration of the discharge cell [108]. Comparable studies in supercapacitors, capacitive de ionization, and capacitive bioanodes showed various parameters to affect

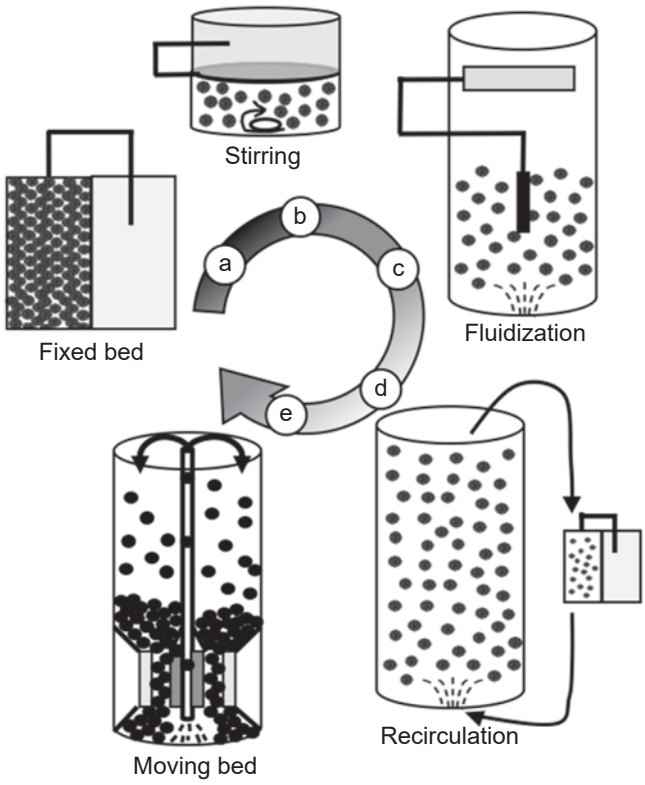

Figure 6.1. Capacitive bioanode reactors. Reproduced from [116], published by Elsevier Ltd., CC BY 4.0 (http://creativecommons.org/licenses/by/4.0/).

capacitive discharging (**Chapter 5**). These parameters were also studied in the moving bed reactor. In **Chapter 5**, the applied potential difference between charged granules and the controlled current collector, the influence of electrical and ionic resistance (through charge transfer path length and bulk electrolyte conductivity), and the flow rate of the moving granular bed were studied for their impact on discharging abiotically charged granules.

6.2. From single granules to moving bed granules

Table 6.1 shows a collection of the results from the experiments reported in this thesis, as well as three results from literature with different reactor configurations. The main performance indicators are the current densities, normalized to membrane area, reactor volume, total granule volume, discharge cell volume, and estimated granule surface area. The selection from literature was made for high current density fluidized bed systems and for similarity of design to the moving bed reactors. For the systems producing high current densities, two fluidization mechanisms were chosen: mechanical stirring [104] (**Figure 6.1b**) and upward liquid fluidization [106] (**Figure 6.1c**). The fluidized bed with an external discharge cell was chosen to compare against the moving bed reactors, as both designs used separated charging and discharging (**Figure 6.1d**) [96].

For the larger scale moving bed reactors, the highest bioanode current density reached was 4.3 mA/cm^3_{cell}, or 0.3 $mA/cm^3_{granules}$ (SMB bioanode, **Chapter 4**) [108], and 27 mA/cm^3_{cell} under abiotic conditions (SMB abiotic, **Chapter 5**). Though the bioanode did not reach the high current density of single bioanode granules (77 $mA/cm^3_{granule}$), the abiotic discharge showed the promising potential of the moving bed reactor as bioanode. A significant improvement was made compared to the current density of previous fluidized bed reactors. Compared to the smaller scale reactors from literature, 1 mL and 80 mL granules (in 7 mL cell resp. 680 mL reactor), the best performing moving bed bioanode produced 3 – 20 times higher current per volume of the discharge cell (22 mL granules). The fluidized bed, with the external discharge cell, had a similar volume to the smaller moving bed reactor (SMB), 2.2 L [96] and 1.5 L (SMB) with 0.4 L of granules in both [96,108]. The longer contact time, for the granules in the SMB discharge cell, resulted in 12 times higher current density.

In the experiments, the discharge process of capacitive granules was studied in relation to several parameters: A) contact time, B) contact resistance, C) charging and discharging, D) faradaic and capacitive contributions to the discharge current for fixed and moving bed systems, E) driving force of the potential difference (**Table 6.1**: ΔE) between charged granules and the current collector, F) the distance between granules and current collector, G) bulk electrolyte conductivity, and H) the residence time in the discharge cell. These parameters were studied in four cell configurations (SG, FB, SMB, LMB, see 6.1), as either bioanodes (experiments using parameters A − F) [87,107,108] or under abiotic conditions (experiments using parameters E − H) (**Chapter 5**). In this section, I will discuss parameters A − D, by using the data in **Table 6.1**. Parameters E − H were discussed in detail in **Chapter 4** and **Chapter 5**. The ΔE was used to calculate the discharge resistivity to compare the various systems in **Table 6.1**.

The contact time was studied by comparing the current density produced by the LMB reactor to fluidized bed bioanodes reported in literature. The highest reported current density was 1.6 mA/cm^3 (granule volume) in a small cell, where contact, through collision, was forced by the stirring motion [104]. A slightly larger system, where the anode was immersed in the granular bed of 80 mL, produced 0.2 mA/cm^3 [106]. The contact between charged granules and the anode was incidental in the upward fluidized reactor configuration. The largest difference between reactors using separated charging and discharging [96,107,108] was the residence time for contact in the discharge cell. Whereas the residence time in the discharge cell was 0.5 seconds in the fluidized bed [96], the residence time was 27 seconds (at the time of highest recorded current) in the LMB [107], and 23 seconds in the SMB [108]. Assuming the granules were evenly distributed over the fluidized bed reactor [96], the granules in the discharge cell produced 0.3 mA/cm^3, which was 5 (LMB, [107]) and 12 (SMB, [108]) times less than the volumetric current in discharge cells.

In the moving bed bioanodes, the charging and discharging times are related to the volumes, in which the granules are located, and the flowrate of the granules, resulting from the gas lift. The volume of the granules outside of the discharge cell versus volume of the discharge cell thus equates to the charging and discharging time. The ratio, between the charging and discharging times, is an important factor in determining the efficiency of using the charge storage of the granules [88] and can be changed in the moving bed reactors by adjusting the ratio between the two volumes. In **Chapter 4**, we showed a high discharge current requires that the charging time is long enough to fully charge the granules, before discharging [108].

As the charge recovered in the discharge cell, the volume of granules outside of the discharge cell does not directly contribute to the volumetric current density in the reactor (both for normalization to the total volume of granules, as well to reactor volume). Both moving bed reactor volumes were over-dimensioned to account for future experiments with larger volumes of granules. For instance, the small moving bed (SMB) reactor produced 4.3 mA/cm^3 in the discharge cell, but only 0.257 mA/cm^3 for the total granule volume, or even 66 A/m$^3_{reactor}$ (0.066 mA/cm^3) [108]. The charging in the moving bed bioanodes was never seen to limit the current produced, and therefore the total granule volume was likely excessive for the used discharge cells: only as much charge can be stored as was discharged from the fully charged granules [107,108]. The high percentage of granules outside of the discharge cell, 86% for the LMB and 94% for the SMB, should be reduced to match the effectiveness of the discharging in the bioanode reactor. This would increase the current density per total granule volume and per reactor volume. Optimizing discharging is thus essential [87,88,107,108,116], which means the resistance in the discharge cell should be minimized.

The electrical contact between granules provides a path for the electrons stored in the electrical double layer (EDL) [118], via the carbon material, to the current collector. Simultaneously, cations stored, with the electrons, in the EDL are released in the electrolyte in the discharge cell [96]. Thus, the resistance for the granular bed in the discharge cell can be viewed as 4 components (seen in **Figure 6.2**): 1) granular material, 2) contact (both with the current collector and between granules with biofilm), 3) ionic resistance from the electrolyte, and 4) ion transport resistance from the porosity.

The maximum resistance during discharging, hereafter called the discharge resistance, can be calculated for all configurations, by using the projected area, the cell width, the potential difference ΔE (between the current collector and the charged granules) [108], and the current (**Chapter 5**). As a result of using the ΔE, the discharge resistance is an indicator of how well the potential difference is used to recover the charge.

The ΔE and discharge resistance are shown in **Table 6.1**, where the ΔE for the systems from literature was estimated based on the reported anode potential and the fully charged at the thermodynamic equilibrium potential of acetate (-0.49 V vs Ag/AgCl, see chapter 1.2).

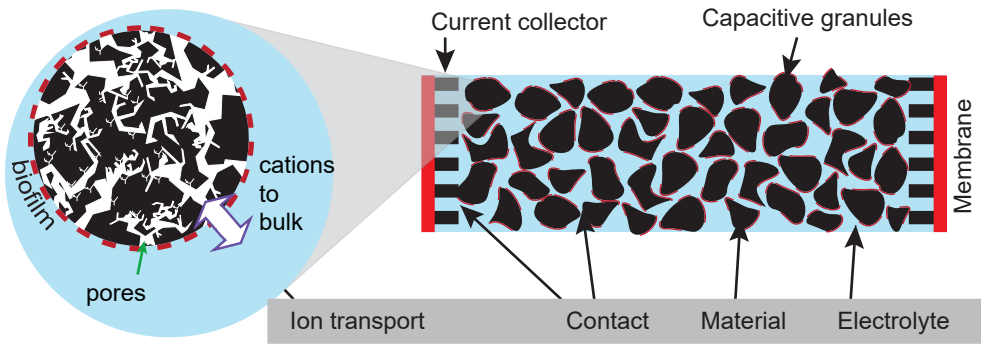

Figure 6.2. Resistances in the granular bed in the discharge cell of a moving bed reactor. The dark red parts on the surface of the granules represent the electroactive biofilm. Modified from ref [87] and chapter 5.

Differences in contact resistance resulted from the various manners of contact used in this thesis. In the single granule (SG) experiments [87], the contact with the current collector was direct: there was no contact resistance with other granules. In the fixed bed (FB) experiments, the granular bed was pressed against the current collector [108], resulting in low contact resistance with the current collector, but added contact resistance between the granules compared to the SG experiments. The contact resistance in the small moving bed (SMB, [108]) and large moving bed (LMB [107]) reactors was highest, as no forced contact was made between the granules themselves or with the current collector.

The fixed bed cells had the lowest discharge resistivity among the experiments in this thesis. The next lowest was at the time of the maximum current of the SMB bioanode (the discharge resistance increased 6 times between day 15 and day 42, due to fouling of the anode) [108]. The discharge resistivity of the single PK granule [87] was 95 Ohm.cm, the third lowest. The single PK granule may thus even have underperformed due to a higher contact resistance than the fixed bed. The LMB bioanode had the highest resistivity during discharging [107]. The biofilm itself may have increased the contact resistance as well, which would have affected the moving bed reactors more as the biofilm in the fixed bioanode (SG and FB) experiments [87,108] could only grow on surfaces not involved in the contact already.

The influence of the cylindrical shape of the LMB discharge cell [107], as opposed to the planar shape in the SMB [108], may be a factor in this increased resistivity. However, as the ohmic resistance over the granular bed in the LMB could not be measured due to the cell configuration, any effect of the discharge cell shape on the resistivity over the granular bed requires more study. In this, I recommend attention is given to the granular and electrolyte flow in the discharge cell, for example using computational fluid dynamics to model the behavior of the flow.

The moving bed reactors had a packed-like moving bed in the discharge cell. The carbon weight%, chosen instead of the volume% due to differences in bulk density, was 49% in the discharge cell of the moving bed reactors [107,108], as opposed to 5% in the upward fluidized system [106] and 10% in the fluidized bed reactor with an external discharge cell [96] (assuming equal distribution over the fluidized bed systems).

The lower current density in the FB experiment, compared to the SMB bioanode, was correlated to the lower ΔE [108]. The effect of the ΔE can also be seen from the similar discharge resistivity, but lower current density, in the bioanode ([108], **Chapter 4**) and abiotic SMB experiments (**Chapter 5**) with a cell width of 10 mm. This suggests the high capacitive current in the SMB bioanode experiment [108] can be further increased by increasing the anode potential. At the time the anode potential was changed during the experiment, no such increase in current was observed. This discrepancy was explained by the increased granular bed resistance (**Chapter 4**) [108].

As shown in **Chapter 5**, the discharging resistance was lower with higher recovered charge, as a result of a higher applied ΔE, higher salinity, and decreased distance to the current collector. It was shown the discharge process was more affected by the electrical resistance than by the ionic resistance, in relation to the bulk electrolyte conductivity. This is a stark contrast to traditional (i.e. fixed) bed resistances, and shows the electrical resistance of the capacitive moving bed should be improved further. However, as the release of ions during discharging increases the local conductivity of the electrolyte (**Chapter 5**), the influence of the electrical resistance may always be greater than the influence of the bulk ionic conductivity.

This changes the challenge of voltage losses over the electrochemical cell, from high ionic resistance due to low conductivity electrolyte, to engineering for reduced electrical resistance. This is especially good news for the application of the moving bed bioanode for treatment of low conductivity wastewater, one of the great challenges for bioelectrochemical systems (see section 1.2).

Although the discharge resistance is an important measure of the losses in the discharge cell, the actual ΔE inside the discharge cell is lower than the maximum ΔE, which was calculated from the charged granules before they were discharged. In the length of the cell, the ΔE will have decreased, as the potential of the granules increased as more charge is recovered. Over the width of the cell, the ΔE will have decreased due to the gradient of resistance and the current over the granular bed. These gradients in the discharge cell were affected by the residence time as well, where a shorter residence time diluted the concentration of released ions more, compared to a long residence time, thus affecting the ohmic resistance in the discharge cell (**Chapter 5**). How increase in local electrolyte conductivity interacts with the residence time in moving bed bioanode reactors should be investigated, as the ΔE for bioanodes is mainly determined by how well the granules are charged before the discharge cell.

The discharge of the charged granules results in a capacitive peak current on top of the faradaic current, which allows high current densities to be achieved [85,86]. In the moving bed bioanodes, the separated charging and discharging produced a continuous discharge current in the discharge cell [107,108], therefore the current density per volume of discharge cell is relevant.

Electroactive bacteria (EAB) produce a faradaic current by oxidizing dissolved organics. The faradaic current, was measured in the single granule (SG) and fixed bed (FB) experiments after continuous potential control [87,108]. The faradaic current of the granules in the moving bed reactors is the current measured in the granular activity test experiments, where the current from a small sample of granules from the bioanode reactor was measured in a separate test cell [107,108]. The contact in the test cell was ensured by compacting the sample of granules tightly against the anode [107,108], resulting in contact resistances closer to fixed bed situation, than in the moving bed which had no pressure to the anode at all. For the faradaic current in the discharge cell of the moving bed, the activity is a best estimate, as differences in resistance result in differences in anode potential over the measured granules.

As bioanode activity is a surface related process, the faradaic current is best compared when normalized to the surface of the granules where the EAB may grow [88]. This surface area can be calculated by approximating spherical granules [88,116], and calculating the number of granules by dividing the total granule volume by the volume of a single granule. For the comparison of current per granule surface area, all values (**Table 6.1**) are selected for the bioanodes controlled at -0.3 V vs Ag/AgCl. The faradaic current produced by the small SG bioanode was 26 $A/m^2_{single\ granule}$. This current density is reduced to 7 $A/m^2_{granules}$ when the surface area is estimated from the bulk granule volume: the electrolyte occupies the remaining volume [87]. In the FB, SMB, and LMB experiments a different type of granule was used.

The average diameter of these granules (type HR5) was 0.65 mm [107,108]. The fixed granular bed bioanodes produced 0.2 $A/m^2_{granule}$. The faradaic current in the moving bed reactors, as the granular activity, increased over time. On day 10, the faradaic current was 0.02 $A/m^2_{granules}$, and on day 42/44 (SMB/LMB) [107,108], the current had increased to 0.05 $A/m^2_{granules}$.

Table 6.1. Table 11. An overview of the results and various parameters of the four capacitive bioanode configurations in this thesis

				Volume (mL)						Current density				Contribution to discharge current (%)		
Setup (chapter)[ref]	**Granule type**	**Cell width (mm)**	**Area (cm^2)**	**$V_{granules}$ [envelope] bulk[a]**	**$V_{reactor}$**	**V_{cell}**	**Residence time (s)**	**ΔE (mV)**	**Resistivity (Ohm.cm)**	**A/m^2_{cell}**	**$A/m^3_{reactor}$**	**$mA/cm^3_{granules}$ [envelope] bulk[a]**	**mA/cm^3_{cell}**	**Faradaic**	**Capacitive**	**Faradaic ($A/m^2_{granule}$)[b]**
Single granule (SG) (**2**)[5]	PK	3[c]	1.3	[10×10^{-3}] 35×10^{-3}	-	1	180 out of 240[d]	86	95[e]	6		[77] 22	0.8	84%	16%	[26.4] 7.4
Fixed bed (FB) (**4**)[8]	HR5 0.5 – 0.8 mm	5	22.3	17	-	11	60 out of 120[d]	46	38	24			3.2	54%	45%	0.19
		10	22.3	28		22	60 out of 120[d]	66	17	39			3.2	54%	46%	0.19
Large moving bed reactor (LMB) bioanode (day 10) (**3**) [6]		8	137	1200	7700	163	27	455	295	19	34	0.2	1.6	22%	78%	
Activity test cell LMB (day 10) (**3**) [6]								-	-	-	-	0.4	-			0.02
LMB bioanode (day 44) (**3**) [6]								505	280	23	40	0.3	1.9	65%	35%	
Activity test cell LMB (day 41) (**3**) [6]											-	1.2	-			0.05
Small moving bed reactor (SMB) bioanode (day 10) (**4**) [8]		10	22.3	375	1458	22	23	271	63	43	66	0.3	4.3	10%	90%	
Activity test cell SMB (day 15) (**4**) [8]											-	0.4	-			0.02
SMB bioanode (day 42) (**4**) [8]								478	382	13	19	0.1	1.3	100%[f]	0%	
Activity test cell SMB (day 42) (**4**) [8]											-	1.8	-			0.05
SMB abiotic (**5**)		5	44.6	375	1458	22	194	284	87	33	100	0.4	7			
		5	44.6				194	471	59	80	245	1.0	16			
		10	22.3				194	471	63	74	114	0.4	7			
		5	44.6				194	438	46	95	290	1.1	19			
		5	44.6				67	479	40	121	369	1.4	24			
		5	44.6				194	482	37	133	408	1.6	27			
Fluidized bed, external discharge cell [4]	GAC 1240	10	11	392	2200	22	0.5	~200[g]	604	1.3	0.7	4×10^{-3}	6.5×10^{-2} (0.3[h])			
Fluidized bed [12]	GAC 0.6 – 1 mm	23[i]	2.6	80	680	-	-	~700[j]	764	2.4	25	0.2	-			
Stirred cell [9]	GAC 30x30	15[k]	2.4	1.1	-	7	-	~100	259	2.6	-	1.6	0.3			

a) The envelope volume differs from the bulk volume by the exclusion of interparticle space from the envelope. For granular bed situations, the bulk volume is more accurate, as the interparticle space affects the volume occupied in the system.
b) The current at -0.3V vs Ag/AgCl controlled potential.
c) Calculated from the envelope volume of the single granules.
d) The discharge time out of the total cycle time: e.g. 60 seconds charging and 60 seconds discharging.
e) Resistivity dimensions of single granule estimated from the projected surface area ($4\pi r^2$) and the radius (½ of the cell width).
f) The activity of the granules was 1.8 mA/cm^3 on day 42, at 0V vs Ag/AgCl (the same potential as the discharge cell at the time).
g) Assumes fully charged granules are discharged at an anode potential of -0.3 V vs Ag/AgCl.
h) Volume of granules in the discharge cell (22 mL) was 4 mL.
i) Radius of reactor column
j) Assumes fully charged granules are discharged at an anode potential of +0.2 V vs Ag/AgCl.
k) Radius of cylindrical cell

The differences in configurations and operation give rise to various limitations imposed on the development of the biofilm. For instance: i) the access of the biofilm to substrate and buffer [95], was much better for the single granules compared to the granular bed electrodes (only 1% of the cell volume was occupied by the granule, compared to 49% granules in the discharge cells of the moving bed reactors), ii) growth time (3 – 9 times longer for the single granules than in the fixed and moving bed reactors [87,107,108], iii) shear stress on the surface of the granules in the moving bed [107] which was lower for the single granules and in the fixed bed, and iv) the contact resistance reduces the anode potential the bioanode granules experience over the width of the bed, which reduces the current produced at that potential [74,85,87,95,237–242].

The capacitive current, from the stored charge during charging, is released as a peak current [85,87,100]. For fixed capacitive bioanodes, the capacitive peak is clearly visible, but for the moving bed reactors the capacitive peak originates from each granule that makes contact with the anode (or through the granular bed) and the overlapping discharges of individual granules are measured as a continuous discharge current [108]. The capacitive current depends on the total stored charge in the volumetric capacitance of the granules (F/cm^3), the voltage driving the discharging, the time in contact for discharging, and the resistance (**Chapter 5**). **Table 6.1** shows the capacitive contribution to the current density in the (discharge) cell in the various configurations studied in this thesis.

Based on the calculated charge transfer, during the intermittent charging and discharging cycles, the capacitive contribution to the discharge in the SG experiments [87], were 16% (PK) and 19% (GAC) (**Chapter 2**). In the fixed bed (FB) experiments, the capacitive contribution was 45%, for both a 5 and 10 mm granular bed (**Chapter 4**) [108]. For the intermittent control of the fixed capacitive bioanodes, the discharge time was found to be the determining factor for the contribution of the capacitive current. As the capacitive peak decreases towards the faradaic current, the contribution of the faradaic current increases over the discharge time [88,108]. As the discharge time of the single granules (180s) [87] was 3 times longer than in the fixed bed reactors [108], the 2.5 – 2.9 times lower capacitive contribution can be explained.

In the moving bed reactors (**Table 6.1**), the capacitive contribution to the discharge current was calculated from the discharge current and the faradaic current, using the granule activity for the anode potential the reactors were operated at. The capacitive contribution was 78% (LMB) and 90% (SMB), after the first 10 days of operation. After another 30 days, the capacitive contribution of the LMB decreased to 35%. In the SMB bioanode experiment, on day 44, the activity was 1.8 mA/cm^3 while the discharge current was 1.3 mA/cm^3. The discharge current in the reactor was over 3 times lower, than the maximum in the SMB bioanode, because of the increased resistance in the discharge cell (**Chapter 4**) [108]. In **Table 6.1**, the capacitive contribution to the discharge current is therefore noted as 0% but may have been higher. Despite this uncertainty, it can be noted, however, that the growth of the biofilm (seen as the increased faradaic current) could be a factor in decreasing the capacitive current. For the application of the capacitive bioanodes, investigating the effect of the biofilm on the discharging process is therefore important, as it may be possible to control by engineering the granules and the shear forces that act on the biofilm (**Chapter 3**).

In the abiotic SMB experiments, the discharge current was fully capacitive. The current densities are the average over the discharge time of each part of the experiment (**Chapter 5**). The current density of the experiments, performed under similar conditions to the SMB bioanode (low bulk electrolyte conductivity and ~0.3 V driving force), had a similar current density, 33 A/m^2, to the bioanode, 43 A/m^2. The abiotic experiment, however, was performed using a different cell configuration, where the maximum distance to the current collector was 5 instead of 10 mm (bioanode), resulting in 7 mA/cm^3 in the discharge cell in the abiotic SMB experiment, compared to 4.3 mA/cm^3 in the SMB bioanode experiment. The importance of optimizing the discharge cell compared to the total volume of granules was shown, both in relation to the surface area of the anode [107], as well as the volume of the discharge cell [108]. In **Chapter 5** this was implemented by doubling the surface area per volume of discharge cell. As a result, the average current density increased from 74 A/m^2 to 80 A/m^2 (**Table 6.1**). This shows the benefit of the additional anode surface area (with associated membrane and counter electrode) for the discharge process, under abiotic conditions.

As the current density and the discharge resistance were similar between the 10 mm cell with of the abiotic and biotic experiments, changing the cell configuration from 10 mm width to 5 mm width, is expected improve the discharge current from the bioanodes as well. The decreased distance to the current collector resulted in 2.1 times more discharge in the abiotic experiment (**Chapter 5**), would mean an increase in discharge current from 4.3 to 9.1 mA/cm^3 for the SMB bioanode [108].

6.3. Improvements to the moving bed reactor

Several recommendations for engineering improvements were made in **Chapters 3, 4 & 5**. These can be divided in three categories: i) discharge cell, ii) charging and discharging volumes, iii) granules, including their biofilm. In this section, improving the resistance over the granular bed will be discussed in relation to these categories.

Decreasing the electrical and ionic resistances in the discharge cell, was in this thesis achieved via a reduced distance to the current collector in the discharge cell in the abiotic system (**Chapter 5**). Reducing the path length over the width of the granular bed (to the current collector and membrane) [108], can most optimally be accomplished by use of a tubular electrode, through which the granular bed flows: the maximum distance between granules and current collector is then the radius of the tube.

Such a reduced width poses challenges in terms of flowability. As the moving bed relies on the flow of granules for a capacitive current from charged granules, an increased clogging risk due to a narrow cell is undesired. Smaller granule size would be favorable, because the risk of clogging is related to the size of the granules in relation to the width of the cell through which the granules flow [243,244]. Improving the resistance via the width of the granular bed, or size of the granules, is limited because the moving bed depends on settling of the granules into a granular bed, as well as for separation from the liquid flowrate at the top of the reactor. In addition, if the granules become too small, the packing may result in the space between the particles to become small enough for the capillary force to overcome the force required for the movement in the bed and the transport in the gas lift. In relation to real wastewater, narrowing the width of the discharge cell increases the risk of clogging due to suspended solids [90,91]. This may be mitigated by using a washing compartment to separate suspended solids, as well as sheared off biofilm, from the water stream, as used in continuous sand filter systems [152], after which the moving bed reactor was designed [107].

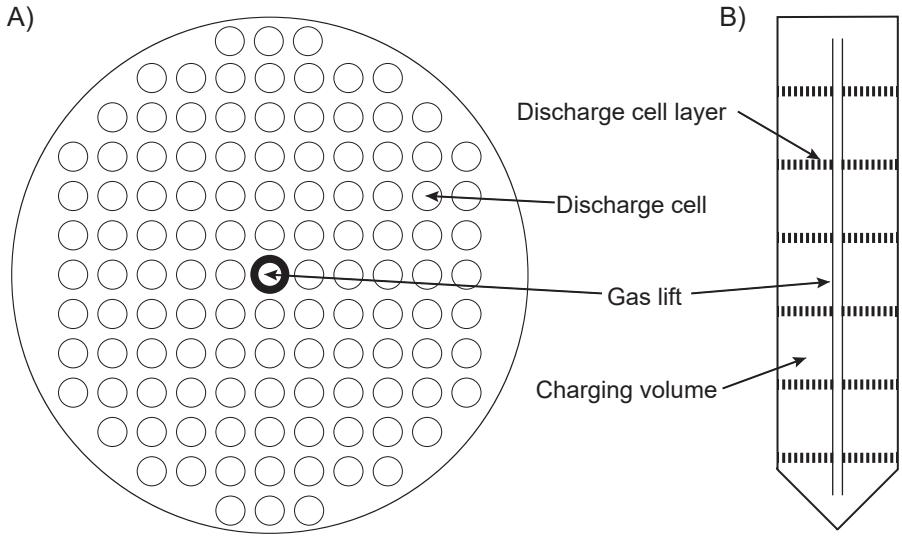

Figure 6.3. A) Example of multiple discharge cells in B) multiple, horizontal, layers of a tubular reactor vessel, with a gas lift in the middle. Designed after a pilot scale air lift reactor concept [245].

As mentioned, the discharge time, for a moving bed bioanode, relates to the residence time of the granules in the cell, which is determined by the length of the discharge cell and the granular flowrate [107,108]. The granular flowrate in the moving bed reactor designs of this thesis was determined by the gas lift flowrate. By dividing the flow of the granules over multiple discharge cells (see **Figure 6.3A** for an example), the granule flowrate through one discharge cell is reduced, further increasing the contact time for discharging.

When the discharge cell is optimized, the number of discharge cells – which equates to the available surface area for discharging – can be optimized to the total granule volume: the ratio of charging to discharging. Larger scale reactors could benefit from vertically positioned layers of discharge cells, with charging volumes in between (**Figure 6.3B**), through which the granular bed moves. The separation with the charging volumes will result in fully charged granules entering the discharge cell for high capacitive current densities (**Chapter 4 & 5**) [108].

Large scale electrochemical reactors are often hampered by ohmic losses over the electrochemical cell, resulting in potential and current distribution over the anode. Such a potential distribution, also between the electrodes and reference electrodes, may give rise to control issues and therefore the current is often controlled instead of the electrode potential. Control over the current may still be preferred for a larger moving bed reactor [107]. Multiple discharge cells would of course reduce the economical benefits of the separated charging and discharging. The costs should thus be weighted against the produced electrical power or the more valuable hydrogen or other chemicals [71].

Further improving the electrical conductivity over the granular bed in the discharge cell can best be sought by improving the granules themselves. The resistance over the granular bed, though clearly affected by the path length, is also affected by the resistivity of the granules. In terms of electrical resistance, the material properties as well as the contact resistance determine the voltage loss over the width of the cell. In addition, the biofilm itself may add another layer which increases the contact resistance. The effect of the biofilm on the contact resistance should be further investigated, however the outer surface of the granules (where the electrical contact likely occurred) in the moving bed reactor was clean of bacteria, as an effect of the shear stress induced by the constant movement [107].

The electrical conductivity of the granules is affected by the type of carbon. For instance, the conductivity of graphite powder is at least 10 times lower than activated carbon, when applying pressure to the powder bed to measure the material resistance independent of the contact resistance. Without the added pressure, the resistivity of the activated carbon powder increased 10 times to 1 Ohm.cm [246], which is a situation closer to the resistivity of the activated carbon granules in the moving bed. However, the size of the granules also affects the resistivity, where decreasing the particle size from 45 to 3 µm more than doubled the resistivity [246], which is another restriction for reducing the particle size.

Metallic current collectors have lower resistivity than carbon [207,246] and could have potential as bioanodes [247]. For instance, pure copper has a resistivity of 1.7×10^{-6} Ohm.cm [207] and titanium 42×10^{-6} Ohm.cm [76], both several orders of magnitude lower than the resistivity of carbon. Pure metallic particles do not have the supercapacitive properties of porous activated carbon, however, and therefore integrating metallic conductance properties and supercapacitive carbon materials will be necessary. There are three likely pathways to combining these properties: activated carbon coated with metal, metal coated with activated carbon, and activating a mixture of metal and pre-cursor carbon material (for instance via polymer carbonization and activation [248]).

Partial metallic granules will have a higher density than unmodified granules, which is beneficial in relation to the settling of the granules: for the same settling velocity, the granules can be smaller [249]. What the relation between conductivity and granule size is for the modified granules, as well as how this affects the contact resistance of the moving bed should be investigated, as smaller granules would allow for a thinner discharge cell which decreases the granular bed resistance as well.

Choosing the granule size involves the ratio of width over granule diameter to minimize the risk of clogging [243,244]. In the experiments, the granule diameter was between 10 and 16 times smaller than the 8 mm width of the LMB discharge cell (which was the thinnest cell of the two moving bed reactors). If a ratio of 10 is chosen, and the granules are selected for 0.5 mm (as opposed to the range of 0.5 to 0.8 mm for the HR type granules in this thesis), the width of the cell can be reduced to 5 mm, or a 2.5 mm tubular radius. Further reducing the granule size may be possible, but the relationship between contact resistance in the moving bed and the size of the granules should be further investigated to make that determination, and care should be taken that a higher particle density increases the energy cost of the gas lift (in gas pressure and gas flow) [249].

Another benefit of smaller granules is lower ion transport resistance [116], because ion transport resistance decreases for lower path length [86]. This also manifests as a higher capacitance, as the voltage drop over the ionic resistance in the pores is reduced and more charge per volt is stored [100]. The capacitance of modified granules should be investigated as well, as the metallic component will reduce the volumetric capacitance: either via blocking pores as a coating, or merely by its fraction of the particle volume. In addition, for long term operation, coatings should adhere enough to overcome loss of the coating via friction of the moving bed.

Decreasing the ion transport resistance by decreasing the granule size can be applied in a limited fashion due to other restrictions on particle size. Aside from settling and contact resistance, the ionic resistance in the electrolyte of the granular bed may also be affected by the granule size, as the available path through the electrolyte could be constricted by the packing density of the granular bed [204]. How this affects the discharge process in the moving bed should be investigated, as the non-rigid nature of the moving bed will be influencing the ion transport resistance in the electrolyte between the granules [249].

During discharging ions are released from the porous granules into the electrolyte [96]. This was shown to increase the local electrolyte in the discharge cell significantly (**Chapter 5**). As such, improving the ion transport from the pores may significantly improve the discharge further by increasing the rate ion discharge [250]. Different pore width and volume contribute to different aspects of charge transfer [250]. The different pore types are described using pore size distributions, expressed as the pore volume and surface area (**Chapter 2**): micropores have pore widths below 2 nm, mesopores between 2 and 50 nm and macropores above 50 nm [87]. While micropores are associated with the capacitance, because of the high surface area per pore volume, the mesopores are associated with ion transport [250].

The PK and GAC granules have 40% resp. 20% mesopores (**Chapter 2**) [87], but the granules in the moving bed reactors (type HR5, **Chapters 3,4 & 5**) have only 0.3% mesopores per volume. The HR granules, however, have the highest micropore area of 1100 m^2/g [107] compared to 764 m^2/g (PK) and 885 (GAC) m^2/g [87]. The total capacitance, or stored charge per volt, is affected by both the micropore area (stored charge) and the voltage difference (reduced by ion transport resistance in the meso/macropore volume, and the carbon structure for the electrical material resistance) [100]. Previous studies have shown that ordered mesoporous carbon have a higher capacitance, which was associated with a decrease in ion transport resistance [251]. Another influence on the ion transport, is the (hydrated) size of the ions [252]. In the abiotic experiments the composition of the electrolyte was relatively simple compared to the synthetic wastewater used in the bioanode experiments. As such, the ion composition of wastewater may influence the discharging process as well [253].

When modifying activated carbon, attention should be given that increasing the mesoporosity may be detrimental for the microporosity. Another downside of a large meso- and macroporous structure is a higher brittleness [116]. As the coconut-based HR granules were specifically chosen for their high hardness (HR type granules have a hardness of 97 on a scale of 100 [254]) to prevent significant degradation of the granules.

Long term operation of bioanodes requires biocompatibility with the granule surface. Carbon anodes, especially rough graphite over flat graphite, perform well in this regard. The granular bioanodes make use of the roughness of activated carbon, which increases the biofilm available surface area [255]. The proposed modifications to combine metallic properties with activated carbon require consideration to biocompatibility. Metals such as gold, silver, copper,

nickel, cobalt, titanium, and stainless steel have been used as conductive surface for bioanode growth [247]. Though specifically silver and copper are used for their antimicrobial properties, EAB produced current densities comparable to graphite on the copper and silver anodes [247]. The stability of the metallic granules should be investigated, as for instance the onset of copper oxidation is at 0 V vs Ag/AgCl, which could occur in the moving bed reactors [107,108].

In the moving bed reactor, the volume of biofilm present on the granules was significantly lower than was observed to grow on the single granules [107]. Though the higher amount of biofilm may show as a high faradaic current (see section 6.2), there are downsides of thicker and aged electroactive biofilms. As the biofilm ages, the older bacteria may become inactive thus reducing the activity of the total biofilm volume [256]. In thicker biofilms, mass transport limitations pose constraints on the current density, from diffusion of substrate and products from the oxidation [69], as well as possible restricted ion transport, out of the porosity, over the biofilm, into the electrolyte. The influence of the biofilm on the discharging process should be investigated further, as it is currently unknown if the biofilm inhibits electrical contact or ion transport.

Shear stress was shown to limit growth of EAB on the surface of the granules [107], thus ensuring thin biofilms on the surface. However, inside the larger pores, a thicker and aged biofilm is likely to remain shielded from the friction in the moving bed. The same friction may cause degradation of manufactured granules, such as granulated powder particles or particles coated with powder and a binder [85].

To improve the removal of old biofilm, and maintaining a thin biofilm, a smoother surface may be preferable, where access to the meso- and micropores is still available but microbial growth is less shielded from the shear forces. To maintain a presence of EAB, the carbon surface may be modified to enhance biofilm attachment, for example a surface with increased hydrophilicity [166]. Choosing to enhance hydrophilicity may also improve the capacitance, as better "wetting" can result in lower ion transfer resistance and higher volumetric capacitance [257], though care must be taken the modification of surface chemistry is not detrimental to the specific surface area [258,259].

In short, the granules should be a) modified for higher electrical conductivity, through integration of metallic components, b) reduced in size, for which the settling rate can be balanced due to an increased density from the metallic components, c) modified for higher mesoporosity, for decreased ionic resistance in the porosity, d) biocompatible, and e) have a smooth surface with surface chemistry modifications to balance biofilm thinning with biofilm attachment in the high shear environment of the moving bed.

When the improved granules are discharged in multiple tubular discharge cells, with a minimum granular bed with of 10 times the diameter of the granules, the discharging is optimized. The charging volume, as total volume of granules, is then balanced to the available discharging surface area. The volume outside of the total granule volume can then be minimized for producing the highest volumetric current per reactor volume.

6.4. Future of moving bed electrodes in microbial electrochemical technologies

As shown in this thesis, application of bioanodes for wastewater treatment faces several challenges: 1) low conductivity, 2) clogging, 3) methanogen competition, and 4) low current densities, and fluidized bed bioanodes were identified as a solution to these challenges. The moving bed reactor showed great promise for producing high current densities and tackle the challenge of low conductivity. The moving bed reactor produced 1.9 – 4.3 mA/cm^3_{cell}, between 3 and 20 times higher current than the previous highest performing reactors, and at a larger scale. We have shown that using the capacitive charge storage, for separate charging and discharging, provides an alternative path for scaling up bioelectrochemical systems, as opposed to increasing the volume by stacking multiple electrochemical cells [107].

Though 3.5 mA/cm^3 per volume of the reactor was not reached, which was desired to compete with AD, the moving bed bioanode did produce 4.3 mA/cm^3 in the discharge cell. With minimal adjustments (adding another current collector, and associated membrane and cathode, to the other side of the granular bed), would result in 9 mA/cm^3 (assuming the same improvement ratio holds for bioanodes as for abiotic discharging). Implementation of the proposed improvements to the discharge cell, granules, and reactor, would improve the current to the desired high current density. The most promising finding is the reduced ionic resistance due to ion release during discharging, which makes the moving bed capacitive bioanode uniquely suited as larger scale bioanode reactors.

Application of moving bed bioanodes in Microbial Fuel Cells for production of electrical power is still promising, when applied to decrease external power demands of wastewater treatment plants. However, due to the rapid rate of implementation of sustainable electricity production from solar and wind [260], implementation of MFCs as a competitive technology for electricity production may be difficult. When the moving bed reactor is applied as Microbial Electrolysis Cells, more product options, like generation of hydrogen or other high-value products are available, which improve the cost-benefit analysis [71].

Activated carbon has been used for various adsorption processes, such as noxious gasses, medicine residues, pesticides, and metals [261]. Recently, pilot scale testing of powdered activated carbon for micropollutant removal has been started in wastewater treatment plants [262]. Application of granular activated carbon as capacitive bioanodes may allow for new possibilities of combining the adsorption processes with treatment of dissolved organics. The electroactive biofilm can act as an interface for attachment of a more diverse microbial community, containing for instance those microorganisms that have been shown to degrade micropollutants such as medicine residues [263]. The reductive potential of charged granules could even accelerate certain adsorption processes. For instance, metals, with a higher reduction potential than the oxidation potential of acetate, like copper [264,265] will be electroplated on the surface of the granules. As copper in solution is toxic to micro-organisms, the removal of copper may reduce the toxicity of the wastewater (effluent) [264]. Of course, the granules should be replaced more often to harvest the copper, but they can potentially be regenerated for reuse.

During the abiotic experiment, we showed that cathodic operation of the discharge cell was able to charge the moving granular bed. Therefore, using the moving bed as a biocathode may be another avenue for research. If hydrogen formation can be successfully suppressed, this could be used for microbial electrosynthesis processes, like the production of acetate or medium chain fatty acids [53–55].

With this research, new directions for design of microbial electrochemical systems have been explored and studied. Further improvement of discharging, and insight in how to control the process, will help to further bring the moving bed reactor towards scaling up for practical application.

Ösbyträsk, Sweden

References

References

[1] M. Qadir, P. Drechsel, B. Jiménez Cisneros, Y. Kim, A. Pramanik, P. Mehta, O. Olaniyan, Global and regional potential of wastewater as a water, nutrient and energy source, Nat. Resour. Forum. 44 (2020) 40–51. https://doi.org/10.1111/1477-8947.12187.

[2] W.P. Cunningham, M.A. Cunningham, Principles of environmental science, 6th ed., 2011.

[3] L.A. Lawton, G.A. Codd, Cyanobacterial (Blue-Green Algal) Toxins and their Significance in UK and European Waters, Water Environ. J. 5 (1991) 460–465. https://doi.org/10.1111/j.1747-6593.1991.tb00643.x.

[4] J. Abellán, Water supply and sanitation services in modern Europe: developments in 19th-20th centuries, in: XII Int. Congr. Spanish Assoc. Econ. Hist., University of Salamanca Water, 2017.

[5] Eurostat, Energy, Transport and environment statistics. 2019 edition, Publications Office of the European Union, Luxembourg, 2019. https://doi.org/10.2785/660147.

[6] A. Ullah, S. Hussain, A. Wasim, M. Jahanzaib, Development of a decision support system for the selection of wastewater treatment technologies, Sci. Total Environ. 731 (2020) 139158. https://doi.org/10.1016/j.scitotenv.2020.139158.

[7] M. Maktabifard, E. Zaborowska, J. Makinia, Achieving energy neutrality in wastewater treatment plants through energy savings and enhancing renewable energy production, Springer Netherlands, 2018. https://doi.org/10.1007/s11157-018-9478-x.

[8] A. Capodaglio, G. Olsson, Energy Issues in Sustainable Urban Wastewater Management: Use, Demand Reduction and Recovery in the Urban Water Cycle, Sustainability. 12 (2019) 266. https://doi.org/10.3390/su12010266.

[9] P.L. McCarty, J. Bae, J. Kim, Domestic Wastewater Treatment as a Net Energy Producer–Can This be Achieved?, Environ. Sci. Technol. 45 (2011) 7100–7106. https://doi.org/10.1021/es2014264.

[10] A. Raheem, V.S. Sikarwar, J. He, W. Dastyar, D.D. Dionysiou, W. Wang, M. Zhao, Opportunities and challenges in sustainable treatment and resource reuse of sewage sludge: A review, Chem. Eng. J. 337 (2018) 616–641. https://doi.org/10.1016/j.cej.2017.12.149.

[11] L. Appels, J. Baeyens, J. Degrève, R. Dewil, Principles and potential of the anaerobic digestion of waste-activated sludge, Prog. Energy Combust. Sci. 34 (2008) 755–781. https://doi.org/10.1016/j.pecs.2008.06.002.

[12] M. Pronk, M.K. de Kreuk, B. de Bruin, P. Kamminga, R. Kleerebezem, M.C.M. van Loosdrecht, Full scale performance of the aerobic granular sludge process for sewage treatment, Water Res. 84 (2015) 207–217. https://doi.org/10.1016/j.watres.2015.07.011.

[13] S. Bengtsson, A. Werker, M. Christensson, T. Welander, Production of polyhydroxyalkanoates by activated sludge treating a paper mill wastewater, Bioresour. Technol. 99 (2008) 509–516. https://doi.org/10.1016/j.biortech.2007.01.020.

[14] Y. di Chen, R. Wang, X. Duan, S. Wang, N. qi Ren, S.H. Ho, Production, properties, and catalytic applications of sludge derived biochar for environmental remediation, Water Res. 187 (2020) 116390. https://doi.org/10.1016/j.watres.2020.116390.

[15] Q. Fu, D. Wang, X. Li, Q. Yang, Q. Xu, B.J. Ni, Q. Wang, X. Liu, Towards hydrogen production from waste activated sludge: Principles, challenges and perspectives, Renew. Sustain. Energy Rev. 135 (2021) 110283. https://doi.org/10.1016/j.rser.2020.110283.

[16] H. Geng, Y. Xu, L. Zheng, H. Gong, L. Dai, X. Dai, An overview of removing heavy metals from sewage sludge: Achievements and perspectives, Environ. Pollut. 266 (2020) 115375. https://doi.org/10.1016/j.envpol.2020.115375.

[17] J.N. Russell, C.K. Yost, Alternative, environmentally conscious approaches for removing antibiotics from wastewater treatment systems, Chemosphere. 263 (2021) 128177. https://doi.org/10.1016/j.chemosphere.2020.128177.

[18] M. Wu, W. Tang, S. Wu, H. Liu, C. Yang, Fate and effects of microplastics in wastewater treatment processes, Sci. Total Environ. 757 (2021) 143902. https://doi.org/10.1016/j.scitotenv.2020.143902.

[19] V. Ajao, R. Fokkink, F. Leermakers, H. Bruning, H. Rijnaarts, H. Temmink, Bioflocculants from wastewater: Insights into adsorption affinity, flocculation mechanisms and mixed particle flocculation based on biopolymer size-fractionation, J. Colloid Interface Sci. 581 (2021) 533–544. https://doi.org/10.1016/j.jcis.2020.07.146.

[20] L.T. Angenent, K. Karim, M.H. Al-Dahhan, B.A. Wrenn, R. Domiguez-Espinosa, Production of bioenergy and biochemicals from industrial and agricultural wastewater, Trends Biotechnol. 22 (2004) 477–485. https://doi.org/10.1016/j.tibtech.2004.07.001.

[21] G. Lettinga, A.F.M. van Velsen, S.W. Hobma, W. de Zeeuw, A. Klapwijk, Use of the upflow sludge blanket (USB) reactor concept for biological wastewater treatment, especially for anaerobic treatment, Biotechnol. Bioeng. 22 (1980) 699–734. https://doi.org/10.1002/bit.260220402.

[22] J.B. van Lier, F.P. van der Zee, C.T.M.J. Frijters, M.E. Ersahin, Celebrating 40 years anaerobic sludge bed reactors for industrial wastewater treatment, Rev. Environ. Sci. Biotechnol. 14 (2015) 681–702. https://doi.org/10.1007/s11157-015-9375-5.

[23] D. Sudmalis, M.C. Gagliano, R. Pei, K. Grolle, C.M. Plugge, H.H.M. Rijnaarts, G. Zeeman, H. Temmink, Fast anaerobic sludge granulation at elevated salinity, Water Res. 128 (2018) 293–303. https://doi.org/10.1016/j.watres.2017.10.038.

[24] C.A.L. Chernicharo, J.B. van Lier, A. Noyola, T. Bressani Ribeiro, Anaerobic sewage treatment: state of the art, constraints and challenges, Rev. Environ. Sci. Biotechnol. 14 (2015) 649–679. https://doi.org/10.1007/s11157-015-9377-3.

[25] Q. Liao, J. Chang, C. Herrmann, A. Xia, Bioreactors for Microbial Biomass and Energy Conversion, Springer Singapore, Singapore, 2018. https://doi.org/10.1007/978-981-10-7677-0.

[26] T.H. Pham, K. Rabaey, P. Aelterman, P. Clauwaert, L. De Schamphelaire, N. Boon, W. Verstraete, Microbial Fuel Cells in Relation to Conventional Anaerobic Digestion Technology, Eng. Life Sci. 6 (2006) 285–292. https://doi.org/10.1002/elsc.200620121.

[27] S.B. Idso, B.A. Kimball, M.G. Anderson, J.R. Mauney, Effects of atmospheric CO2 enrichment on plant growth: the interactive role of air temperature, Agric. Ecosyst. Environ. 20 (1987) 1–10. https://doi.org/10.1016/0167-8809(87)90023-5.

[28] C.J.N. Buisman, Biotechnological Sulphide Removal with Oxygen, (1989) 122.

[29] J.R. Cunha, C. Schott, R.D. van der Weijden, L.H. Leal, G. Zeeman, C. Buisman, Calcium phosphate granules recovered from black water treatment: A sustainable substitute for mined phosphorus in soil fertilization, Resour. Conserv. Recycl. 158 (2020) 104791. https://doi.org/10.1016/j.resconrec.2020.104791.

[30] M.C. Potter, Electrical effects accompanying the decomposition of organic compounds, Proc. R. Soc. London. Ser. B, Contain. Pap. a Biol. Character. (1911) 260–276.

[31] B. Cohen, Thirty-second Annual Meeting of the Society of American Bacteriologists, J Bacteriol. 21 (1931) 1–60.

[32] J.B. Davis, H.F. Yarbrough Jr., Preliminary experiments on a microbial fuel cell, Science (80-.). 137 (1962) 615–616. https://doi.org/10.1126/science.137.3530.615.

[33] K. Lewis, Symposium on bioelectrochemistry of microorganisms. IV. Biochemical fuel cells., Bacteriol. Rev. 30 (1966) 101–113. https://doi.org/10.1128/mmbr.30.1.101-113.1966.

[34] J.B.A. Arends, W. Verstraete, 100 years of microbial electricity production: Three concepts for the future, Microb. Biotechnol. 5 (2012) 333–346. https://doi.org/10.1111/j.1751-7915.2011.00302.x.

[35] K. Rabaey, Bioelectrochemical systems: from extracellular electron transfer to biotechnological application, IWA publishing, London, UK, 2010.

[36] B.E. Logan, B. Hamelers, R. Rozendal, U. Schröder, J. Keller, S. Freguia, P. Aelterman, W. Verstraete, K. Rabaey, Microbial Fuel Cells: Methodology and Technology †, Environ. Sci. Technol. 40 (2006) 5181–5192. https://doi.org/10.1021/es0605016.

[37] R.A. Rozendal, E. Leone, J. Keller, K. Rabaey, Efficient hydrogen peroxide generation from organic matter in a bioelectrochemical system, Electrochem. Commun. 11 (2009) 1752–1755. https://doi.org/10.1016/j.elecom.2009.07.008.

[38] R.A. Rozendal, H.V.M. Hamelers, G. Euverink, S. Metz, C.J.N. Buisman, Principle and perspectives of hydrogen production through biocatalyzed electrolysis, Int. J. Hydrogen Energy. 31 (2006) 1632–1640. https://doi.org/10.1016/j.ijhydene.2005.12.006.

[39] B.E. Logan, D. Call, S. Cheng, H.V.M. Hamelers, T.H.J.A. Sleutels, A.W. Jeremiasse, R.A. Rozendal, Microbial Electrolysis Cells for High Yield Hydrogen Gas Production from Organic Matter, Environ. Sci. Technol. 42 (2008) 8630–8640. https://doi.org/10.1021/es801553z.

[40] R. a Rozendal, H.V.M. Hamelers, R.J. Molenkamp, C.J.N. Buisman, Performance of single chamber biocatalyzed electrolysis with different types of ion exchange membranes., Water Res. 41 (2007) 1984–94. https://doi.org/10.1016/j.watres.2007.01.019.

[41] T.H.J.A. Sleutels, H.V.M. Hamelers, R.A. Rozendal, C.J.N. Buisman, Ion transport resistance in Microbial Electrolysis Cells with anion and cation exchange membranes, Int. J. Hydrogen Energy. 34 (2009) 3612–3620. https://doi.org/10.1016/j.ijhydene.2009.03.004.

[42] C.J.N. Buisman, R. Rozendal, Bio-electrochemical process for producing hydrogen, WO2005005981A2, 2005.

[43] M. Rodríguez Arredondo, P. Kuntke, A. ter Heijne, C.J.N. Buisman, The concept of load ratio applied to bioelectrochemical systems for ammonia recovery, J. Chem. Technol. Biotechnol. 94 (2019) 2055–2061. https://doi.org/10.1002/jctb.5992.

[44] Y. Lei, M. Du, P. Kuntke, M. Saakes, R. van der Weijden, C.J.N. Buisman, Energy Efficient Phosphorus Recovery by Microbial Electrolysis Cell Induced Calcium Phosphate Precipitation, ACS Sustain. Chem. Eng. 7 (2019) 8860–8867. https://doi.org/10.1021/acssuschemeng.9b00867.

[45] X. Cao, X. Huang, P. Liang, K. Xiao, Y. Zhou, X. Zhang, B.E. Logan, A new method for water desalination using microbial desalination cells, Environ. Sci. Technol. 43 (2009) 7148–7152. https://doi.org/10.1021/es901950j.

[46] D. Liu, M. Roca-Puigros, F. Geppert, L. Caizán-Juanarena, S.P. Na Ayudthaya, C. Buisman, A. ter Heijne, Granular Carbon-Based Electrodes as Cathodes in Methane-Producing Bioelectrochemical Systems, Front. Bioeng. Biotechnol. 6 (2018) 1–10. https://doi.org/10.3389/fbioe.2018.00078.

[47] F. Geppert, D. Liu, M. van Eerten-Jansen, E. Weidner, C. Buisman, A. ter Heijne, Bioelectrochemical Power-to-Gas: State of the Art and Future Perspectives, Trends Biotechnol. 34 (2016) 879–894. https://doi.org/10.1016/j.tibtech.2016.08.010.

[48] D. Liu, L. Zhang, S. Chen, C. Buisman, A. Ter Heijne, Bioelectrochemical enhancement of methane production in low temperature anaerobic digestion at 10 °C, Water Res. 99 (2016) 281–287. https://doi.org/10.1016/j.watres.2016.04.020.

[49] D. Liu, T. Zheng, C. Buisman, A. Ter Heijne, Heat-Treated Stainless Steel Felt as a New Cathode Material in a Methane-Producing Bioelectrochemical System, ACS Sustain. Chem. Eng. 5 (2017) 11346–11353. https://doi.org/10.1021/acssuschemeng.7b02367.

[50] K. Rabaey, R. a Rozendal, Microbial electrosynthesis - revisiting the electrical route for microbial production., Nat. Rev. Microbiol. 8 (2010) 706–16. https://doi.org/10.1038/nrmicro2422.

[51] S.D. Molenaar, P. Saha, A.R. Mol, T.H.J.A. Sleutels, A. ter Heijne, C.J.N. Buisman, Competition between methanogens and acetogens in biocathodes: A comparison between potentiostatic and galvanostatic control, Int. J. Mol. Sci. 18 (2017). https://doi.org/10.3390/ijms18010204.

[52] S.D. Molenaar, A.R. Mol, T.H.J.A. Sleutels, A. ter Heijne, C.J.N. Buisman, Microbial Rechargeable Battery: Energy Storage and Recovery through Acetate, Environ. Sci. Technol. Lett. 3 (2016) 144–149. https://doi.org/10.1021/acs.estlett.6b00051.

[53] S.M.T. Raes, L. Jourdin, C.J.N. Buisman, D.P.B.T.B. Strik, Bioelectrochemical Chain Elongation of Short-Chain Fatty Acids Creates Steering Opportunities for Selective Formation of n-Butyrate, n-Valerate or n-Caproate, ChemistrySelect. 5 (2020) 9127–9133. https://doi.org/10.1002/slct.202002001.

[54] S.M.T. Raes, L. Jourdin, C.J.N. Buisman, D.P.B.T.B. Strik, Continuous Long-Term Bioelectrochemical Chain Elongation to Butyrate, ChemElectroChem. 4 (2017) 386–395. https://doi.org/10.1002/celc.201600587.

[55] L. Jourdin, S.M.T. Raes, C.J.N. Buisman, D.P.B.T.B. Strik, Critical biofilm growth throughout unmodified carbon felts allows continuous bioelectrochemical chain elongation from CO2 up to caproate at high current density, Front. Energy Res. 6 (2018) 1–15. https://doi.org/10.3389/fenrg.2018.00007.

[56] D.R. Lovley, The microbe electric: conversion of organic matter to electricity, Curr. Opin. Biotechnol. 19 (2008) 564–571. https://doi.org/10.1016/j.copbio.2008.10.005.

[57] D.R. Lovley, Electromicrobiology, Annu. Rev. Microbiol. 66 (2012) 391–409. https://doi.org/10.1146/annurev-micro-092611-150104.

[58] B.E. Logan, R. Rossi, A. Ragab, P.E. Saikaly, Electroactive microorganisms in bioelectrochemical systems, Nat. Rev. Microbiol. 17 (2019) 307–319. https://doi.org/10.1038/s41579-019-0173-x.

[59] C. Koch, F. Harnisch, Is there a Specific Ecological Niche for Electroactive Microorganisms?, ChemElectroChem. 3 (2016) 1282–1295. https://doi.org/10.1002/celc.201600079.

[60] C.I. Torres, A.K. Marcus, H.S. Lee, P. Parameswaran, R. Krajmalnik-Brown, B.E. Rittmann, A kinetic perspective on extracellular electron transfer by anode-respiring bacteria, FEMS Microbiol. Rev. 34 (2010) 3–17. https://doi.org/10.1111/j.1574-6976.2009.00191.x.

[61] R. Kumar, L. Singh, A.W. Zularisam, Exoelectrogens: Recent advances in molecular drivers involved in extracellular electron transfer and strategies used to improve it for microbial fuel cell applications, Renew. Sustain. Energy Rev. 56 (2016) 1322–1336. https://doi.org/10.1016/j.rser.2015.12.029.

[62] P. Winaikij, P. Sreearunothai, K. Sombatmankhong, Probing mechanisms for microbial extracellular electron transfer (EET) using electrochemical and microscopic characterisations, Solid State Ionics. 320 (2018) 283–291. https://doi.org/10.1016/j.ssi.2018.02.044.

[63] G. Reguera, K.D. McCarthy, T. Mehta, J.S. Nicoll, M.T. Tuominen, D.R. Lovley, Extracellular electron transfer via microbial nanowires, Nature. 435 (2005) 1098–1101. https://doi.org/10.1038/nature03661.

[64] S. Tejedor-Sanz, J.R. Quejigo, A. Berná, A. Esteve-Núñez, The Planktonic Relationship Between Fluid-Like Electrodes and Bacteria: Wiring in Motion, ChemSusChem. (2017) 1–9. https://doi.org/10.1002/cssc.201601329.

[65] S. Freguia, K. Rabaey, Z. Yuan, J. Keller, Electron and Carbon Balances in Microbial Fuel Cells Reveal Temporary Bacterial Storage Behavior During Electricity Generation, Environ. Sci. Technol. 41 (2007) 2915–2921. https://doi.org/10.1021/es062611i.

[66] N. Uría, X. Muñoz Berbel, O. Sánchez, F.X. Muñoz, J. Mas, Transient Storage of Electrical Charge in Biofilms of Shewanella oneidensis MR-1 Growing in a Microbial Fuel Cell, Environ. Sci. Technol. 45 (2011) 10250–10256. https://doi.org/10.1021/es2025214.

[67] A. ter Heijne, M.A. Pereira, J. Pereira, T. Sleutels, Electron Storage in Electroactive Biofilms, Trends Biotechnol. 39 (2020) 34–42. https://doi.org/10.1016/j.tibtech.2020.06.006.

[68] S.C. Popat, C.I. Torres, Critical transport rates that limit the performance of microbial electrochemistry technologies, Bioresour. Technol. 215 (2016) 265–273. https://doi.org/http://dx.doi.org/10.1016/j.biortech.2016.04.136.

[69] A.C.L. de Lichtervelde, A. ter Heijne, H.V.M. Hamelers, P.M. Biesheuvel, J.E. Dykstra, Theory of Ion and Electron Transport Coupled with Biochemical Conversions in an Electroactive Biofilm, Phys. Rev. Appl. 12 (2019) 014018. https://doi.org/10.1103/PhysRevApplied.12.014018.

[70] S. Chen, G. He, Q. Liu, F. Harnisch, Y. Zhou, Y. Chen, M. Hanif, S. Wang, X. Peng, H. Hou, U. Schröder, Layered corrugated electrode macrostructures boost microbial bioelectrocatalysis, Energy Environ. Sci. 5 (2012) 9769. https://doi.org/10.1039/c2ee23344d.

[71] T.H.J.A. Sleutels, A. ter Heijne, C.J.N. Buisman, H.V.M. Hamelers, Bioelectrochemical Systems: An Outlook for Practical Applications, ChemSusChem. 5 (2012) 1012–1019. https://doi.org/10.1002/cssc.201100732.

[72] A. Kadier, Y. Simayi, P. Abdeshahian, N.F. Azman, K. Chandrasekhar, S. Kalil, A comprehensive review of microbial electrolysis cells (MEC) reactor designs and configurations for sustainable hydrogen gas production, Alexandria Eng. J. 55 (2016) 427–443. https://doi.org/10.1016/j.aej.2015.10.008.

[73] T.H.J.A. Sleutels, L. Darus, H.V.M. Hamelers, C.J.N. Buisman, Effect of operational parameters on Coulombic efficiency in bioelectrochemical systems, Bioresour. Technol. 102 (2011) 11172–11176. https://doi.org/http://dx.doi.org/10.1016/j.biortech.2011.09.078.

[74] T. Sleutels, S. Molenaar, A. ter Heijne, C. Buisman, Low Substrate Loading Limits Methanogenesis and Leads to High Coulombic Efficiency in Bioelectrochemical Systems, Microorganisms. 4 (2016) 7. https://doi.org/han.

[75] T.H.J.A. Sleutels, A. ter Heijne, P. Kuntke, C.J.N. Buisman, H.V.M. Hamelers, Membrane Selectivity Determines Energetic Losses for Ion Transport in Bioelectrochemical Systems, ChemistrySelect. 2 (2017) 3462–3470. https://doi.org/10.1002/slct.201700064.

[76] R.A. Rozendal, H.V.M. Hamelers, K. Rabaey, J. Keller, C.J.N. Buisman, Towards practical implementation of bioelectrochemical wastewater treatment, Trends Biotechnol. 26 (2008) 450–459. https://doi.org/10.1016/j.tibtech.2008.04.008.

[77] M. Wang, Z. Wang, X. Gong, Z. Guo, The intensification technologies to water electrolysis for hydrogen production - A review, Renew. Sustain. Energy Rev. 29 (2014) 573–588. https://doi.org/10.1016/j.rser.2013.08.090.

[78] P. Aelterman, K. Rabaey, H.T. Pham, N. Boon, W. Verstraete, Continuous electricity generation at high voltages and currents using stacked microbial fuel cells, Environ. Sci. Technol. 40 (2006) 3388–3394. https://doi.org/10.1021/es0525511.

[79] M.G. Waller, T.A. Trabold, Review of microbial fuel cells for wastewater treatment: Large-scale applications, future needs and current research gaps, in: ASME 2013 11th Int. Conf. Fuel Cell Sci. Eng. Technol. Collocated with ASME 2013 Heat Transf. Summer Conf. ASME 2013 7th Int. Conf. Energy Sustain. FUELCELL 2013, 2013. https://doi.org/10.1115/FuelCell2013-18185.

[80] H. Rismani-Yazdi, S.M. Carver, A.D. Christy, O.H. Tuovinen, Cathodic limitations in microbial fuel cells: An overview, J. Power Sources. 180 (2008) 683–694. https://doi.org/10.1016/j.jpowsour.2008.02.074.

[81] A. ter Heijne, H.V.M. Hamelers, C.J.N. Buisman, Microbial Fuel Cell Operation with Continuous Biological Ferrous Iron Oxidation of the Catholyte, Environ. Sci. Technol. 41 (2007) 4130–4134. https://doi.org/10.1021/es0702824.

[82] T.H.J.A.T.H.J.A. Sleutels, R. Lodder, H.V.M. Hamelers, C.J.N. Buisman, Improved performance of porous bio-anodes in microbial electrolysis cells by enhancing mass and charge transport, Int. J. Hydrog. Energy. 34 (2009) 9655–9661. https://doi.org/10.1016/j.ijhydene.2009.09.089.

[83] A. Pina, A. Amaya, J. Marcuzzo, A. Rodrigues, M. Baldan, N. Tancredi, A. Cuña, Supercapacitor Electrode Based on Activated Carbon Wool Felt, J. Carbon Res. 4 (2018) 24. https://doi.org/10.3390/c4020024.

[84] C. Feng, Z. Lv, X. Yang, C. Wei, Anode modification with capacitive materials for a microbial fuel cell: an increase in transient power or stationary power, Phys. Chem. Chem. Phys. 16 (2014) 10464–10472. https://doi.org/10.1039/C4CP00923A.

[85] A. Deeke, T.H.J.A. Sleutels, H.V.M. Hamelers, C.J.N. Buisman, Capacitive bioanodes enable renewable energy storage in microbial fuel cells, Environ. Sci. Technol. 46 (2012) 3554–3560. https://doi.org/10.1021/es204126r.

[86] A. Deeke, T.H.J.A. Sleutels, A. ter Heijne, H.V.M. Hamelers, C.J.N. Buisman, Influence of the thickness of the capacitive layer on the performance of bioanodes in Microbial Fuel Cells, J. Power Sources. 243 (2013) 611–616. https://doi.org/10.1016/j.jpowsour.2013.05.195.

[87] C. Borsje, D. Liu, T.H.J.A. Sleutels, C.J.N. Buisman, A. ter Heijne, Performance of single carbon granules as perspective for larger scale capacitive bioanodes, J. Power Sources. 325 (2016) 690–696. https://doi.org/10.1016/j.jpowsour.2016.06.092.

[88] L. Caizán-Juanarena, I. Servin-Balderas, X. Chen, C.J.N. Buisman, A. ter Heijne, Electrochemical and microbiological characterization of single carbon granules in a multi-anode microbial fuel cell, J. Power Sources. 435 (2019) 126514. https://doi.org/10.1016/j.jpowsour.2019.04.042.

[89] B.E. Logan, M.J. Wallack, K.-Y.Y. Kim, W. He, Y. Feng, P.E. Saikaly, Assessment of Microbial Fuel Cell Configurations and Power Densities, Environ. Sci. Technol. Lett. 2 (2015) 206–214. https://doi.org/10.1021/acs.estlett.5b00180.

[90] D. Jiang, M. Curtis, E. Troop, K. Scheible, J. McGrath, B. Hu, S. Suib, D. Raymond, B. Li, A pilot-scale study on utilizing multi-anode/cathode microbial fuel cells (MAC MFCs) to enhance the power production in wastewater treatment, Int. J. Hydrogen Energy. 36 (2011) 876–884. https://doi.org/10.1016/j.ijhydene.2010.08.074.

[91] C. Munoz-Cupa, Y. Hu, C. Xu, A. Bassi, An overview of microbial fuel cell usage in wastewater treatment, resource recovery and energy production, Sci. Total Environ. 754 (2021) 142429. https://doi.org/10.1016/j.scitotenv.2020.142429.

[92] H.T. Pham, N. Boon, P. Aelterman, P. Clauwaert, L. De Schamphelaire, P. Van Oostveldt, K. Verbeken, K. Rabaey, W. Verstraete, High shear enrichment improves the performance of the anodophilic microbial consortium in a microbial fuel cell, Microb. Biotechnol. 1 (2008) 487–496. https://doi.org/10.1111/j.1751-7915.2008.00049.x.

[93] P. Liang, R. Duan, Y. Jiang, X. Zhang, Y. Qiu, X. Huang, One-year operation of 1000-L modularized microbial fuel cell for municipal wastewater treatment, Water Res. 141 (2018). https://doi.org/10.1016/j.watres.2018.04.066.

[94] S. Georg, I. de Eguren Cordoba, T. Sleutels, P. Kuntke, A. ter Heijne, C.J.N. Buisman, Competition of electrogens with methanogens for hydrogen in bioanodes, Water Res. 170 (2020) 115292. https://doi.org/10.1016/j.watres.2019.115292.

[95] P. Aelterman, S. Freguia, J. Keller, W. Verstraete, K. Rabaey, The anode potential regulates bacterial activity in microbial fuel cells, Appl. Microbiol. Biotechnol. 78 (2008) 409–418. https://doi.org/10.1007/s00253-007-1327-8.

[96] A. Deeke, T.H.J.A. Sleutels, T.F.W. Donkers, H.V.M. Hamelers, C.J.N. Buisman, A. ter Heijne, Fluidized Capacitive Bioanode As a Novel Reactor Concept for the Microbial Fuel Cell, Environ. Sci. Technol. 49 (2015) 1929–1935. https://doi.org/10.1021/es503063n.

[97] A. Dekker, A. ter Heijne, M. Saakes, H.V.M. Hamelers, C.J.N. Buisman, Analysis and improvement of a scaled-up and stacked microbial fuel cell, Environ. Sci. Technol. 43 (2009) 9038–9042. https://doi.org/10.1021/es901939r.

[98] M. Lu, S. Chen, S. Babanova, S. Phadke, M. Salvacion, A. Mirhosseini, S. Chan, K. Carpenter, R. Cortese, O. Bretschger, Long-term performance of a 20-L continuous flow microbial fuel cell for treatment of brewery wastewater, J. Power Sources. 356 (2017) 274–287. https://doi.org/10.1016/j.jpowsour.2017.03.132.

[99] Y. Feng, W. He, J. Liu, X. Wang, Y. Qu, N. Ren, A horizontal plug flow and stackable pilot microbial fuel cell for municipal wastewater treatment, Bioresour. Technol. 156 (2014) 132–138. https://doi.org/10.1016/j.biortech.2013.12.104.

[100] L. Caizán-Juanarena, C. Borsje, T. Sleutels, D. Yntema, C. Santoro, I. Ieropoulos, F. Soavi, A. ter Heijne, Combination of bioelectrochemical systems and electrochemical capacitors: Principles, analysis and opportunities, Biotechnol. Adv. 39 (2020) 107456. https://doi.org/10.1016/j.biotechadv.2019.107456.

[101] A. Dewan, H. Beyenal, Z. Lewandowski, Intermittent energy harvesting improves the performance of microbial fuel cells, Environ. Sci. Technol. 43 (2009) 4600–4605. https://doi.org/10.1021/es8037092.

[102] X. Zhang, A. Prévoteau, R.O. Louro, C.M. Paquete, K. Rabaey, Periodic polarization of electroactive biofilms increases current density and charge carriers concentration while modifying biofilm structure, Biosens. Bioelectron. (2018). https://doi.org/10.1016/j.bios.2018.08.045.

[103] J. Fernández, J. Bonastre, J. Molina, A.I. del Río, F. Cases, Study on the specific capacitance of an activated carbon cloth modified with reduced graphene oxide and polyaniline by cyclic voltammetry, Eur. Polym. J. 92 (2017) 194–203. https://doi.org/10.1016/j.eurpolymj.2017.04.044.

[104] J. Liu, F. Zhang, W. He, X. Zhang, Y. Feng, B.E. Logan, Intermittent contact of fluidized anode particles containing exoelectrogenic biofilms for continuous power generation in microbial fuel cells, J. Power Sources. 261 (2014) 278–284. https://doi.org/10.1016/j.jpowsour.2014.03.071.

[105] J. Li, Z. Ge, Z. He, A fluidized bed membrane bioelectrochemical reactor for energy-efficient wastewater treatment, Bioresour. Technol. 167 (2014) 310–315. https://doi.org/10.1016/j.biortech.2014.06.034.

[106] S. Tejedor-Sanz, J.M. Ortiz, A. Esteve-Núñez, Merging microbial electrochemical systems with electrocoagulation pretreatment for achieving a complete treatment of brewery wastewater, Chem. Eng. J. 330 (2017) 1068–1074. https://doi.org/10.1016/j.cej.2017.08.049.

[107] C. Borsje, T. Sleutels, M. Saakes, C.J.N. Buisman, A. ter Heijne, The granular capacitive moving bed reactor for the scale up of bioanodes, J. Chem. Technol. Biotechnol. 94 (2019) 2738–2748. https://doi.org/10.1002/jctb.6091.

[108] C. Borsje, T. Sleutels, W. Zhang, W. Feng, C.J.N. Buisman, A. ter Heijne, Making the best use of capacitive current: Comparison between fixed and moving granular bioanodes, J. Power Sources. 489 (2021) 229453. https://doi.org/10.1016/j.jpowsour.2021.229453.

[109] R. Kaiser, A. Kulczyk, D. Rich, R.J. Willey, J. Minicucci, B. MacIver, Effect of pore size distribution of commercial activated carbon fabrics on the adsorption of CWA simulants from the liquid phase, Ind. Eng. Chem. Res. 46 (2007) 6126–6132. https://doi.org/10.1021/ie061429n.

[110] J. Rodrigo Quejigo, S. Tejedor-Sanz, A. Esteve-Núñez, F. Harnisch, Bed electrodes in microbial electrochemistry: setup, operation and characterization, ChemTexts. 5 (2019) 4. https://doi.org/10.1007/s40828-019-0078-3.

[111] G. Kreysa, Particle phase conductivity of a fluidized bed electrode, Electrochim. Acta. 25 (1980) 813–818. https://doi.org/http://dx.doi.org/10.1016/0013-4686(80)90032-8.

[112] J.N. Hiddleston, A.F. Douglas, Current/potential relationships and potential distribution in fluidized bed electrodes, Electrochim. Acta. 15 (1970) 431–443. https://doi.org/http://dx.doi.org/10.1016/0013-4686(70)87003-7.

[113] B.K. Ferreira, Three-dimensional electrodes for the removal of metals from dilute solutions: A review, Miner. Process. Extr. Metall. Rev. 29 (2008) 330–371. https://doi.org/10.1080/08827500802045586.

[114] J. Liu, F. Zhang, W. He, W. Yang, Y. Feng, B.E. Logan, A microbial fluidized electrode electrolysis cell (MFEEC) for enhanced hydrogen production, J. Power Sources. 271 (2014) 530–533. https://doi.org/10.1016/j.jpowsour.2014.08.042.

[115] X. Wang, X. Yue, Q. Guo, Production of Electricity during Wastewater Treatment Using Fluidized-Bed Microbial Fuel Cells, Chem. Eng. Technol. 37 (2014) 703–708. https://doi.org/10.1002/ceat.201300241.

[116] L. Caizán-Juanarena, T. Sleutels, C. Borsje, A. ter Heijne, Considerations for application of granular activated carbon as capacitive bioanode in bioelectrochemical systems, Renew. Energy. 157 (2020) 782–792. https://doi.org/10.1016/j.renene.2020.05.049.

[117] K. Rabaey, W. Verstraete, Microbial fuel cells: novel biotechnology for energy generation, Trends Biotechnol. 23 (2005) 291–298. https://doi.org/http://dx.doi.org/10.1016/j.tibtech.2005.04.008.

[118] E. Frackowiak, F. Béguin, Carbon materials for the electrochemical storage of energy in capacitors, Carbon N. Y. 39 (2001) 937–950. https://doi.org/http://dx.doi.org/10.1016/S0008-6223(00)00183-4.

[119] A. Schneuwly, R. Gallay, Properties and applications of supercapacitors: From the state-of-the-art to future trends, in: PCIM 2000, Nürnberg, Germany, 2000.

[120] S. Porada, R. Zhao, A. van der Wal, V. Presser, P.M. Biesheuvel, Review on the science and technology of water desalination by capacitive deionization, Prog. Mater. Sci. 58 (2013) 1388–1442. https://doi.org/10.1016/j.pmatsci.2013.03.005.

[121] P.A. Webb, Volume and density determinations for particle technologists, Micromeritics Instrum. Corp. 2 (2001) 1.

[122] E.A. Wolin, M.J. Wolin, R.S. Wolfe, Formation of Methane by Bacterial Extracts, J. Biol. Chem. 238 (1963) 2882–2886. http://www.jbc.org/content/238/8/2882.short.

[123] Z. Ren, H. Yan, W. Wang, M.M. Mench, J.M. Regan, Characterization of Microbial Fuel Cells at Microbially and Electrochemically Meaningful Time scales, Environ. Sci. Technol. 45 (2011) 2435–2441. https://doi.org/10.1021/es103115a.

[124] J. Jagiello, J.P. Olivier, 2D-NLDFT adsorption models for carbon slit-shaped pores with surface energetical heterogeneity and geometrical corrugation, Carbon N. Y. 55 (2013) 70–80. https://doi.org/http://dx.doi.org/10.1016/j.carbon.2012.12.011.

[125] D.R. Bond, D.R. Lovley, Electricity Production by Geobacter sulfurreducens Attached to Electrodes, Appl. and Environ. Microb. 69 (2003) 1548–1555. https://doi.org/10.1128/aem.69.3.1548-1555.2003.

[126] G.D. Schrott, P.S. Bonanni, L. Robuschi, A. Esteve-Nuñez, J.P. Busalmen, Electrochemical insight into the mechanism of electron transport in biofilms of Geobacter sulfurreducens, Electrochim. Acta. 56 (2011) 10791–10795. https://doi.org/10.1016/j.electacta.2011.07.001.

[127] P.T. Ha, H. Moon, B.H. Kim, H.Y. Ng, I.S. Chang, Determination of charge transfer resistance and capacitance of microbial fuel cell through a transient response analysis of cell voltage, Biosens. Bioelectron. 25 (2010) 1629–1634. https://doi.org/10.1016/j.bios.2009.11.023.

[128] Z. Lv, D. Xie, F. Li, Y. Hu, C. Wei, C. Feng, Microbial fuel cell as a biocapacitor by using pseudo-capacitive anode materials, J. Power Sources. 246 (2014) 642–649. https://doi.org/10.1016/j.jpowsour.2013.08.014.

[129] L. Han, K.G. Karthikeyan, M.A. Anderson, K.B. Gregory, Exploring the impact of pore size distribution on the performance of carbon electrodes for capacitive deionization, J. Colloid Interface Sci. 430 (2014) 93–99. https://doi.org/10.1016/j.jcis.2014.05.015.

[130] S. Porada, L. Borchardt, M. Oschatz, M. Bryjak, J.S. Atchison, K.J. Keesman, S. Kaskel, P.M. Biesheuvel, V. Presser, Direct prediction of the desalination performance of porous carbon electrodes for capacitive deionization, Energy Environ. Sci. 6 (2013) 3700. https://doi.org/10.1039/c3ee42209g.

[131] G. Gryglewicz, J. Machnikowski, E. Lorenc-Grabowska, G. Lota, E. Frackowiak, Effect of pore size distribution of coal-based activated carbons on double layer capacitance, Electrochim. Acta. 50 (2005) 1197–1206. https://doi.org/10.1016/j.electacta.2004.07.045.

[132] C. Santoro, S. Babanova, K. Artyushkova, J.A. Cornejo, L. Ista, O. Bretschger, E. Marsili, P. Atanassov, A.J. Schuler, Influence of anode surface chemistry on microbial fuel cell operation, Bioelectrochemistry. 106 (2015) 141–149. https://doi.org/10.1016/j.bioelechem.2015.05.002.

[133] F. Zhang, K.S. Jacobson, P. Torres, Z. He, Effects of anolyte recirculation rates and catholytes on electricity generation in a litre-scale upflow microbial fuel cell, Energy Environ. Sci. 3 (2010) 1347. https://doi.org/10.1039/c001201g.

[134] S. Freguia, K. Rabaey, Z. Yuan, J. Keller, Non-catalyzed cathodic oxygen reduction at graphite granules in microbial fuel cells, Electrochim. Acta. 53 (2007) 598–603. https://doi.org/10.1016/j.electacta.2007.07.037.

[135] D. Jiang, B. Li, Granular activated carbon single-chamber microbial fuel cells (GAC-SCMFCs): A design suitable for large-scale wastewater treatment processes, Biochem. Eng. J. 47 (2009) 31–37. https://doi.org/10.1016/j.bej.2009.06.013.

[136] J. Jagiello, Stable Numerical Solution of the Adsorption Integral Equation Using Splines, Langmuir. 10 (1994) 2778–2785. https://doi.org/10.1021/la00020a045.

[137] T.H.J.A. Sleutels, H.V.M. Hamelers, C.J.N. Buisman, Reduction of pH buffer requirement in bioelectrochemical systems, Environ. Sci. Technol. 44 (2010) 8259–8263. https://doi.org/10.1021/es101858f.

[138] B.E. Logan, K. Rabaey, Conversion of Wastes into Bioelectricity and Chemicals by Using Microbial Electrochemical Technologies, Science (80-.). 337 (2012) 686–690. https://doi.org/10.1126/science.1217412.

[139] P. Kuntke, T.H.J.A. Sleutels, M. Rodríguez Arredondo, S. Georg, S.G. Barbosa, A. ter Heijne, H.V.M. Hamelers, C.J.N. Buisman, (Bio)electrochemical ammonia recovery: progress and perspectives, Appl. Microbiol. Biotechnol. 102 (2018) 3865–3878. https://doi.org/10.1007/s00253-018-8888-6.

[140] R.D. Cusick, B.E. Logan, Phosphate recovery as struvite within a single chamber microbial electrolysis cell, Bioresour. Technol. 107 (2012) 110–115. https://doi.org/10.1016/j.biortech.2011.12.038.

[141] A. Janicek, Y. Fan, H. Liu, Design of microbial fuel cells for practical application: a review and analysis of scale-up studies, Biofuels. 5 (2014) 79–92. https://doi.org/10.4155/bfs.13.69.

[142] P. Clauwaert, S. Mulenga, P. Aelterman, W. Verstraete, Litre-scale microbial fuel cells operated in a complete loop, Appl. Microbiol. Biotechnol. 83 (2009) 241–247. https://doi.org/10.1007/s00253-009-1876-0.

[143] J. Greenman, I.A. Ieropoulos, Allometric scaling of microbial fuel cells and stacks: The lifeform case for scale-up, J. Power Sources. 356 (2017) 365–370. https://doi.org/10.1016/j.jpowsour.2017.04.033.

[144] P. Zamora, T. Georgieva, A. ter Heijne, T.H.J.A. Sleutels, A.W. Jeremiasse, M. Saakes, C.J.N. Buisman, P. Kuntke, Ammonia recovery from urine in a scaled-up Microbial Electrolysis Cell, J. Power Sources. 356 (2017) 491–499. https://doi.org/10.1016/j.jpowsour.2017.02.089.

[145] V.G. Gude, Wastewater treatment in microbial fuel cells – an overview, J. Clean. Prod. 122 (2016) 287–307. https://doi.org/10.1016/j.jclepro.2016.02.022.

[146] D. Jiang, B. Li, Novel electrode materials to enhance the bacterial adhesion and increase the power generation in microbial fuel cells (MFCs), Water Sci. Technol. 59 (2009) 557–563. https://doi.org/10.2166/wst.2009.007.

[147] J. Houghton, C. Santoro, F. Soavi, A. Serov, I. Ieropoulos, C. Arbizzani, P. Atanassov, Supercapacitive microbial fuel cell: Characterization and analysis for improved charge storage/delivery performance, Bioresour. Technol. 218 (2016) 552–560. https://doi.org/10.1016/j.biortech.2016.06.105.

[148] C. Santoro, F. Soavi, A. Serov, C. Arbizzani, P. Atanassov, Self-powered supercapacitive microbial fuel cell: The ultimate way of boosting and harvesting power, Biosens. Bioelectron. 78 (2016) 229–235. https://doi.org/10.1016/j.bios.2015.11.026.

[149] F. Soavi, L.G. Bettini, P. Piseri, P. Milani, C. Santoro, P. Atanassov, C. Arbizzani, Miniaturized supercapacitors: key materials and structures towards autonomous and sustainable devices and systems, J. Power Sources. 326 (2016) 717–725. https://doi.org/10.1016/j.jpowsour.2016.04.131.

[150] X. Liu, J. Wu, Q. Guo, Analysis of organic compounds' degradation and electricity generation in anaerobic fluidized bed microbial fuel cell for coking wastewater treatment, Environ. Technol. 38 (2017) 3115–3121. https://doi.org/10.1080/09593330.2017.1290147.

[151] S. Oka, Fluidized bed, in: A-to-Z Guid. to Thermodyn. Heat Mass Transf. Fluids Eng., Begellhouse, 2006. https://doi.org/10.1615/AtoZ.f.fluidized_bed.

[152] U.R. Hjelmner, H.F. Larsson, Method for the filtration of a suspension or emulsion, US4126546B1, 1977. https://doi.org/10.1057/9780230607156.

[153] S.D. Molenaar, T. Sleutels, J. Pereira, M. Iorio, C. Borsje, J.A. Zamudio, F. Fabregat-Santiago, C.J.N. Buisman, A. ter Heijne, In situ Biofilm Quantification in Bioelectrochemical Systems by using Optical Coherence Tomography, ChemSusChem. 11 (2018) 2171–2178. https://doi.org/10.1002/cssc.201800589.

[154] A.J.B. Zehnder, B.A. Huser, T.D. Brock, K. Wuhrmann, Characterization of an acetate-decarboxylating, non-hydrogen-oxidizing methane bacterium, Arch. Microbiol. 124 (1980) 1–11. https://doi.org/10.1007/BF00407022.

[155] P. Liang, C. Zhang, Y. Jiang, Y. Bian, H. Zhang, X. Sun, X. Yang, X. Zhang, X. Huang, Performance enhancement of microbial fuel cell by applying transient-state regulation, Appl. Energy. 185 (2017) 582–588. https://doi.org/10.1016/j.apenergy.2016.10.130.

[156] Y. Wang, Q. Wen, Y. Chen, J. Yin, T. Duan, Enhanced Performance of a Microbial Fuel Cell with a Capacitive Bioanode and Removal of Cr (VI) Using the Intermittent Operation, Appl. Biochem. Biotechnol. 180 (2016) 1372–1385. https://doi.org/10.1007/s12010-016-2173-x.

[157] C. Picioreanu, M.C.M. van Loosdrecht, J.J. Heijnen, A theoretical study on the effect of surface roughness on mass transport and transformation in biofilms, Biotechnol. Bioeng. 68 (2000) 355–369. https://doi.org/10.1002/(SICI)1097-0290(20000520)68:4<355::AID-BIT1>3.0.CO;2-A.

[158] P. Champigneux, C. Renault-Sentenac, D. Bourrier, C. Rossi, M.L. Delia, A. Bergel, Effect of surface nano/micro-structuring on the early formation of microbial anodes with Geobacter sulfurreducens: Experimental and theoretical approaches, Bioelectrochemistry. 121 (2018) 191–200. https://doi.org/10.1016/j.bioelechem.2018.02.005.

[159] M. Pierra, M. Golozar, X. Zhang, A. Prévoteau, M. De Volder, D. Reynaerts, K. Rabaey, Growth and current production of mixed culture anodic biofilms remain unaffected by sub-microscale surface roughness, Bioelectrochemistry. 122 (2018) 213–220. https://doi.org/10.1016/j.bioelechem.2018.04.002.

[160] P. Chong, B. Erable, A. Bergel, Effect of pore size on the current produced by 3-dimensional porous microbial anodes: A critical review, Bioresour. Technol. 289 (2019). https://doi.org/10.1016/j.biortech.2019.121641.

[161] K. Guo, A. Prévoteau, S.A. Patil, K. Rabaey, Engineering electrodes for microbial electrocatalysis, Curr. Opin. Biotechnol. 33 (2015) 149–156. https://doi.org/10.1016/j.copbio.2015.02.014.

[162] D. Puyol, D.J. Batstone, T. Hülsen, S. Astals, M. Peces, J.O. Krömer, Resource recovery from wastewater by biological technologies: Opportunities, challenges, and prospects, Front. Microbiol. 7 (2017) 1–23. https://doi.org/10.3389/fmicb.2016.02106.

[163] B.E. Logan, Microbial Fuel Cells, Wiley, 2008. https://books.google.nl/books?id=cXnc2wmrE9gC.

[164] S. Chen, G. Liu, R. Zhang, B. Qin, Y. Luo, Development of the microbial electrolysis desalination and chemical-production cell for desalination as well as acid and alkali productions, Environ. Sci. Technol. 46 (2012) 2467–2472. https://doi.org/10.1021/es203332g.

[165] R. Rousseau, L. Etcheverry, E. Roubaud, R. Basséguy, M.L. Délia, A. Bergel, Microbial electrolysis cell (MEC): Strengths, weaknesses and research needs from electrochemical engineering standpoint, Appl. Energy. 257 (2020). https://doi.org/10.1016/j.apenergy.2019.113938.

[166] K. Guo, S. Freguia, P.G. Dennis, X. Chen, B.C. Donose, J. Keller, J.J. Gooding, K. Rabaey, Effects of Surface Charge and Hydrophobicity on Anodic Biofilm Formation, Community Composition, and Current Generation in Bioelectrochemical Systems, Environ. Sci. Technol. 47 (2013) 7563–70. https://doi.org/10.1021/es400901u.

[167] X. Xie, C. Criddle, Y. Cui, Design and fabrication of bioelectrodes for microbial bioelectrochemical systems, Energy Environ. Sci. 8 (2015) 3418–3441. https://doi.org/10.1039/C5EE01862E.

[168] B. Li, J. Zhou, X. Zhou, X. Wang, B. Li, C. Santoro, M. Grattieri, S. Babanova, K. Artyushkova, P. Atanassov, A.J. Schuler, Surface modification of microbial fuel cells anodes: Approaches to practical design, Electrochim. Acta. 134 (2014). https://doi.org/10.1016/j.electacta.2014.04.136.

[169] G.D. Saratale, R.G. Saratale, M.K. Shahid, G. Zhen, G. Kumar, H.S. Shin, Y.G. Choi, S.H. Kim, A comprehensive overview on electro-active biofilms, role of exo-electrogens and their microbial niches in microbial fuel cells (MFCs), Chemosphere. 178 (2017). https://doi.org/10.1016/j.chemosphere.2017.03.066.

[170] A.J. Lewis, A.P. Borole, Adapting microbial communities to low anode potentials improves performance of MECs at negative potentials, Electrochim. Acta. 254 (2017) 79–88. https://doi.org/10.1016/j.electacta.2017.09.085.

[171] Z. Dong, H. Wang, S. Tian, Y. Yang, H. Yuan, Q. Huang, T.-S. Song, J. Xie, Fluidized granular activated carbon electrode for efficient microbial electrosynthesis of acetate from carbon dioxide, Bioresour. Technol. 269 (2018) 203–209. https://doi.org/10.1016/j.biortech.2018.08.103.

[172] Y.-C. Wu, Q.-X. Deng, Z.-J. Wang, Y. Zheng, D.-L. Li, F. Zhao, Comparative analysis of the bacterial community on anodic biofilms in sediment microbial fuel cell under open and closed circuits, Huanjing Kexue/Environmental Sci. 37 (2016). https://doi.org/10.13227/j.hjkx.201606199.

[173] X. Zhu, M.D. Yates, M.C. Hatzell, H.A. Rao, P.E. Saikaly, B.E. Logan, Microbial Community Composition Is Unaffected by Anode Potential, Environ. Sci. Technol. 48 (2014) 1352–1358. https://doi.org/10.1021/es501982m.(2).

[174] A.J. Lewis, A.P. Borole, Adapting microbial communities to low anode potentials improves performance of MECs at negative potentials, Electrochim. Acta. 254 (2017) 79–88. https://doi.org/10.1016/j.electacta.2017.09.085.

[175] Y. Sun, J. Wei, P. Liang, X. Huang, Electricity generation and microbial community changes in microbial fuel cells packed with different anodic materials, Bioresour. Technol. 102 (2011) 10886–10891. https://doi.org/10.1016/j.biortech.2011.09.038.

[176] A.J. Slate, K.A. Whitehead, D.A.C. Brownson, C.E. Banks, Microbial fuel cells: An overview of current technology, Renew. Sustain. Energy Rev. 101 (2019) 60–81. https://doi.org/10.1016/j.rser.2018.09.044.

[177] G.C. Premier, I.S. Michie, H.C. Boghani, K.R. Fradler, J.R. Kim, Reactor design and scale-up, in: Microb. Electrochem. Fuel Cells, Elsevier, 2016: pp. 215–244. https://doi.org/10.1016/B978-1-78242-375-1.00007-1.

[178] A.G. Dixon, M. Nijemeisland, E.H. Stitt, Packed Tubular Reactor Modeling and Catalyst Design using Computational Fluid Dynamics, Adv. Chem. Eng. 31 (2006) 307–389. https://doi.org/10.1016/S0065-2377(06)31005-8.

[179] L. González-Gutiérrez, C. Frontana, E. Martínez, Upflow fixed bed bioelectrochemical reactor for wastewater treatment applications, Bioresour. Technol. 176 (2015) 292–295. https://doi.org/10.1016/j.biortech.2014.11.018.

[180] M. Kitching, R. Butler, E. Marsili, Microbial bioelectrosynthesis of hydrogen: Current challenges and scale-up, Enzyme Microb. Technol. 96 (2017) 1–13. https://doi.org/10.1016/j.enzmictec.2016.09.002.

[181] X.A. Walter, J. You, J. Winfield, U. Bajarunas, J. Greenman, I.A. Ieropoulos, From the lab to the field: Self-stratifying microbial fuel cells stacks directly powering lights, Appl. Energy. 277 (2020). https://doi.org/10.1016/j.apenergy.2020.115514.

[182] A.E. Franks, N. Malvankar, K.P. Nevin, Bacterial biofilms: The powerhouse of a microbial fuel cell, Biofuels. 1 (2010) 589–604. https://doi.org/10.4155/bfs.10.25.

[183] M.R. Khan, E. Baranitharan, D.M.R. Prasad, C.K. Cheng, Fast Biofilm Formation and Its Role on Power Generation in Palm Oil Mill Effluent Fed Microbial Fuel Cell, MATEC Web Conf. 62 (2016) 1–6. https://doi.org/10.1051/04002.

[184] P. Aelterman, M. Versichele, M. Marzorati, N. Boon, W. Verstraete, Loading rate and external resistance control the electricity generation of microbial fuel cells with different three-dimensional anodes, Bioresour Technol. 99 (2008) 8895–8902. https://doi.org/10.1016/j.biortech.2008.04.061.

[185] Y. Ye, J. Guo, B. Pan, S. Cheng, Effect of anode double-layered capacitance on performance of microbial fuel cell, Huagong Xuebao/CIESC J. 66 (2015) 773–778. https://doi.org/10.11949/j.issn.0438-1157.20140978.

[186] S. Kato, Biotechnological aspects of microbial extracellular electron transfer, Microbes Environ. 30 (2015) 133–139. https://doi.org/10.1264/jsme2.ME15028.

[187] C. Santoro, M. Kodali, N. Shamoon, A. Serov, F. Soavi, I. Merino-Jimenez, I. Gajda, J. Greenman, I. Ieropoulos, P. Atanassov, Increased power generation in supercapacitive microbial fuel cell stack using Fe–N–C cathode catalyst, J. Power Sources. 412 (2019) 416–424. https://doi.org/10.1016/j.jpowsour.2018.11.069.

[188] C. Santoro, C. Flores-Cadengo, F. Soavi, M. Kodali, I. Merino-Jimenez, I. Gajda, J. Greenman, I. Ieropoulos, P. Atanassov, Ceramic Microbial Fuel Cells Stack: Power generation in standard and supercapacitive mode, Sci. Rep. 8 (2018) 1–12. https://doi.org/10.1038/s41598-018-21404-y.

[189] F. Poli, J. Seri, C. Santoro, F. Soavi, Boosting Microbial Fuel Cell Performance by Combining with an External Supercapacitor: An Electrochemical Study, ChemElectroChem. 7 (2020) 893–903. https://doi.org/10.1002/celc.201901876.

[190] P. Liang, W. Wu, J. Wei, L. Yuan, X. Xia, X. Huang, Alternate Charging and Discharging of Capacitor to Enhance the Electron Production of Bioelectrochemical Systems, Environ. Sci. Technol. 45 (2011) 6647–6653. https://doi.org/10.1021/es200759v.

[191] M.C. Hatzell, Y. Kim, B.E. Logan, Powering microbial electrolysis cells by capacitor circuits charged using microbial fuel cell, J. Power Sources. 229 (2013) 198–202. https://doi.org/10.1016/j.jpowsour.2012.12.006.

[192] Y. Kim, M.C. Hatzell, A.J. Hutchinson, B.E. Logan, Capturing power at higher voltages from arrays of microbial fuel cells without voltage reversal, Energy Environ. Sci. 4 (2011) 4662–4667. https://doi.org/10.1039/c1ee02451e.

[193] F. Grondin, M. Perrier, B. Tartakovsky, Microbial fuel cell operation with intermittent connection of the electrical load, J. Power Sources. 208 (2012) 18–23. https://doi.org/10.1016/j.jpowsour.2012.02.010.

[194] F. Soavi, C. Santoro, Supercapacitive operational mode in microbial fuel cell, Curr. Opin. Electrochem. 22 (2020) 1–8. https://doi.org/10.1016/j.coelec.2020.03.009.

[195] W. Kong, Q. Guo, X. Wang, X. Yue, Electricity Generation from Wastewater Using an Anaerobic Fluidized Bed Microbial Fuel Cell, Ind. Eng. Chem. Res. 50 (2011) 12225–12232. https://doi.org/10.1021/ie2007505.

[196] Y. Liu, X. Sun, D. Yin, L. Cai, L. Zhang, Suspended anode-type microbial fuel cells for enhanced electricity generation, RSC Adv. 10 (2020) 9868–9877. https://doi.org/10.1039/C9RA08288C.

[197] J. Li, S. Luo, Z. He, Cathodic fluidized granular activated carbon assisted-membrane bioelectrochemical reactor for wastewater treatment, Sep. Purif. Technol. 169 (2016) 241–246. https://doi.org/10.1016/j.seppur.2016.06.014.

[198] X.A. Walter, C. Santoro, J. Greenman, I. Ieropoulos, Scaling up self-stratifying supercapacitive microbial fuel cell, Int. J. Hydrogen Energy. (2020). https://doi.org/10.1016/j.ijhydene.2020.06.070.

[199] W. Zhao, W. Fu, S. Chen, H. Xiong, L. Lan, M. Jiang, S.A. Patil, S. Chen, High-capacitance bioanode circumvents bioelectrochemical reaction transition in the voltage-reversed serially-stacked air-cathode microbial fuel cell, J. Power Sources. 468 (2020) 228402. https://doi.org/10.1016/j.jpowsour.2020.228402.

[200] A. ter Heijne, H.V.M. Hamelers, M. Saakes, C.J.N. Buisman, Performance of non-porous graphite and titanium-based anodes in microbial fuel cells, Electrochim. Acta. 53 (2008) 5697–5703. https://doi.org/10.1016/j.electacta.2008.03.032.

[201] C.T. Rueden, J. Schindelin, M.C. Hiner, B.E. DeZonia, A.E. Walter, E.T. Arena, K.W. Eliceiri, ImageJ2: ImageJ for the next generation of scientific image data, BMC Bioinformatics. 18 (2017) 529. https://doi.org/10.1186/s12859-017-1934-z.

[202] K. To, P.-Y. Lai, H.K. Pak, Jamming of Granular Flow in a Two-Dimensional Hopper, Phys. Rev. Lett. 86 (2001) 71–74. http://link.aps.org/doi/10.1103/PhysRevLett.86.71.

[203] Y.U.E. Xuehai, W. Xuyun, Z. Shuju, K. Weifang, G.U.O. Qingjie, W.F. Kong, Q.J. Guo, X.Y. Wang, X.H. Yue, Electricity Generation from Wastewater Using an Anaerobic Fluidized Bed Microbial Fuel Cell, Ind. Eng. Chem. Res. 50 (2011) 12225–12232. https://doi.org/10.1021/ie2007505.

[204] V.M. Fischer, In situ electrochemical regeneration of activated carbon, 2001.

[205] C.R. Dennison, M. Beidaghi, K.B. Hatzell, J.W. Campos, Y. Gogotsi, E.C. Kumbur, Effects of flow cell design on charge percolation and storage in the carbon slurry electrodes of electrochemical flow capacitors, J. Power Sources. 247 (2014) 489–496. https://doi.org/10.1016/j.jpowsour.2013.08.101.

[206] B. Marinho, M. Ghislandi, E. Tkalya, C.E. Koning, G. de With, Electrical conductivity of compacts of graphene, multi-wall carbon nanotubes, carbon black, and graphite powder, Powder Technol. 221 (2012) 351–358. https://doi.org/10.1016/j.powtec.2012.01.024.

[207] C. Zhong, Y. Deng, W. Hu, J. Qiao, L. Zhang, J. Zhang, A review of electrolyte materials and compositions for electrochemical supercapacitors, Chem. Soc. Rev. 44 (2015) 7484–7539. https://doi.org/10.1039/C5CS00303B.

[208] H.A. Andreas, Self-Discharge in Electrochemical Capacitors: A Perspective Article, J. Electrochem. Soc. 162 (2015) A5047–A5053. https://doi.org/10.1149/2.0081505jes.

[209] Rosemount Analytical, Conductance data for commonly used chemicals, 2010. https://www.emerson.com/documents/automation/manual-conductance-data-for-commonly-used-chemicals-rosemount-en-68896.pdf (accessed January 28, 2021).

[210] R.C. Weast, D.R. Lide, Electrical conductivity of aqueous solutions, in: CRC Handb. Chem. Phys. 70th Ed., CRC Press, Boca Raton, 1989: p. D-221.

[211] H. Cohen, S.E. Eli, M. Jõgi, M.E. Suss, Suspension Electrodes Combining Slurries and Upflow Fluidized Beds, ChemSusChem. 9 (2016) 3045–3048. https://doi.org/10.1002/cssc.201601008.

[212] J. Schindelin, I. Arganda-Carreras, E. Frise, V. Kaynig, M. Longair, T. Pietzsch, S. Preibisch, C. Rueden, S. Saalfeld, B. Schmid, J.-Y. Tinevez, D.J. White, V. Hartenstein, K. Eliceiri, P. Tomancak, A. Cardona, Fiji: an open-source platform for biological-image analysis, Nat. Methods. 9 (2012) 676–682. https://doi.org/10.1038/nmeth.2019.

[213] R. Zhao, P.M. Biesheuvel, H. Miedema, H. Bruning, A. van der Wal, Charge efficiency: A functional tool to probe the double-layer structure inside of porous electrodes and application in the modeling of capacitive deionization, J. Phys. Chem. Lett. 1 (2010) 205–210. https://doi.org/10.1021/jz900154h.

[214] S. Porada, J. Lee, D. Weingarth, V. Presser, Continuous operation of an electrochemical flow capacitor, Electrochem. Commun. 48 (2014) 178–181. https://doi.org/10.1016/j.elecom.2014.08.023.

[215] S.I. Jeon, H.R. Park, J.G. Yeo, S. Yang, C.H. Cho, M.H. Han, D.K. Kim, Desalination via a new membrane capacitive deionization process utilizing flow-electrodes, Energy Environ. Sci. 6 (2013) 1471–1475. https://doi.org/10.1039/c3ee24443a.

[216] K. Tang, S. Yiacoumi, Y. Li, J. Gabitto, C. Tsouris, Optimal conditions for efficient flow-electrode capacitive deionization, Sep. Purif. Technol. 240 (2020) 116626. https://doi.org/10.1016/j.seppur.2020.116626.

[217] K.B. Hatzell, J. Eller, S.L. Morelly, M.H. Tang, N.J. Alvarez, Y. Gogotsi, Direct observation of active material interactions in flowable electrodes using X-ray tomography, Faraday Discuss. 199 (2017) 511–524. https://doi.org/10.1039/C6FD00243A.

[218] S. Yang, J. Choi, J. Yeo, S. Jeon, H. Park, D.K. Kim, Flow-Electrode Capacitive Deionization Using an Aqueous Electrolyte with a High Salt Concentration, Environ. Sci. Technol. 50 (2016) 5892–5899. https://doi.org/10.1021/acs.est.5b04640.

[219] A. Rommerskirchen, Y. Gendel, M. Wessling, Single module flow-electrode capacitive deionization for continuous water desalination, Electrochem. Commun. 60 (2015) 34–37. https://doi.org/10.1016/j.elecom.2015.07.018.

[220] A. Rommerskirchen, A. Kalde, C.J. Linnartz, L. Bongers, G. Linz, M. Wessling, Unraveling charge transport in carbon flow-electrodes: Performance prediction for desalination applications, Carbon N. Y. 145 (2019) 507–520. https://doi.org/10.1016/j.carbon.2019.01.053.

[221] S. Porada, D. Weingarth, H.V.M. Hamelers, M. Bryjak, V. Presser, P.M. Biesheuvel, ab D. Weingarth, H. V M Hamelers, M. Bryjak, V. Presser, P.M. Biesheuvel ef, Carbon flow electrodes for continuous operation of capacitive deionization and capacitive mixing energy generation - SI, J. Mater. Chem. A. 2 (2014) 9313. https://doi.org/10.1039/c4ta01783h.

[222] J.W. Campos, M. Beidaghi, K.B. Hatzell, C.R. Dennison, B. Musci, V. Presser, E.C. Kumbur, Y. Gogotsi, Investigation of carbon materials for use as a flowable electrode in electrochemical flow capacitors, Electrochim. Acta. 98 (2013) 123–130. https://doi.org/10.1016/j.electacta.2013.03.037.

[223] N.C. Hoyt, E. Agar, E.A. Nagelli, R. Savinell, J. Wainright, Electrochemical Impedance Spectroscopy of Flowing Electrosorptive Slurry Electrodes, J. Electrochem. Soc. 165 (2018) E439–E444. https://doi.org/10.1149/2.0051810jes.

[224] M. Boota, K.B. Hatzell, M. Beidaghi, C.R. Dennison, E.C. Kumbur, Y. Gogotsi, Activated carbon spheres as a flowable electrode in electrochemical flow capacitors, J. Electrochem. Soc. 161 (2014) A1078–A1083. https://doi.org/10.1149/2.072406jes.

[225] M. Boota, K.B. Hatzell, M. Alhabeb, E.C. Kumbur, Y. Gogotsi, Graphene-containing flowable electrodes for capacitive energy storage, Carbon N. Y. 92 (2015) 142–149. https://doi.org/10.1016/j.carbon.2015.04.020.

[226] C.R. Dennison, Y. Gogotsi, E.C. Kumbur, In situ distributed diagnostics of flowable electrode systems: resolving spatial and temporal limitations, Phys. Chem. Chem. Phys. 16 (2014) 18241. https://doi.org/10.1039/C4CP02820A.

[227] F. Liu, O. Coronell, D.F. Call, Electricity generation using continuously recirculated flow electrodes in reverse electrodialysis, J. Power Sources. 355 (2017) 206–210. https://doi.org/10.1016/j.jpowsour.2017.04.061.

[228] C. Zhang, K.B. Hatzell, M. Boota, B. Dyatkin, M. Beidaghi, D. Long, W. Qiao, E.C. Kumbur, Y. Gogotsi, Highly porous carbon spheres for electrochemical capacitors and capacitive flowable suspension electrodes, Carbon N. Y. 77 (2014) 155–164. https://doi.org/10.1016/j.carbon.2014.05.017.

[229] R. Gloukhovski, M.E. Suss, Measurements of the Electric Conductivity of MWCNT Suspension Electrodes with Varying Potassium Bromide Electrolyte Ionic Strength, J. Electrochem. Soc. 167 (2020) 020528. https://doi.org/10.1149/1945-7111/ab6a88.

[230] K.B. Hatzell, M. Boota, Y. Gogotsi, Materials for suspension (semi-solid) electrodes for energy and water technologies, Chem. Soc. Rev. 44 (2015) 8664–8687. https://doi.org/10.1039/C5CS00279F.

[231] J. Ma, P. Liang, X. Sun, H. Zhang, Y. Bian, F. Yang, J. Bai, Q. Gong, X. Huang, Energy recovery from the flow-electrode capacitive deionization, J. Power Sources. 421 (2019) 50–55. https://doi.org/10.1016/j.jpowsour.2019.02.082.

[232] T.J. Petek, N.C. Hoyt, R.F. Savinell, J.S. Wainright, Characterizing slurry electrodes using electrochemical impedance spectroscopy, J. Electrochem. Soc. 163 (2016) A5001–A5009. https://doi.org/10.1149/2.0011601jes.

[233] N.C. Hoyt, R.F. Savinell, J.S. Wainright, Modeling of flowable slurry electrodes with combined faradaic and nonfaradaic currents, Chem. Eng. Sci. 144 (2016) 288–297. https://doi.org/http://dx.doi.org/10.1016/j.ces.2016.01.048.

[234] J. Kang, T. Kim, H. Shin, J. Lee, J.I. Ha, J. Yoon, Direct energy recovery system for membrane capacitive deionization, Desalination. 398 (2016) 144–150. https://doi.org/10.1016/j.desal.2016.07.025.

[235] L. Wang, P.M. Biesheuvel, S. Lin, Reversible thermodynamic cycle analysis for capacitive deionization with modified Donnan model, J. Colloid Interface Sci. 512 (2018) 522–528. https://doi.org/10.1016/j.jcis.2017.10.060.

[236] G.J. Doornbusch, J.E. Dykstra, P.M. Biesheuvel, M.E. Suss, Fluidized bed electrodes with high carbon loading for water desalination by capacitive deionization, J. Mater. Chem. A. 4 (2016) 3642–3647. https://doi.org/10.1039/C5TA10316A.

[237] P.G. Dennis, B. Virdis, I. Vanwonterghem, A. Hassan, P. Hugenholtz, G.W. Tyson, K. Rabaey, Anode potential influences the structure and function of anodic electrode and electrolyte-associated microbiomes, Sci. Rep. 6 (2016). https://doi.org/10.1038/srep39114.

[238] H.-S. Lee, C.I. Torres, B.E. Rittmann, Effects of Substrate Diffusion and Anode Potential on Kinetic Parameters for Anode-Respiring Bacteria, Environ. Sci. Technol. 43 (2009) 7571–7577. https://doi.org/10.1021/es9015519.

[239] D. Pinto, T. Coradin, C. Laberty-Robert, Effect of anode polarization on biofilm formation and electron transfer in Shewanella oneidensis/graphite felt microbial fuel cells, Bioelectrochemistry. 120 (2018) 1–9. https://doi.org/10.1016/j.bioelechem.2017.10.008.

[240] H.V.M. Hamelers, A. ter Heijne, N. Stein, R.A. Rozendal, C.J.N. Buisman, Butler-Volmer-Monod model for describing bio-anode polarization curves, Bioresour. Technol. 102 (2011) 381–387. https://doi.org/10.1016/j.biortech.2010.06.156.

[241] M. Sharma, S. Bajracharya, S. Gildemyn, S.A. Patil, Y. Alvarez-Gallego, D. Pant, K. Rabaey, X. Dominguez-Benetton, A critical revisit of the key parameters used to describe microbial electrochemical systems, Electrochim. Acta. 140 (2014) 191–208. https://doi.org/10.1016/j.electacta.2014.02.111.

[242] J. Bosch, K.-Y. Lee, S.-F. Hong, F. Harnisch, U. Schröder, R.U. Meckenstock, Metabolic Efficiency of Geobacter sulfurreducens Growing on Anodes with Different Redox Potentials, Curr. Microbiol. 68 (2014) 763–768. https://doi.org/10.1007/s00284-014-0539-2.

[243] K. To, Effect of hopper angles on jamming probability in 2-dimensional hoppers, Chinese J. Phys. 40 (2002) 379–386. http://www.scopus.com/inward/record.url?eid=2-s2.0-0036391593&partnerID=40&md5=98a20ea07dca2907e00351cfb4677bcf.

[244] P.G. Lafond, M.W. Gilmer, C.A. Koh, E.D. Sloan, D.T. Wu, A.K. Sum, Orifice jamming of fluid-driven granular flow, Phys. Rev. E. 87 (2013) 42204. http://link.aps.org/doi/10.1103/PhysRevE.87.042204.

[245] J.G. Majeed, E. Békásy-Molnár, Design correlations of an air-lift tube reactor, Gas Sep. Purif. 9 (1995) 101–109. https://doi.org/http://dx.doi.org/10.1016/0950-4214(95)93947-I.

[246] A.G. Pandolfo, G.J. Wilson, T.D. Huynh, A.F. Hollenkamp, The influence of conductive additives and inter-particle voids in carbon EDLC electrodes, Fuel Cells. 10 (2010) 856–864. https://doi.org/10.1002/fuce.201000027.

[247] A. Baudler, I. Schmidt, M. Langner, A. Greiner, U. Schröder, Does it have to be carbon? Metal anodes in microbial fuel cells and related bioelectrochemical systems, Energy Environ. Sci. 8 (2015) 2048–2055. https://doi.org/10.1039/C5EE00866B.

[248] C. Wu, X. Wang, B. Ju, L. Jiang, H. Wu, Q. Zhao, L. Yi, Supercapacitive performance of nitrogen-enriched carbons from carbonization of polyaniline/activated mesocarbon microbeads, J. Power Sources. 227 (2013) 1–7. https://doi.org/10.1016/j.jpowsour.2012.11.028.

[249] W.C. Yang, Handbook of Fluidization and Fluid-Particle Systems, Taylor & Francis, 2003. https://books.google.nl/books?id=n_UqkwcFbwkC.

[250] M. Liu, L. Gan, W. Xiong, Z. Xu, D. Zhu, L. Chen, Development of MnO 2 /porous carbon microspheres with a partially graphitic structure for high performance supercapacitor electrodes, J. Mater. Chem. A. 2 (2014) 2555–2562. https://doi.org/10.1039/C3TA14445C.

[251] Y. Zhai, Y. Dou, D. Zhao, P.F. Fulvio, R.T. Mayes, S. Dai, Carbon Materials for Chemical Capacitive Energy Storage, Adv. Mater. 23 (2011) 4828–4850. https://doi.org/10.1002/adma.201100984.

[252] X. Wen, D. Zhang, L. Shi, T. Yan, H. Wang, J. Zhang, Three-dimensional hierarchical porous carbon with a bimodal pore arrangement for capacitive deionization, J. Mater. Chem. 22 (2012) 23835–23844. https://doi.org/10.1039/c2jm35138b.

[253] S.J. Seo, H. Jeon, J.K. Lee, G.Y. Kim, D. Park, H. Nojima, J. Lee, S.H. Moon, Investigation on removal of hardness ions by capacitive deionization (CDI) for water softening applications, Water Res. 44 (2010) 2267–2275. https://doi.org/10.1016/j.watres.2009.10.020.

[254] Eurocarb, Datasheet HR5 18x35, 2006.

[255] L. Caizán-Juanarena, J.R. Krug, F.J. Vergeldt, J.M. Kleijn, A.H. Velders, H. Van As, A. ter Heijne, 3D biofilm visualization and quantification on granular bioanodes with magnetic resonance imaging, Water Res. 167 (2019) 115059. https://doi.org/10.1016/j.watres.2019.115059.

[256] D. Sun, S. Cheng, A. Wang, F. Li, B.E. Logan, K. Cen, Temporal-Spatial Changes in Viabilities and Electrochemical Properties of Anode Biofilms, Environ. Sci. Technol. 49 (2015) 5227–5235. https://doi.org/10.1021/acs.est.5b00175.

[257] H. Yoo, M. Min, S. Bak, Y. Yoon, H. Lee, A low ion-transfer resistance and high volumetric supercapacitor using hydrophilic surface modified carbon electrodes, J. Mater. Chem. A. 2 (2014) 6663. https://doi.org/10.1039/c4ta00158c.

[258] G. Pognon, T. Brousse, D. Bélanger, Effect of molecular grafting on the pore size distribution and the double layer capacitance of activated carbon for electrochemical double layer capacitors, Carbon N. Y. 49 (2011) 1340–1348. https://doi.org/10.1016/j.carbon.2010.11.055.

[259] T. Menanteau, C. Benoît, T. Breton, C. Cougnon, Enhancing the performance of a diazonium-modified carbon supercapacitor by controlling the grafting process, Electrochem. Commun. 63 (2016) 70–73. https://doi.org/10.1016/j.elecom.2015.12.014.

[260] IRENA, Renewable Power Generation Costs in 2019, Abu Dhabi, 2020. https://www.irena.org/-/media/Files/IRENA/Agency/Publication/2018/Jan/IRENA_2017_Power_Costs_2018.pdf.

[261] R.C. Bansal, M. Goyal, Activated Carbon Adsorption, CRC Press, 2005. https://books.google.nl/books?id=VUluBwAAQBAJ.

[262] M. Mulder, G. Rijs, C. Uijterlinde, Stowa - Innovatieprogramma microverontreinigingen uit RWZI-afvalwater, 2019.

[263] V. Abromaitis, V. Racys, P. van der Marel, R.J.W.W. Meulepas, Biodegradation of persistent organics can overcome adsorption-desorption hysteresis in biological activated carbon systems, Chemosphere. 149 (2016) 183–189. https://doi.org/10.1016/j.chemosphere.2016.01.085.

[264] P.R. Motos, R. V. Weijden, A. ter Heijne, M. Saakes, C.J. Buisman, T.H. Sleutels, High Rate Copper and energy recovery in Microbial Fuel Cells, Front. Microbiol. 6 (2015) 1–8. https://doi.org/10.3389/fmicb.2015.00527.

[265] E. Ntagia, P. Rodenas, A. Ter Heijne, C.J.N. Buisman, T.H.J.A. Sleutels, Hydrogen as electron donor for copper removal in bioelectrochemical systems, Int. J. Hydrogen Energy. 41 (2016) 5758–5764. https://doi.org/10.1016/j.ijhydene.2016.02.058.


R

Monster, The Netherlands

Summary

Summary

Municipal and industrial activities produce large volumes of wastewater. Discharge of wastewater containing organics leads to deoxygenation of surface waters, resulting in degradation of our natural environment. Removal of the organics requires wastewater treatment. Globally, aerobic treatment is the most used technology for removal of organics from wastewater. Aerobic treatment requires energy input for active oxygenation and treatment of waste biomass (also called waste activated sludge) grown from the organics. The waste activated sludge can be digested anaerobically to produce biogas, which allows some energy to be recovered to heat and power the treatment of wastewater. New technological developments combine aerobic and anaerobic environments in granular sludge to consume organics, nitrogen and phosphorous, and have lowered the required energy input.

The organics in wastewater contain chemical energy, which can be recovered by anaerobic processes. Anaerobic digestion (AD) can be used in Upflow Anaerobic Sludge Bed (UASB) reactors to directly produce biogas from the organics in wastewater, without producing waste sludge first. The biogas contains 80% combustible methane, from which 30% can be recovered as electrical power, and the rest is produced as heat which is needed to heat the UASB reactor for sufficient methanogenic productivity. Before combustion, H_2S removal is required to prevent corrosion of the engines and other components. In practice, 26% of the energy in organics can be recovered as electrical power.

Bioelectrochemical systems (BESs) make use of electroactive bacteria that can interact with electrodes. The bacteria grow as a biofilm on the anode, called a bioanode, and oxidize organics. Bioanodes are theoretically able to convert 100% (except for some biomass growth) of the organics to electrical current, in contrast to the 26% in AD. The electrons, freed in the oxidation, are transferred through an electrical circuit as an electrical current to the cathode. At the cathode, a reduction reaction takes place, using the electrons originating from the bioanode. For increased efficiency and selectivity, an ion exchange membrane is placed between the anode and cathode electrolyte compartments. Ions cross over from the anode and cathode, to preserve charge neutrality. Microbial Fuel Cells (MFCs) are bioelectrochemical systems which generate electrical power from a positive cell voltage between the anode and cathode. Microbial Electrolysis Cells (MECs) are bioelectrochemical systems which generate products at the cathode, for which an applied cell voltage is required (and thus negative compared to the MFCs). Common products in MECs are hydrogen and NaOH. The cell voltage, generated by the potential difference between cathode and anode, is reduced by voltage losses. These voltage losses mean that, in practice, there is less power produced or the efficiency of production of valuable products is reduced.

Traditional bioelectrochemical cell designs require space to prevent clogging, caused by solids in the wastewater or biomass grown on the anode (often high m^2/m^3 structures) in the cell. The wide spacing, between anode and cathode, results in voltage losses due to low conductivity of the wastewater, thus decreasing the energy recovered from the organics. Electroactive bacteria and methanogenic archaea grow under similar conditions, such as substrate concentration and pH. Low substrate concentrations controlled via organic loading rate are hypothesized to allow electroactive bacteria to outcompete methanogenic archaea. Traditional cell designs do not allow for high volumetric activity, which is required for treatment of high loading rates, as the limited space restricts the available surface area per volume. Bioelectrochemical systems have yet to produce high current densities,

especially at larger scale, which is a limitation compared to anaerobic digestion. Fluidized capacitive bioanodes promise to tackle these challenges for BESs, in particular with regards to scaling up the technology. The use of activated carbon granules in fluidized capacitive bioanodes allows for intermittent charge storage and large surface area for the bioanode per volume.

Electrons, from the oxidation, and cations, from the bulk solution, are stored in electrical double layers on the surface of the pores in the porous granules. Charging the granules, by the oxidation by the bioanode, occurred in open circuit: not in contact with a potential controlled anode. The charging decreases the electric potential of the granule, and the capacitance is full when the thermodynamic equilibrium of the oxidation reaction is reached. During discharging, the electrons are released into the anode, while cations – adsorbed in the electrical double layers during the charging – are released back into the electrolyte. The electric potential of the granules increases during discharging.

The release of ions would increase the conductivity of the wastewater, reducing voltage losses, and the high surface area of activated carbon granules would allow for high volumetric activity. However, fluidized bed reactors presented in literature have yet to reach high current densities. To recover more charge and produce higher currents, this thesis is focused on studying the discharge of the capacitive granules.

As the capabilities of the granules were largely unknown, we studied single carbon granules as capacitive bioanodes, in a 1 mL cell, to discover the maximum achievable current density. In **Chapter 2**, single activated carbon granules, with volumes below 1 mm^3, were shown to store and release large amounts of charge: on average 73 C/cm^3 over 40 cycles, compared to 18 C/cm^3 from a non-capacitive graphite granule. When the charge was released during discharging, a capacitive peak current was produced on top of the faradaic current, produced by the bioanode, resulting in 77 $mA/cm^3_{granule}$ during the discharging phase. The discharging time, essential for harvesting the charge produced and stored, was deemed too incidental in de existing fluidized bed reactors. Indeed, the highest current of those reactors was produced by forcing contact with the anode through stirring. The moving bed reactor was designed for the granules to have a long contact time by creating a moving bed of capacitive granules at the anode in the discharge cell. This was accomplished by removing the active fluidization for contacting, which allowed the granules to settle into a packed bed like formation. A gas lift was used to transport the granules from below the discharge cell, to the top of the reactor, thus moving the active fluidization to the gas lift. Additionally, the use of the gas lift allowed slower movement, thus increasing the time for discharging at the anode. In the moving bed reactor, charging occurred when not in the discharge cell: not in contact with the anode. Discharging occurred when the granules were in the discharge cell: electrical charge was transferred from granule to granule, and from granule to anode. The discharge current consisted of both the faradaic charge and the capacitive charge from the bioanode granules. Because charged granules were continuously discharged, a continuous current was generated. This is in contrast with fixed granules, where the discharging needs to be alternated with charging: an intermittent current is generated.

Two versions of the moving bed reactor were developed. The largest bioanode reactor was presented in **Chapter 3**. The reactor volume was 7.7 L, containing 1.2 L of granules, flowing through a 163mL discharge cell. The reactor was a tubular construction with a cylindrical discharge cell. The maximum discharge current was 1.9 mA/cm^3_{cell} (257 $A/m^3_{granules}$,

daily average). This current was mainly produced by the passing granules (23 A/m^2 with granules, versus 1.4 A/m^2 when the granules were removed). The activity of the granules was measured in an external cell, where the current produced by a sample of granules from the reactor was measured. This activity increased over time, but eventually stagnated: the same pattern of growth and stagnation (or rather stabilization) of the reactor current was observed.

The stagnation in the current was explained by observation of the biofilm on the granules via Scanning Electron Microscopy (SEM) imaging: the biofilm only grew in the larger pores on the surface of the granules. Slow discharging, seen during discharging without charging (stopped influent), indicated that, though the current density was significantly improved compared to the previous fluidized bioanode reactors, the discharging should be further improved to reach the results of the single granule study.

In **Chapter 4**, the second version of the moving bed had a planar discharge cell of 22mL, through which 0.4L of granules flowed, in a total reactor volume of 1.5L. The maximum current was 4.3 mA/cm^3_{cell}. The planar cell configuration allowed direct comparison with a fixed bed bioanode of similar cell construction. When viewed over the continuous cycle of charging and discharging, the moving bed bioanode produced double the current of the fixed bed, though the current was similar when compared to the fixed bed discharging only. The high discharge current in the moving bed was attributed to the discharge of fully charged granules, resulting from a long discharge time compared to charging time in the moving bed. Investigating in the discharge cell configuration in the fixed bed showed discharging using the anode closest to the membrane produced the highest discharge current. A wider fixed bed, 10 mm instead of 5 mm wide granule bed, produced overall more charge, though the volumetric current density was the same for both.

Discharging was further studied under abiotic conditions in **Chapter 5**. The charged granules (charged via a cathodic current in the discharge cell) were discharged under different conditions. The discharge increased: with higher potential difference ΔE (between the anode and the charged granules), with higher bulk electrolyte conductivity, with decreased maximum distance to the anode (by discharging from both sides of the granular bed) and for a shorter residence time of the granules in the cell. The experiments showed the discharge process was affected more by the electrical resistance than the ionic resistance, although both influenced the transferred charge.

Analysis of the discharge resistance pointed to a reduced resistance at higher transferred charge. This was explained by the release of ions during discharging increased the local conductivity in the cell. The released ions increased the conductivity of the bulk electrolyte on average by 40% (depending on the experimental conditions). This increase in conductivity was diluted when the flowrate of the granular bed, thus the electrolyte, was increased, but due to more charged granules passing during the discharge time the charge was still higher than when the flowrate was low.

In the **Chapter 6**, the various results are discussed. The four cell configurations used in this thesis were discussed: single granules fixed to a wire current collector, a fixed granular bed, a moving bed reactor of 1.5 L with a discharge cell similar to the fixed bed setup, and a moving bed reactor of 7.7 L with a tubular discharge cell. A comparison was made for: 1) the contact time (moving bed), or discharge time (fixed bioanodes), 2) contact resistance, 3) ratio between charging and discharging, and 4) the faradaic and capacitive contributions to the discharge current. In **Chapters 3, 4 and 5** recommendations were given for engineering

improvements. These recommendations were used, together with improvements resulting from **Chapter 6**, to discuss improving 1) the discharge cell for a tubular design, 2) the charging and discharging volumes in a multi discharge cell reactor for large scale implementation, and 3) the granules in relation to electrical resistance, ion transport resistance, and the biofilm presence on the granules.

The bioanode experiments showed the moving bed produced 3 – 20 times higher current density in the discharge cell compared to previous fluidized bed reactors from literature. Although the aim of 3.5 mA/cm^3, for competition with anaerobic digestion, was not reached in the reactor, the moving bed bioanode did produce 4.3 mA/cm^3 in the discharge cell. If improvements are implemented, this current density can be increased and bring the reactor performance closer to the desired goal.

The discharge of ions in the discharge cell increased the local electrolyte conductivity, and the electrical resistance was more important for the discharge process than the bulk ionic resistance. These findings show the moving bed reactor has great promise as an alternative for scaling up bioelectrochemical systems. Future improvements should focus on improving the electrical resistance in the discharge cell, and to match the total volume of granules to the discharge cell and the reactor volume, to bring the current density on the discharge cell closer to the total reactor performance.

Calo Pola, Spain

List of publications

C. Borsje, D. Liu, T.H.J.A. Sleutels, C.J.N. Buisman, A. ter Heijne, Performance of single carbon granules as perspective for larger scale capacitive bioanodes, J. Power Sources. 325 (2016) 690–696. https://doi.org/10.1016/j.jpowsour.2016.06.092. **(Chapter 2)**

C. Borsje, T. Sleutels, M. Saakes, C.J.N. Buisman, A. ter Heijne, The granular capacitive moving bed reactor for the scale up of bioanodes, J. Chem. Technol. Biotechnol. 94 (2019) 2738–2748. https://doi.org/10.1002/jctb.6091. **(Chapter 3)**

C. Borsje, T. Sleutels, W. Zhang, W. Feng, C.J.N. Buisman, A. ter Heijne, Making the best use of capacitive current: Comparison between fixed and moving granular bioanodes, J. Power Sources. 489 (2021) 229453. https://doi.org/10.1016/j.jpowsour.2021.229453. **(Chapter 3)**

C. Borsje, T. Sleutels, C.J.N. Buisman, A ter Heijne, Improving the discharge of capacitive granules in a moving bed reactor, J. Environ. Chem. Eng. (submitted 2021). **(Chapter 4)**

S.D. Molenaar, T. Sleutels, J. Pereira, M. Iorio, **C. Borsje**, J.A. Zamudio, F. Fabregat-Santiago, C.J.N. Buisman, A. ter Heijne, In situ Biofilm Quantification in Bioelectrochemical Systems by using Optical Coherence Tomography, ChemSusChem. 11 (2018) 2171–2178. https://doi.org/10.1002/cssc.201800589.

L. Caizán-Juanarena, **C. Borsje**, T. Sleutels, D. Yntema, C. Santoro, I. Ieropoulos, F. Soavi, A. ter Heijne, Combination of bioelectrochemical systems and electrochemical capacitors: Principles, analysis and opportunities, Biotechnol. Adv. 39 (2020) 107456. https://doi.org/10.1016/j.biotechadv.2019.107456.

L. Caizán-Juanarena, T. Sleutels, **C. Borsje**, A. ter Heijne, Considerations for application of granular activated carbon as capacitive bioanode in bioelectrochemical systems, Renew. Energy. 157 (2020) 782–792. https://doi.org/10.1016/j.renene.2020.05.049.

Pannenhoef, The Netherlands

Acknowledgements

Acknowlegdements

In the seven years since I started with the research in this thesis, I have had the pleasure to meet, and to work with, many remarkable people while working in the inspiring work environments of the department of environmental technology and Wetsus.

Annemiek, thank you for challenging me to take up the capacitive adventure and for all your support. I enjoyed our walking talks in Wageningen and Rhenen a lot. Even though our Wetsus meetings were usually short, I appreciated your ability to make the most of the time.

Tom, thank you for your guidance at Wetsus. I appreciated how you were always open for a talk and your input was always valued. Thank you for all the advice, especially during the writing.

Cees, thank you for your support and for challenging my ambitions and for providing me the opportunity to do this research at ETE and Wetsus.

Thank you **Dandan**, for introducing me in the intriguing world of bioelectrochemistry. I enjoyed my time as your student and our talks and discussions in the years after.

Leire, my capacitive partner-in-crime. I enjoyed your positive attitude during this challenging research. I always looked forward to our meetings and enjoyed our shared trips to Rome, China, France, and New Castle. Also, my thanks for often providing a guest bed in Wageningen.

Michel and **Philipp**, thank you for your guidance in my electrochemical experiments and lab tips and tricks. **Michel**, I especially appreciate your enthusiasm and creative input! **Bert**, you are a good listener. Thank you for your advice. I hope we can share our photography some more later.

I want to thank my various officemates. I felt quite welcome and enjoyed the talks and discussions in the 'office of happiness' with **Yin, Sofia, Jorrit, Louis, Ilse, Enas, Suyash, Tania, Zexin, Antoine, Rita, Nandini,** and **Naghme**. I also had a good time with **Fabian, Sandra, Yang, Rebeca, Paulina,** and **Natascha** in the upstairs office.

My thanks to the members and participants of the Resource Recovery theme for your support and input.

I want to thank the analytical and technical team of Wetsus. Special thanks to **Jan Tuinstra**, who helped me built the many parts, pieces, and components of my various experimental setups. I enjoyed working together a lot! Thank you **JJ, Ernst, Harm, John, Wim, Marianne, Lisette, Jelmer, Mieke Jan Willem, Janneke,** and **Agnieszka**. And my thanks to **Gerrit** and **Rienk**, who were very helpful with their logistics and IT support.

My thanks to the secretarial teams of ETE and Wetsus. **Liesbeth**, **Gea**, **Helena**, **Linda**, **Marnejaeike**, **Trienke**, **Jeanette**, **Anke**, **Esther**, **Jannie**, and **Willy**. Thank you for all your help over the years.

Gerben, **Riet** and **Catharine**, your efforts made the cantine and drinks at Wetsus an enjoyable experience. Thank you for the improvements to the menu for the diets and wishes, and your openness for a friendly chat.

Thanks to my students **Wouter**, **Menur**, **Julian**, **Wandi**, **Siqi** and **Wenzhou**, for your help exploring the various research topics and for all your contributions. **Hardy**, **Ricardo**, **Patrick**, **Victor A**, and **Steffen**: I enjoyed organizing the practicals together.

To my colleagues and friends at ETE, thank you for many enjoyable Christmas dinners, department trips, the study trip to China, and the meetings with the Biorecovery group and the Bioelectrochemistry group. **Emelius**, **Lucia**, **Pim**, **Rieks**, **Sanne**, **Delaram**, **Laura**, **Huub**,

Miriam, **David**, **Pradip**, **Vinnie**, **Dandan**, **Momo**, the interesting travel companions on the ETE trip of 2016, and many more. Thank you for making ETE feel welcome.

My thanks to my colleagues and friends, past and present, **Prashanth**, **Gaofeng**, **Jordy**, **Jan Willem**, **Victor T**, **Jouke**, **Joeri**, **Rik**, **Kaustub**, **Joeri**, **Fabian**, **Diego**, **Gijs**, **Catarina**, **Qingdian**, **Rose**, **Barbara**, **Shuyana**, **Sandra**, **Raquel**, **Maarten**, **Pau**, **Sam**, **Mariana**, **Yang**, **Steffen**, **Mariana**, **João**, **Victor A**, **Maarten B**, **Caroline**, **Martijn**, **Veerle**, **Roel**, **João**, **Lisette**, and many more, who made life at Wetsus and in Leeuwarden a pleasant experience.

Raquel, I appreciate your insights. **Sandra**, I enjoyed our summer swims very much! **Steffen**, you are a great listener! **Sebastian**, you always inject a bit of fun in any situation. Thanks for being a great housemate – though a bit too much heat sometimes! **Sam**, thank you for being a good friend, housemate, lab partner, co-bioanode researcher, and now paranymph! You've been at my side through this PhD adventure. I really enjoyed the late-night insights, talks and discussions.

My paranymphs **Sam** and **Sebastian** thank you for supporting me in the last months!

To my family, Pa en Yvonne, en Ma, bedankt voor alle goede zorgen en het luisterend oor tijdens dit avontuur. Opa, je bent mijn inspiratie voor het uitvinder-zijn. Mijn broertjes en zusjes, mijn neefje en nichtje, jullie inspireren mijn doorzettingsvermogen.

Casper Borsje, 28-05-2021

Markermeer, The Netherlands

About the author

Casper was born on 15 November 1986 in Houten, a town in the center of the Netherlands. He finished his high school studies in 2005 at the Katholieke Scholengemeenschap Etten-Leur. After some years studying in Nijmegen and Enschede, he graduated cum laude in the study Environmental Management and Technology, a Bachelor of Applied Science of Avans University of Applied Sciences. Casper continued his studies of the environmental sciences and sustainability challenges at Wageningen University, with the Master of Science program of Environmental Sciences and the major of Environmental Technology.

His first foray into bioelectrochemistry started with his MSc thesis, where he investigated the behavior of single carbon granules as capacitive bioanodes in microbial fuel cells, at the department of Environmental Technology. Casper graduated in July 2015, after finishing an internship at Wetsus. He started immediately after, in August 2015, with his PhD research in Capacitive bioanodes for electricity production with Microbial Fuel Cells at the department of Environmental Technology of Wageningen University. The research took place in Leeuwarden at Wetsus, European centre of excellence for sustainable water technology. His studies focused on the larger scale application of activated carbon granules as capacitive bioanodes. The capacitive bioanode granules allow for electroless charging, by storing charge produced by electroactive bacteria that consume substrate from wastewater, and the production of an electrical during discharging in an electrochemical cell.

Netherlands Research School for the
Socio-Economic and Natural Sciences of the Environment

D I P L O M A

for specialised PhD training

The Netherlands research school for the
Socio-Economic and Natural Sciences of the Environment
(SENSE) declares that

Casper Borsje

born on 15 November 1986 in Houten, The Netherlands

has successfully fulfilled all requirements of the
educational PhD programme of SENSE.

Wageningen, 28 May 2021

Chair of the SENSE board

Prof. dr. Martin Wassen

The SENSE Director

Prof. Philipp Pattberg

The SENSE Research School has been accredited by the Royal Netherlands Academy of Arts and Sciences (KNAW)

KONINKLIJKE NEDERLANDSE
AKADEMIE VAN WETENSCHAPPEN

The SENSE Research School declares that **Casper Borsje** has successfully fulfilled all requirements of the educational PhD programme of SENSE with a work load of 43.3 EC, including the following activities:

SENSE PhD Courses

- Environmental research in context (2016)
- Research in context activity: 'Biological Water Treatment practical (MSc Water Technology, Wetsus Academy); course management and development' (2016-2018);

Other PhD and Advanced MSc Courses

- European Summer School for Electrochemical Engineering, Wetsus (2015)
- Workshop on Up-scaling of bioelectrochemical Systems, Wetsus (2016)
- Presentation course, Wetsus (2015)
- Graphical abstract workshop, Wetsus (2016)
- Student supervision course, Wetsus (2016)
- Communication styles, Wetsus (2017)
- Talent course, Wetsus (2017)
- Project and Time management, Wageningen Graduate Schools (2017)
- Efficient writing strategies, Wageningen Graduate Schools (2019)
- Career perspectives, Wetsus (2020)

External training at a foreign research institute

- Tailoring the interface of porous graphite granules and electroactive biofilms for efficient bioelectrochemical systems, Exchange program with University of Rennes, Van Gogh research programme (2016)

Management and Didactic Skills Training

- Chairing and organizing weekly lunch presentations at Wetsus (2016)
- Organized and chaired 'Mini-symposium in honor of the defense of Dandan Liu' (2018)
- Organized a visit to Evides (2018)
- Supervising one BSc student with thesis (2016)
- Supervising five MSc students with thesis (2016-2019)

Selection of Oral Presentations

- *The capacitive moving bed reactor to scale up bioanodes*, EU-ISMET 2018, 12-14 September 2018, Newcastle upon Tyne, United Kingdom
- *The granular capacitive moving bed reactor for the scale up of bioanodes*, Environmental Technology for impact (ETEi 2020), 3-4 June 2020, Wageningen (online), The Netherlands

SENSE coordinator PhD education

Dr. ir. Peter Vermeulen

The research was supported by the Dutch Technology Foundation STW, which is part of the Netherlands Organization for Scientific Research (NWO), and which is partly funded by the Ministry of Economic Affairs (VENI grant no 13631).

This work was performed in the cooperation framework of Wetsus, European Centre of Excellence for Sustainable Water Technology (www.wetsus.eu). Wetsus is co-funded by the Dutch Ministry of Economic Affairs and Ministry of Infrastructure and Environment, the European Union Regional Development Fund, the Province of Fryslân and the Northern Netherlands Provinces. The authors thank the participants of the research theme 'Resource Recovery' for the fruitful discussions and their financial support.

Financial support from both Wageningen University and Wetsus for printing this thesis is gratefully acknowledged.

Cover design by Casper Borsje
Photo by Casper Borsje – Mistaya Canyon, Canada

Photos between chapters by Casper Borsje

Printed by ProefschriftMaken